LUND UNIVERSITY

MASTER THESIS

Efficient Modeling of a Flexible Beam in Dymola using Coupled Substructures in a Floating Frame of Reference Formulation

Author:
Anders ERICSSON
Anton KJELLANDER

Supervisor:
Mathias STRANDBERG
Per LIDSTRÖM

A thesis submitted in fulfilment of the requirements
for the degree of Master of Science

in the

Division of Mechanics
Department of Mechanical Engineering

October 2015

"My powers are ordinary. Only my application brings me success."

Sir Isaac Newton

Abstract

Efficient Modeling of a Flexible Beam in Dymola using Coupled Substructures in a Floating Frame of Reference Formulation

by Anders Ericsson

Anton Kjellander

In this Master Thesis a three dimensional Euler-Bernoulli beam model was implemented in the simulation software Dymola. The beam model is based on the Floating Frame of Reference formulation combined with the Craig-Bampton method. The theory is developed with the scope to capture the dynamic and static responses of a beam model in a compact and computer efficient implementation. The Thesis includes derivation of kinematic description, mass matrix, stiffness matrix and force vectors of an Euler-Bernoulli beam in three-dimensional space. Two one-dimensional models have been derived as well. The implementation in Dymola is described together with validation of the model, discussion and conclusions. The validation of the model shows great accuracy in static loading both in elongation, torsion and bending. Excitation of eigenfrequencies is possible but the results slightly differs from the analytical solutions. Dynamic tests of the beam model shows realistic responses but further testing on this subject is recommended. Compatibility with other components in Dymola works fine. However there are some minor issues that should be solved to enhance the efficiency. Overall the static and dynamic responses of the beam model works sufficiently well.

Acknowledgements

Contents

List of Figures

List of Tables

Symbols

ϵ	Strain	$-$
u	Displacement	m
F	Force	N
A	Cross section area	m^2
L	Beam length	m
h	Height of cross section	m
b	Width of cross section	m
ρ	Density	kgm^{-3}
v	Poisson's ratio	$-$
E	Elasticity modulus	Pa
c	Wave speed	ms^{-1}
M	Bending moment/Torque	Nm
G	Shear modulus	Pa
K	Torsional stiffness factor	m^4
θ	Angular displacement	rad
J_x	Moment of inertia around the x-axis per unit length	kgm
I_i	Planar second moment of area, $i = y, z$	m^4
w	Deflection	m
$\mathbf{r}_p$	Position vector to point p	m
$\mathbf{R}$	Position vector to origin of local coordinate system	m
$\mathbf{A}$	Transformation matrix, local to global	$-$
$\bar{\mathbf{u}}$	Local position vector	m
$\bar{\mathbf{u}}_0$	Initial local position vector	m
$\bar{\mathbf{u}}_f$	Local deformation vector	m
$\mathbf{S}$	Shape function matrix	$-$
$\mathbf{q}_f$	Generalized deformation coordinates	m
$\bar{\mathbf{u}}_c$	Vector to cross section	m
$\bar{\mathbf{u}}_{p/c}$	Vector in the plane of the cross section	m
$\bar{\mathbf{u}}_r$	Translational deformation vector	m

$\bar{\mathbf{u}}_\theta$	Deformation vector due to rotation	m
$\mathbf{A}_f$	Transformation matrix depending on angular displacement	$-$
$\boldsymbol{\theta}_f$	Angular deformation vector	rad
$\mathbf{S}_r$	Shape function matrix associated with translation	$-$
$\mathbf{S}_\theta$	Shape function matrix associated with rotation	$-$
$\bar{\boldsymbol{\omega}}$	Angular velocity in local frame	$rads^{-1}$
$\bar{\boldsymbol{\alpha}}$	Angular acceleration in local frame	$rads^{-2}$
$\boldsymbol{\theta}$	Rotational coordinates describing the location of local coordinate system	$-$
$\bar{\mathbf{G}}$	Matrix describing relation between angular velocity and time derivative angular representation	$-$ $-$
$\mathbf{q}$	Generalized coordinate vector	$-$
$\mathbf{a}_v$	Vector associated with quadratic velocity	$-$
N_i	Static shape functions, $i = x, y, z, \theta_x, \theta_y, \theta_z$	$-$
S_i	Dynamic shape functions, $i = x, y, z, \theta_x, \theta_y, \theta_z$	$-$
T	Kinetic energy	J
$\mathbf{M}$	Mass matrix	$-$
$\mathbf{m}_{ii}$	Components of the mass matrix, $i = R, \theta, $f	$-$
U_0	Strain energy per unit area	Jm^{-2}
$\boldsymbol{\sigma}_{ij}$	Stress tensor, $i, j = 1, 2, 3$	Pa
$\mathrm{d}\boldsymbol{\epsilon}_{ij}^*$	Strain increment tensor, $i, j = 1, 2, 3$	$-$
K	Stiffness matrix	$-$
K_{ff}	Stiffness associated with deformation coordinates	$-$
δW_F	Virtual work off all forces	J
δW_s	Virtual work of elastic forces	J
δW_e	Virtual work of external forces	J
δW_g	Virtual work of gravitational forces	J
$\mathbf{Q}_e$	External force vector	$-$
$\mathbf{Q}_g$	Gravitational force vector	$-$
δW_I	Virtual work of Inertia forces	J
$\mathbf{C}$	Damping matrix	$-$
η	Rayleigh damping coefficient	$-$
δ	Rayleigh damping coefficient	$-$
$\mathbf{g}$	Gravitational vector	ms^{-2}

Chapter 1

Introduction

1.1 Background

The Master Thesis project was proposed by Modelon AB, a Swedish company with
an expertise within physical modeling, simulation and optimization of dynamic systems.
Their expertise focuses on Dymola, a dynamic modeling software written in the equation
based language Modelica. A majority of Modelon's customers are manufacturers within
the automotive industry, an industry with short development cycles that demand efficient
and accurate modeling of complex mechanical systems.

Advanced models of mechanical systems need to take into account structural elasticity
of different components. Currently the Modelica standard library only supports rigid
components. Beams are important structural elements that are used in many different
mechanical applications. Adding support for elasticity will improve model accuracy
especially for models with large structures or loads (such as a heavy vehicle drive line).

Since Dymola is a software most widely used in modeling of large mechanical systems the
need for a efficient and yet relative simple beam model is required to maintain certain
standards in computational time. The purpose has been to create a structural beam
component that provides information concerning dynamics and deformation as a part
of large multibody systems. Common information within structural mechanics such as
internal stresses and strains has been disregarded in favour of reducing the complexity
of the model.

1.2 Objectives and Delimitations

The objectives specified from Modelon AB were from the start

- Review of the model reduction methods with special focus on Floating Frame of Reference formulation combined with Craig-Bampton method and the Absolute Nodal Coordinates method.

- Review the specifics of object-oriented equation based modeling and identify possible pit-falls with the methods.

- Implementation of the two methods in 3D in form of a Modelica library compatible with the standard multibody library.

- Implementation of the two methods in 1D in form of a Modelica library compatible with the standard rotational and translational libraries.

- Development of test models and performance comparison of the methods.

During the project it was determined that an investigation and implementation of both methods mention above would be to time consuming and focus shifted to the Floating Frame of Reference formulation in combination with the Craig-Bampton method. At first the ambition was also to implement a geometrically parametrized flexible beam i.e. the beam could have a rectangular or circular cross section. However due to lack of time the three-dimensional model was only implemented for a rectangular cross section.

An Euler-Bernoulli beam model is used in this thesis and the limitation on this model is presented in Section 1.5.3. Additionally the following assumptions were also made:

- The material is isotropic and homogeneous.

- The material is linearly elastic and there is no consideration of plastic behaviour.

- The cross-sections of the beam are symmetric around the y- and z-axis.

- Only small strains are considered which in turn implies small angular deformation.

- The geometry of the beam is constant with time and calculated in the reference configuration.

- In the 1D translational model only rectangular cross sections are considered.

- In the 1D rotational model both rectangular and circular cross sections are considered.

- In the 3D model only rectangular cross sections are considered.

These delimitations were made to simplify the model and hence make it more efficient.

1.3 Description of Methodology

Throughout this project the focus has been to implement a flexible beam component based on theory of the Floating Frame of Reference(FFoR) formulation . The FFoR formulation was chosen due to it's capabilities and advantages in modeling multibody systems as well as similarities with the current implementation of components in Dymola. The FFoR formulation is described in detail in Chapters 2, 3 and 4 while the structure in Dymola is described in Chapter 5.

The FFoR formulation is a methodology which structures the equations of flexible multibody systems through the principle of Langrangian Dynamics. It follows from the principle of virtual work and provides the equations of motion for the system. The FFoR formulation can be applied to any flexible multibody system, it is however necessary to provide information regarding the bodies deformable behaviour. The deformation is described through the so called shape functions, which in this project are chosen according to the Craig-Bampton method. The Craig-Bampton method divides the flexible body into coupled substructures which imposes certain constraints on the shape functions. In this project the shape functions of the substructures consists of analytical solutions from the Euler-Bernoulli beam theory, the solutions are derived from both static and dynamic cases of deformation. Where the dynamic shape functions are solutions from a eigenvalue analysis of a vibrating flexible beam. The Craig-Bampton method is further explained in Sections 2.4 to 2.7.

1.4 Previous Work

The project to develop a flexible beam model in Dymola started in 2009. There has previously been two Master Thesis within this topic at Modelon AB. Both of the projects used the Floating Frame of Reference formulation in combination with other theories.

The first project focused on the Finite Element Method [1], the objective was to link Dymola with the FEA software Abaqus in order to run coupled simulations between the two software's. The project encountered different problems due to the underestimation of the workload.

The second project focused on analytical solutions from eigenvalue analysis of vibrating flexible beams [2]. The approach was similar to the one presented in this thesis but the formulation didn't include solutions to static cases of deformation which made the model inefficient for those cases. The model also required the user to specify boundary condition's, a problem which has been solved differently in this project.

1.5 Constitutive Relations within Solid Mechanics

This Section is meant to provide the reader with an review of the constitutive relations used in this report. The beam model is based on these fundamental theories and the equations in this Section are recurring content throughout the report.

1.5.1 Longitudinal Deformation

For a bar with arbitrary cross section geometry the constitutive relation between strain and tensile force can be described as [3, p. 308]

$$\epsilon(x,t) = \frac{\partial u(x,t)}{\partial x}, \qquad F(x,t) = AE\epsilon(x,t) \tag{1.1}$$

where ϵ and $F(x,t)$ is the elongation and tensile force, A is the cross-section area, E the elasticity modulus and $u(x,t)$ the longitudinal displacement a long the x-axis. Here it is assumed that the area and elasticity modulus remain constant through the length of the bar.

1.5.2 Torsional Deformation

In comparison to longitudinal deformation, torsional deformation of a shaft can be described by the following constitutive relation. [3, p. 325]

$$M(x,t) = GK\frac{\partial \theta(x,t)}{\partial x} \tag{1.2}$$

Where $M(x,t)$ is the torque and $\theta(x,t)$ is the torsional angle around the x-axis. G is the shear modulus and K is the torsion stiffness factor depending on the cross section geometry. Both the shear modulus and torsion stiffness is assumed to be constant through the shaft.

1.5.3 Euler Bernoulli Beam Theory

The beam models created in this Master Thesis follows the Euler Bernoulli beam theory. This model was chosen due to it's simplicity in comparison to the Timoshenko beam theory. There are some advantages with the Timoshenko beam theory, such as taking shear deformation into account which makes it more suitable for describing short, thick beams or high frequency excitation. However, it also involves two differential equations instead of one which increases the complexity of the solution. Euler Bernoulli theory is

more widely used and accounted for in the literature, making it a safer choice. These arguments makes it a better candidate for the purpose of implementing a computer efficient model.

In Euler Bernoulli beam theory the following assumptions are made:

- The beams cross sections are considered flat and remain flat after deformation.

- Cross sections that are perpendicular to the centreline of the beam before deformation remains perpendicular after deformation.

- The cross sections of the beam have initially a constant shape through the beam length and the shape of the cross section remains the same after deformation.

These three assumptions imply zero shear deformation and leads to the following constitutive relations [4, p. 115-116]

$$EI\frac{\partial^2 w(x,t)}{\partial x^2} = -M(x,t) \tag{1.3}$$

$$EI\frac{\partial^3 w(x,t)}{\partial x^3} = -T(x,t) \tag{1.4}$$

$$EI\frac{\partial^4 w(x,t)}{\partial x^4} = q(x,t) \tag{1.5}$$

$$\theta(x,t) = \frac{\partial w(x,t)}{\partial x} \tag{1.6}$$

where $w(x,t)$ is the deflection in the bending plane, E the elasticity modulus, I the planar second moment of area around the axis of bending, $M(x,t)$ the bending moment, $T(x,t)$ the shear force and $q(x,t)$ is the applied load per unit length with respect to the x-coordinate .

Chapter 2

Kinematic Description

This Chapter explains the kinematic theory of the deformable beam. It starts from the general formulation provided in the theory of Floating Frame of Reference and applies this to the special case of an Euler Bernoulli beam. The position, velocity and acceleration of any given material point in the beam is derived, which is later connected with the theory of the Craig-Bampton method and the selection of shape functions.

2.1 The Position Vector

In the Floating Frame of Reference formulation the position of an arbitrary point p in any body B can be described by the vector $\mathbf{r}_p$. This vector is defined in a fixed global coordinate system. Introduce a local coordinate system in body B and the position of point p can be described as,[5, p. 192]

$$\mathbf{r}_p = \mathbf{R} + \mathbf{A}\bar{\mathbf{u}} \tag{2.1}$$

where $\mathbf{R}$ is a vector from the origin of the global coordinate system to the origin of the local coordinate system. $\mathbf{A} = \mathbf{A}(\boldsymbol{\theta})$ is the transformation matrix from the local to the global coordinate system, it is defined by the rotational coordinates $\boldsymbol{\theta}$ and has orthogonal properties, i.e. $\mathbf{A}^T\mathbf{A} = \mathbf{I}$. $\bar{\mathbf{u}}$ describes the position of point p in the body B, the bar above the vector denotes that this vector is defined in the local coordinate system. In the case of rigid body motion the vector $\bar{\mathbf{u}}$ remains constant, in the case of body B being a deformable body the vector $\bar{\mathbf{u}}$ changes depending on position and time. The position $\bar{\mathbf{u}}$ can then be defined as

$$\bar{\mathbf{u}} = \bar{\mathbf{u}}_0 + \bar{\mathbf{u}}_f \tag{2.2}$$

where

$$\bar{\mathbf{u}}_0 = \begin{bmatrix} x \\ y \\ z \end{bmatrix} \tag{2.3}$$

describes the initial position of point p in the body and the vector

$$\bar{\mathbf{u}}_f = \begin{bmatrix} u_{f1} \\ u_{f2} \\ u_{f3} \end{bmatrix} \tag{2.4}$$

describes the displacement of p. Using separation of variables $\bar{\mathbf{u}}_f$ can be separated into two functions, one function depending on the position and one function depending on the time[5, p. 190-191]. The deformation vector can then be expressed as

$$\bar{\mathbf{u}}_f(x, y, z, t) = \mathbf{S}(x, y, z)\mathbf{q}_f(t) \tag{2.5}$$

where x, y, z are the Cartesian coordinates in the local coordinate system, $\mathbf{S}(x, y, z)$ is the shape function matrix that describes the shape of the deformation of body B. The shape function matrix contains shape functions for each degree of freedom that has to satisfy the kinematic constraints imposed on the boundary of the deformable body. The vector $\mathbf{q}_f(t)$ contains the generalized coordinates corresponding to the shape functions.

Combining equation (2.1), (2.2) and (2.5) yields the following expression for the position of point p

$$\mathbf{r}_p = \mathbf{R} + \mathbf{A}\Big(\bar{\mathbf{u}}_0 + \mathbf{S}(x, y, z)\mathbf{q}_f(t)\Big) \tag{2.6}$$

This is the general expression for describing the position of a point p on any body B. For a beam under the influence of bending it is needed to consider the deformation due to rotation around the local coordinate axis's. The local position vector $\bar{\mathbf{u}}$ should then be defined as

$$\bar{\mathbf{u}} = \bar{\mathbf{u}}_c + \bar{\mathbf{u}}_{p/c} + \bar{\mathbf{u}}_f = \begin{bmatrix} x \\ 0 \\ 0 \end{bmatrix} + \begin{bmatrix} 0 \\ y \\ z \end{bmatrix} + \mathbf{u}_f \tag{2.7}$$

Where $\bar{\mathbf{u}}_c$ is a vector along the beam axis to the cross section of interest. $\bar{\mathbf{u}}_{p/c}$ is a vector in the plane of the cross section, defined from the beam centreline to the point p. Consult Figure 2.1 where these position vectors are illustrated in a beam with rectangular cross section.
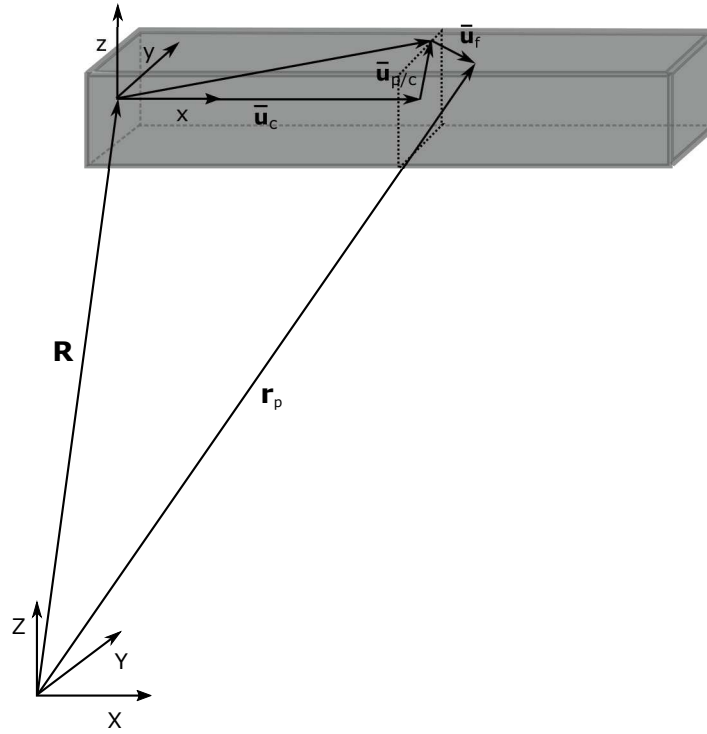
FIGURE 2.1: The position vector $\mathbf{r}_p$ defined in the global coordinate system. The figure also illustrates the two local position vectors $\bar{\mathbf{u}}_c$ and $\bar{\mathbf{u}}_{p/c}$.

The deformation of point p can be divided into two terms. One describing the deformation of the beam centreline and one term describing the deformation due to the cross section subjected to rotational effects.

$$\bar{\mathbf{u}}_f = \bar{\mathbf{u}}_r + \bar{\mathbf{u}}_\theta \tag{2.8}$$

Where

$$\bar{\mathbf{u}}_r = \begin{bmatrix} u_x \\ u_y \\ u_z \end{bmatrix}, \qquad \bar{\mathbf{u}}_\theta = \begin{bmatrix} u_{\theta_x} \\ u_{\theta_y} \\ u_{\theta_z} \end{bmatrix} \tag{2.9}$$

and the deformation $\bar{\mathbf{u}}_\theta$ is defined as

$$\bar{\mathbf{u}}_\theta = \mathbf{A}_f \bar{\mathbf{u}}_{p/c} - \bar{\mathbf{u}}_{p/c} \approx (\mathbf{I} + \tilde{\boldsymbol{\theta}}_f)\bar{\mathbf{u}}_{p/c} - \bar{\mathbf{u}}_{p/c} = \tilde{\boldsymbol{\theta}}_f \bar{\mathbf{u}}_{p/c} = -\tilde{\bar{\mathbf{u}}}_{p/c}\boldsymbol{\theta}_f \tag{2.10}$$

where $\mathbf{A}_f = \mathbf{A}_f(\boldsymbol{\theta}_f)$ is a local rotation matrix that describes the rotation of the cross section and

$$\boldsymbol{\theta}_f = \begin{bmatrix} \theta_x \\ \theta_y \\ \theta_z \end{bmatrix} \tag{2.11}$$

is the angular deformation that arises due to the effects of bending and torsion. In this formulation it is assumed that these angles can be approximated as small such that

$$tan(\boldsymbol{\theta}_f) \approx \mathbf{0} \tag{2.12}$$

Furthermore $\tilde{\bar{\mathbf{u}}}_{p/c}$ and $\tilde{\boldsymbol{\theta}}$ are the skew symmetric matrices of the vectors $\bar{\mathbf{u}}_{p/c}$ and $\boldsymbol{\theta}$ defined as

$$\tilde{\bar{\mathbf{u}}}_{p/c} = \begin{bmatrix} 0 & -z & y \\ z & 0 & 0 \\ -y & 0 & 0 \end{bmatrix}, \qquad \tilde{\boldsymbol{\theta}} = \begin{bmatrix} 0 & -\theta_z & \theta_y \\ \theta_z & 0 & -\theta_x \\ -\theta_y & \theta_x & 0 \end{bmatrix} \tag{2.13}$$

In general the " $\sim$ " sign above a vector denotes the skew symmetric matrix of this vector. Now considering that each degree of freedom in point p can be described by shape functions emerging from the equations in Section 1.5 and therefore only dependent on the local x-coordinate. This implies the following

$$\bar{\mathbf{u}}_r = \mathbf{S}_r(x)\mathbf{q}_f, \qquad \mathbf{S}_r(x) = \begin{bmatrix} \mathbf{S}_x(x) \\ \mathbf{S}_y(x) \\ \mathbf{S}_z(x) \end{bmatrix} \tag{2.14}$$

$$\boldsymbol{\theta}_f = \mathbf{S}_\theta(x)\mathbf{q}_f, \qquad \mathbf{S}_\theta(x) = \begin{bmatrix} \mathbf{S}_{\theta_x}(x) \\ \mathbf{S}_{\theta_y}(x) \\ \mathbf{S}_{\theta_z}(x) \end{bmatrix} \tag{2.15}$$

Where $\mathbf{S}_r(x)$ and $\mathbf{S}_\theta(x)$ are matrices of the size $[3 \times n]$. The vector $\mathbf{q}_f$ is of the size $[n \times 1]$ and n is the number of shape function used. Combining equation (2.14) and (2.15) with (2.8) and inserting into equation (2.10) yields

$$\bar{\mathbf{u}}_f = (\mathbf{S}_r - \tilde{\bar{\mathbf{u}}}_{p/c}\mathbf{S}_\theta)\mathbf{q}_f \tag{2.16}$$

where the shape function matrix $\mathbf{S}$ can be identified as

$$\mathbf{S} = \mathbf{S}(x,y,z) = \mathbf{S}_r(x) - \tilde{\bar{\mathbf{u}}}_{p/c}(y,z)\mathbf{S}_\theta(x) = \begin{bmatrix} \mathbf{S}_x \\ \mathbf{S}_y \\ \mathbf{S}_z \end{bmatrix} - \begin{bmatrix} 0 & -z & y \\ z & 0 & 0 \\ -y & 0 & 0 \end{bmatrix} \begin{bmatrix} \mathbf{S}_{\theta_x} \\ \mathbf{S}_{\theta_y} \\ \mathbf{S}_{\theta_z} \end{bmatrix} \tag{2.17}$$

or in a more explicit form

$$\mathbf{S} = \begin{bmatrix} \mathbf{S}_1 \\ \mathbf{S}_2 \\ \mathbf{S}_3 \end{bmatrix} = \begin{bmatrix} \mathbf{S}_x + z\mathbf{S}_{\theta_y} - y\mathbf{S}_{\theta_z} \\ \mathbf{S}_y - z\mathbf{S}_{\theta_x} \\ \mathbf{S}_z + y\mathbf{S}_{\theta_x} \end{bmatrix} \tag{2.18}$$

which is used to describe the position of point p in equation (2.6).

2.2 The Velocity Vector

The velocity of a arbitrary point p is obtained by differentiating equation (2.1) with respect to time, which yields

$$\dot{\mathbf{r}}_p = \dot{\mathbf{R}} + \dot{\mathbf{A}}\bar{\mathbf{u}} + \mathbf{A}\dot{\bar{\mathbf{u}}} \tag{2.19}$$

where the second term can be written as $\dot{\mathbf{A}}\bar{\mathbf{u}} = -\mathbf{A}\tilde{\bar{\mathbf{u}}}\bar{\boldsymbol{\omega}}$,[5, p. 197] which can be used along with $\dot{\bar{\mathbf{u}}} = \mathbf{S}\dot{\mathbf{q}}_f$ to write the velocity as

$$\dot{\mathbf{r}}_p = \dot{\mathbf{R}} - \mathbf{A}\tilde{\bar{\mathbf{u}}}\bar{\boldsymbol{\omega}} + \mathbf{A}\mathbf{S}\dot{\mathbf{q}}_f \tag{2.20}$$

where $\bar{\boldsymbol{\omega}}[3 \times 1]$ is the angular velocity vector defined in the local coordinate system. The angular velocity depends on the rotational coordinates through [5, p. 52]

$$\bar{\boldsymbol{\omega}} = \bar{\mathbf{G}}\dot{\boldsymbol{\theta}} \tag{2.21}$$

where $\bar{\mathbf{G}} = \bar{\mathbf{G}}(\boldsymbol{\theta})$ is a transformation matrix expressed in the local coordinate system depending on the rotational coordinates of the body. These rotational coordinates can be chosen either as Euler parameters/quaternions, Rodriguez parameters, Euler angles or other coordinates in favour. In this thesis it was decided to use Euler parameters/quaternions since it simplifies the quadratic velocity vector which is further explained in Section 3.6. This implies that the transformation matrices becomes [5, p. 31,51]

$$\boldsymbol{\theta} = \begin{bmatrix} \theta_0 \\ \theta_1 \\ \theta_2 \\ \theta_3 \end{bmatrix}, \qquad \bar{\mathbf{G}} = 2\begin{bmatrix} -\theta_1 & \theta_0 & \theta_3 & -\theta_2 \\ -\theta_2 & -\theta_3 & \theta_0 & \theta_1 \\ -\theta_3 & \theta_2 & -\theta_1 & \theta_0 \end{bmatrix} \tag{2.22}$$

$$\mathbf{A} = \begin{bmatrix} 1 - 2(\theta_2)^2 - 2(\theta_3)^2 & 2(\theta_1\theta_2 - \theta_0\theta_3) & 2(\theta_1\theta_3 + \theta_0\theta_2) \\ 2(\theta_1\theta_2 + \theta_0\theta_3) & 1 - 2(\theta_1)^2 - 2(\theta_3)^2 & 2(\theta_2\theta_3 - \theta_0\theta_1) \\ 2(\theta_1\theta_3 - \theta_0\theta_2) & 2(\theta_2\theta_3 - \theta_0\theta_1) & 1 - 2(\theta_1)^2 - 2(\theta_2)^2 \end{bmatrix} \tag{2.23}$$

where the quaternions need to fulfil the constraint

$$\boldsymbol{\theta}^T\boldsymbol{\theta} = 1 \tag{2.24}$$

However, inserting equation (2.21) into (2.20) yields a final expression for the velocity vector

$$\dot{\mathbf{r}}_p = \dot{\mathbf{R}} - \mathbf{A}\tilde{\bar{\mathbf{u}}}\bar{\mathbf{G}}\dot{\boldsymbol{\theta}} + \mathbf{A}\mathbf{S}\dot{\mathbf{q}}_f = \mathbf{L}\dot{\mathbf{q}} \tag{2.25}$$

where $\mathbf{L}$ is a matrix and $\dot{\mathbf{q}}$ a vector defined as

$$\mathbf{L} = \begin{bmatrix} \mathbf{I} & -\mathbf{A}\tilde{\bar{\mathbf{u}}}\bar{\mathbf{G}} & \mathbf{AS} \end{bmatrix} \tag{2.26}$$

$$\mathbf{q} = \begin{bmatrix} \mathbf{R} \\ \boldsymbol{\theta} \\ \mathbf{q}_f \end{bmatrix}, \qquad \dot{\mathbf{q}} = \begin{bmatrix} \dot{\mathbf{R}} \\ \dot{\boldsymbol{\theta}} \\ \dot{\mathbf{q}}_f \end{bmatrix}, \qquad \ddot{\mathbf{q}} = \begin{bmatrix} \ddot{\mathbf{R}} \\ \ddot{\boldsymbol{\theta}} \\ \ddot{\mathbf{q}}_f \end{bmatrix} \tag{2.27}$$

where $\mathbf{q}$ is the generalized coordinate vector, containing all the generalized coordinates $\mathbf{R}[3 \times 1]$, $\boldsymbol{\theta}[4 \times 1]$ and $\mathbf{q}_f[n \times 1]$ associated with rigid body translation and rotation as well as deformation.

2.3 The Acceleration Vector

Differentiating equation (2.25) with respect to time yields the acceleration of an arbitrary point p

$$\ddot{\mathbf{r}}_p = \dot{\mathbf{L}}\dot{\mathbf{q}} + \mathbf{L}\ddot{\mathbf{q}} \tag{2.28}$$

where everything is known except for $\dot{\mathbf{L}}$, which is given by

$$\dot{\mathbf{L}} = \begin{bmatrix} \mathbf{0} & -\dot{\mathbf{A}}\tilde{\bar{\mathbf{u}}}\bar{\mathbf{G}} - \mathbf{A}\dot{\tilde{\bar{\mathbf{u}}}}\bar{\mathbf{G}} - \mathbf{A}\tilde{\bar{\mathbf{u}}}\dot{\bar{\mathbf{G}}} & \dot{\mathbf{A}}\mathbf{S} \end{bmatrix} \tag{2.29}$$

which leads to the definition of the vector $\mathbf{a}_v$. This vector contains all terms associated with the quadratic velocity formulated in Section 3.6.

$$\mathbf{a}_v = \dot{\mathbf{L}}\dot{\mathbf{q}} = \begin{bmatrix} \mathbf{0} & -\dot{\mathbf{A}}\tilde{\bar{\mathbf{u}}}\bar{\mathbf{G}} - \mathbf{A}\dot{\tilde{\bar{\mathbf{u}}}}\bar{\mathbf{G}} - \mathbf{A}\tilde{\bar{\mathbf{u}}}\dot{\bar{\mathbf{G}}} & \dot{\mathbf{A}}\mathbf{S} \end{bmatrix} \begin{bmatrix} \dot{\mathbf{R}} \\ \dot{\boldsymbol{\theta}} \\ \dot{\mathbf{q}}_f \end{bmatrix} \tag{2.30}$$

By carrying out the matrix multiplication and using the following identities [5, p. 48,52]

$$\bar{\boldsymbol{\omega}} = \bar{\mathbf{G}}\dot{\boldsymbol{\theta}}$$

$$\dot{\mathbf{A}} = \mathbf{A}\tilde{\bar{\boldsymbol{\omega}}} \tag{2.31}$$

$$\dot{\tilde{\bar{\mathbf{u}}}}\bar{\boldsymbol{\omega}} = -\tilde{\bar{\boldsymbol{\omega}}}\mathbf{S}\dot{\mathbf{q}}_f \tag{2.32}$$

Where the algebraic rule

$$\tilde{\mathbf{x}}\mathbf{y} = -\tilde{\mathbf{y}}\mathbf{x} \tag{2.33}$$

and that

$$\dot{\bar{\mathbf{u}}} = \mathbf{S}\dot{\mathbf{q}}_f \tag{2.34}$$

has been used. The vector $\mathbf{a}_v$ becomes

$$\mathbf{a}_v = \mathbf{A}(\tilde{\boldsymbol{\omega}})^2 \bar{\mathbf{u}} - \mathbf{A}\tilde{\bar{\mathbf{u}}}\dot{\mathbf{G}}\dot{\boldsymbol{\theta}} + 2\mathbf{A}\tilde{\boldsymbol{\omega}}\mathbf{S}\dot{\mathbf{q}}_f \tag{2.35}$$

and equation (2.28) can be written as

$$\ddot{\mathbf{r}}_p = \mathbf{L}\ddot{\mathbf{q}} + \mathbf{a}_v = \begin{bmatrix} \mathbf{I} & -\mathbf{A}\tilde{\bar{\mathbf{u}}}\bar{\mathbf{G}} & \mathbf{AS} \end{bmatrix} \begin{bmatrix} \ddot{\mathbf{R}} \\ \ddot{\boldsymbol{\theta}} \\ \ddot{\mathbf{q}}_f \end{bmatrix} + \mathbf{A}(\tilde{\boldsymbol{\omega}})^2 \bar{\mathbf{u}} - \mathbf{A}\tilde{\bar{\mathbf{u}}}\dot{\mathbf{G}}\dot{\boldsymbol{\theta}} + 2\mathbf{A}\tilde{\boldsymbol{\omega}}\mathbf{S}\dot{\mathbf{q}}_f \tag{2.36}$$

2.4 The Craig-Bampton Method

As described in Section 2.1 the Floating Frame of Reference formulation factorizes the deformation in to two parts, namely the shape functions and generalized coordinates. The shape functions represents how the deformation is described dependent on the location within the body while the generalized coordinates are dependent on time. Multiplying them together forms the full displacement field of the body. There are various methods on how to select these shape functions and throughout this project the focus has been on the Craig-Bampton method [6].

The Craig-Bampton method is a reduction technique which divides complex deformable structures in to a assemblage of substructures. Each substructure has its own mass and stiffness matrix associated with a set of generalized coordinates. The set involves two forms of generalized coordinates, boundary generalized coordinates and internal generalized coordinates. The boundary generalized coordinates prescribe the displacements and rotation at the boundaries while the internal generalized coordinates are related to the free vibration modes of the substructure, with completely restrained boundaries. Consequently the two sets of generalized coordinates become decoupled at the boundaries of the substructure and coupled internally.

Applying this method to a Euler-Bernoulli beam model in a Floating Frame of Reference formulation, implies that the shape functions matrix in equation (2.18) should consist of two sets of shape functions, static and dynamic shape functions. The static shape functions correspond to the boundary generalized coordinates while the dynamic shape functions correspond to the internal generalized coordinates. The static shape functions are selected according to what essential boundary conditions are applied to the beam while the dynamic shape functions are calculated for a case of free vibration of the beam while the boundaries are fixed.

This method allows the static shape functions to fully describe the deformation at the boundaries while the dynamics within the body is described as a linear combination of the static and dynamic shape functions. The linear combination of the two within the body together with the generalized deformation coordinates makes it possible to provide time dependent solutions such as vibrations and with high accuracy describe the displacements in a efficient manner.

2.5 Static Shape Functions

The static shape functions or mode shapes are determined in a similar manner as used for a beam element Finite Element Method [7, Chapter 17]. The shape functions are approximated as polynomials that should satisfy the constitutive relations described in Section 1.5, additionally they also need to describe the body's degrees of freedom and the arbitrary motion of these independent from each other. These function are normalized i.e. the function can vary between 0 and 1 if nothing else is stated.

Since these functions are expressed in the local coordinate system which in turn is attached to the beams left end as seen in Figure 2.1, the boundary conditions for all degrees of freedom at $x = 0$ are fixed. While for the right end at $x = L$, the boundary conditions are considered free. This implies that there is no need to determine the static shape functions for the left end since only the right end will move relative the local coordinate system.

2.5.1 Longitudinal Deformation

Let $N_x(x)$ be the static shape function for longitudinal deformation.

$$N_x(x) = \alpha_0 + \alpha_1 x \tag{2.37}$$

This function approximates the form of the displacement $u_x(x,t) = N_x(x)q_f(t)$ along the beams centreline and can represent arbitrary strain through equation (1.1).

Applying the boundary conditions for a beam that is fixed at the left end and free at the right end determines the values of α_0 and α_1, the static shape function then becomes [7, p. 99]

$$N_x(x) = \frac{x}{L} \tag{2.38}$$

2.5.2 Torsional Deformation

As seen in equation (1.2) and (1.1), the constitutive relation for torsional deformation and longitudinal deformation have the same form. This implies that the static shape function used for torsional deformation are equal to the one used for longitudinal deformation, seen in equation (2.38).

$$N_{\theta_x} = \frac{x}{L} \tag{2.39}$$

2.5.3 Bending Deformation

FIGURE 2.2: Degrees of freedom for a beam in the $x - y$ plane.

Consider a beam under the influence of bending in a plane. The simplest possible representation of the beam consists of four degrees of freedom, two deflections and two rotations, (see figure 2.2) and therefore requires that the static shape functions are at least polynomials of the 3rd order. Let $N_y(x)$ be the static shape function for bending in the $x - y$ plane.

$$N_y(x) = \alpha_0 + \alpha_1 x + \alpha_2 x + \alpha_3 x^2 + \alpha_4 x^3 \tag{2.40}$$

This approximation of the shape function satisfies the constitutive relations (1.3), (1.4), (1.5) and (1.6) through $u_y(x,t) = N_y(x)q_f(t)$. It can also describe arbitrary deflection and rotation a long the x-axis.

By using

$$u_y(x,t) = N_y(x)q_f(t), \qquad \theta_z(x,t) = \frac{\partial u_y(x,t)}{\partial x} = \frac{dN_y(x)}{dx}q_f(t) \tag{2.41}$$

where u_y is the bending displacement in y-direction and θ_z is the rotation around the z-axis. Then the shape functions can be derived from letting them fully describe the displacement of each degree of freedom at the boundaries. Since the shape functions are expressed in the local coordinate system attached in the left end, only the displacement at the right end needs to be considered.

Described Displacement	$N(x=0)$	$(\frac{dN}{dx})_{x=0}$	$N(x=L)$	$(\frac{dN}{dx})_{x=L}$
u_3	0	0	1	0
u_4	0	0	0	1

TABLE 2.1: Boundary conditions for static shape functions associated with bending in the $x - y$ plane.

The two cases described in table 2.1 can be used to determine the α_n coefficients in equation (2.40) and implies the following two static shape functions [7, p 326]

$$\begin{cases} N_y^1(x) = \frac{x^2}{L^2}(3 - 2\frac{x}{L}) \\ N_y^2(x) = \frac{x^2}{L}(\frac{x}{L} - 1) \end{cases} \tag{2.42}$$

Here N_y^1 represent the deflection while N_y^2 represent the slope at the right end of the beam. These functions are valid when bending occurs in the $x - y$ plane. When bending in the $x - z$ plane is considered the shape function corresponding to the the slope changes sign. This due to the definition of the right-handed coordinate system, see figure 2.3.

FIGURE 2.3: Degrees of freedom for a beam in the $x - z$ plane.

$$u_z(x,t) = N_z(x)q_f(t), \qquad \theta_y(x,t) = -\frac{\partial u_z(x,t)}{\partial x} = -\frac{dN_z(x)}{dx}q_f(t) \tag{2.43}$$

where u_z is the bending displacement in z-direction and θ_y is the rotation around the y-axis. For this case table 2.1 becomes

Described Displacement	$N(x=0)$	$(\frac{dN}{dx})_{x=0}$	$N(x=L)$	$(\frac{dN}{dx})_{x=L}$
u_3	0	0	1	0
u_4	0	0	0	-1

TABLE 2.2: Boundary conditions for static shape functions associated with bending in the $x - z$ plane.

which yields the following static shape functions

$$\begin{cases} N_z^1(x) = \frac{x^2}{L^2}(3 - 2\frac{x}{L}) \\[2mm] N_z^2(x) = \frac{x^2}{L}(1 - \frac{x}{L}) \end{cases} \tag{2.44}$$

Note that

$$N_z^1 = N_y^1 \qquad\qquad N_z^2 = -N_y^2$$

due to the definition of the right-handed coordinate system.

2.6 Dynamic Shape Functions

According to the Craig-Bampton Method the dynamic shape functions should be determined from a beam under the influence of free vibrations while it's being fixed at both ends. The solution can be derived for each degree of freedom from the constitutive relations in Section 1.5 together with D'Alembert's principle. By assuming that displacements are small, each case of vibration can be described independent from each other and derived individually. This procedure is presented in [3, Chapter 5] where the author solves the free vibration problem for each case.

2.6.1 Longitudinal Vibration

By differentiating equation (1.1) with respect to x, the incremental difference in force between two adjacent cross sections becomes

$$dF(x,t) = AE\frac{\partial^2 u_x(x,t)}{\partial x^2}dx \tag{2.45}$$

when considering dynamics the incremental difference in force can be written as

$$dF(x,t) = A\rho\frac{\partial^2 u_x(x,t)}{\partial t^2}dx \tag{2.46}$$

where ρ is the material density. Combining equation (2.45) and (2.46) together with D'Alembert's principle yields the following equation of motion for an infinitesimal element within the bar [3, p. 308-310]

$$\frac{\partial^2 u_x(x,t)}{\partial t^2} = \alpha^2\frac{\partial^2 u_x(x,t)}{\partial x^2} \tag{2.47}$$

where

$$\alpha^2 = \frac{E}{\rho} \tag{2.48}$$

Recall that the displacement can be written as $u_x(x,t) = S_x(x)q_f(t)$, which separates (2.47) into two differential equations.

$$\frac{d^2 S_x(x)}{dx^2} + p^2 S_x(x) = 0 \tag{2.49}$$

$$\frac{d^2 q_f(t)}{dt^2} + \lambda^2 q_f(t) = 0 \tag{2.50}$$

where

$$p^2 = \frac{\lambda^2}{\alpha^2} \tag{2.51}$$

Equation (2.49) is the differential equation for the normal modes and describes the motion of the bar depending on the location along the x-axis while equation (2.50) describes the motion of the bar depending on time. λ is the eigenfrequency of the free vibration, p is the frequency for corresponding normal mode.

The general solution to equation (2.49) is [3, p. 309]

$$S_x^i(x) = C cos(p_i x) + D sin(p_i x) \qquad i = 1, 2, 3... \tag{2.52}$$

which are the longitudinal shape functions or mode shapes of the free vibration problem. The constants C and D depend on the boundary conditions applied at the bar's ends and i denotes the order of the mode shape.

The boundary conditions for a bar fixed at both ends implies that

$$S_x^i(0) = 0, \qquad S_x^i(L) = 0 \tag{2.53}$$

which combined with the additional condition $|S_{x_i}(x)| \leq 1$ yields the following solution to (2.52)

$$S_x^i(x) = sin(p_i x), \qquad p_i = \frac{i\pi}{L}, \qquad i = 1, 2, 3... \tag{2.54}$$

which are the dynamic shape functions used for longitudinal displacement.

The solution to (2.50) can be obtained in an identical approach, but in this beam model that solution is obtained from equation (3.49) according to the Floating Frame of Reference formulation.

2.6.2 Torsional Vibration

The equation of motion for a shaft under the influence of torsional vibration can in the same manner as the longitudinal case be derived from (1.2) in Section 1.5. Together with the incremental difference in moment between two adjacent cross sections the equation of motion becomes [3, p. 325-326]

$$\frac{\partial^2 \theta_x(x,t)}{\partial t^2} = \beta^2 \frac{\partial^2 \theta_x(x,t)}{\partial x^2} \tag{2.55}$$

where

$$\beta^2 = \frac{GK}{J_x} \tag{2.56}$$

G is the shear modulus, K is the torsion stiffness depending on the geometry of the cross section and J_x is the moment of inertia around the x-axis per unit length. In the case of a circular shaft equation (2.56) can be reduced to

$$\beta^2 = \frac{G}{\rho} \tag{2.57}$$

since $K = \frac{\pi r^4}{2}$ [8, p. 333] and $J_x = \frac{\rho \pi r^4}{2}$ where ρ is the density of the beam and r is the radius of the cross section.

Equation (2.55) can, by knowing that $\theta_x(x,t) = S_{\theta_x}(x)q_f(t)$, be written as two separated differential equations as

$$\frac{d^2 S_{\theta_x}(x)}{dx^2} + h^2 S_{\theta_x}(x) = 0 \tag{2.58}$$

$$\frac{d^2 q_f(t)}{dt^2} + \lambda^2 q_f(t) = 0 \tag{2.59}$$

where (2.58) is identical to (2.49) with the exception of

$$h^2 = \frac{\lambda^2}{\beta^2} \tag{2.60}$$

Both equations share the same general solution and by applying the boundary conditions for a shaft fixed at both ends then the solution for the torsional vibration becomes

$$S_{\theta_x}^i(x) = sin(h_i x), \qquad h_i = \frac{i\pi}{L}, \qquad i = 1, 2, 3... \tag{2.61}$$

2.6.3 Bending Vibration

The applied load per unit length of a free beam in bending can be written as [3, p. 331-332]

$$q = -A\rho\frac{\partial^2 u_y(x,t)}{\partial t^2} \tag{2.62}$$

Note that in equation (2.62) q is applied load per unit length. By using D'Alemberts principle and (2.62) inserted into equation (1.5) yields the following equation of motion for a infinitesimal element within the beam

$$EI\frac{\partial^4 u_y(x,t)}{\partial x^4} = -A\rho\frac{\partial^2 u_y(x,t)}{\partial t^2} \tag{2.63}$$

or

$$\frac{\partial^2 u_y(x,t)}{\partial t^2} + \beta^2\frac{\partial^4 u_y(x,t)}{\partial x^4} = 0 \tag{2.64}$$

$$\beta^2 = \frac{EI}{A\rho}$$

With $u_y(x,t) = S_y(x)q_f(t)$ and the assumption of harmonic motion, e.i. $q_f(t) = A sin(\lambda t) + B cos(\lambda t)$ then the differential equation for the normal modes can be derived from (2.64) as

$$\frac{d^4 S_y(x)}{dx^4} = k^4 S_y(x) \tag{2.65}$$

where $k^4 = \frac{\lambda^2}{\beta^2}$. Equation (2.65) has the general solution [3, p. 331-344]

$$S_y^i(x) = C_1 sin(k_i x) + C_2 cos(k_i x) + C_3 sinh(k_i x) + C_4 cosh(k_i x), \qquad i = 1, 2, 3... \tag{2.66}$$

The boundary conditions for a beam with clamped ends are

$$S_y^i(x = 0) = 0, \qquad S_y^i(x = L) = 0 \tag{2.67}$$

$$(\frac{dS_y^i}{dx})_{x=0} = 0, \qquad (\frac{dS_y^i}{dx})_{x=L} = 0 \tag{2.68}$$

Applying them to (2.66) implies that $C_1 = C_3 = 0$ and $S_y^i(x)$ becomes

$$S_y^i(x) = cos(k_i x) - cosh(k_i x) + C(sin(k_i x) - sinh(k_i x)), \qquad i = 1, 2, 3... \tag{2.69}$$

where

$$C = \frac{C_4}{C_2} = \frac{cos(k_i L) - cosh(k_i L)}{sinh(k_i L) - sin(k_i L)} \tag{2.70}$$

and the eigenfreqency k_i of the normal modes can be obtained by solving [3, p. 343-344]

$$cos(k_i L)cosh(k_i L) = 1 \tag{2.71}$$

Equation (2.69) gives the dynamic shape functions used for bending in the $x - y$ plane, these are exactly the same for bending in the $x - z$ plane or in other words

$$S_z^i = S_y^i \tag{2.72}$$

The slope of the beam is related to the bending according to equation 1.6. It follows that the dynamic mode shapes related to rotation around the y- and z-axis's will be.

$$\mathbf{S}_{\theta_y} = -\frac{d\mathbf{S}_z^i}{dx} \tag{2.73}$$

$$\mathbf{S}_{\theta_z} = \frac{d\mathbf{S}_y^i}{dx} \tag{2.74}$$

where the minus sign is due to the definition of the coordinate system.

2.7   The 3D Shape Function Matrix

As expressed in Section 2.1, the shape function matrix is

$$\mathbf{S} = \begin{bmatrix} \mathbf{S}_1 \\ \mathbf{S}_2 \\ \mathbf{S}_3 \end{bmatrix} = \begin{bmatrix} \mathbf{S}_x + z\mathbf{S}_{\theta_y} - y\mathbf{S}_{\theta_z} \\ \mathbf{S}_y - z\mathbf{S}_{\theta_x} \\ \mathbf{S}_z + y\mathbf{S}_{\theta_x} \end{bmatrix} \tag{2.75}$$

Using the static and dynamic shape functions derived in Section 2.5 and 2.6, the shape function vectors in

$$\mathbf{S}_r = \begin{bmatrix} \mathbf{S}_x \\ \mathbf{S}_y \\ \mathbf{S}_z \end{bmatrix}, \qquad \mathbf{S}_\theta = \begin{bmatrix} \mathbf{S}_{\theta_x} \\ \mathbf{S}_{\theta_y} \\ \mathbf{S}_{\theta_z} \end{bmatrix} \tag{2.76}$$

can be assembled individually as

$$\mathbf{S}_x = \begin{bmatrix} N_x & S_x^1 & \dots & S_x^{n_1} & 0^{n_1+2} & \dots & 0^{n_1+n_2+n_3+n_4+6} \end{bmatrix} \tag{2.77}$$

$$\mathbf{S}_y = \begin{bmatrix} 0 & \dots & 0^{n_1+1} & N_y^1 & S_y^1 & \dots & S_y^{n_2} & 0^{n_1+n_2+3} & \dots & 0^{n_1+n_2+n_3+n_4+5} & N_y^2 \end{bmatrix} \tag{2.78}$$

$$\mathbf{S}_z = \begin{bmatrix} 0 & \dots & 0^{n_1+n_2+2} & N_z^1 & S_z^1 & \dots & S_z^{n_3} \\ & & 0^{n_1+n_2+n_3+4} & \dots & 0^{n_1+n_2+n_3+n_4+4} & N_z^2 & 0 \end{bmatrix} \tag{2.79}$$

$$\mathbf{S}_{\theta_x} = \begin{bmatrix} 0 & \ldots & 0^{n_1+n_2+n_3+3} & N_{\theta_x} & S_{\theta_x}^1 & \ldots & S_{\theta_x}^{n_4} & 0 & 0 \end{bmatrix} \quad (2.80)$$

$$\mathbf{S}_{\theta_y} = \begin{bmatrix} 0 & \ldots & 0^{n_1+n_2+2} & -\frac{\mathrm{d}N_z^1}{\mathrm{d}x} & -\frac{\mathrm{d}S_z^1}{\mathrm{d}x} & \ldots & -\frac{\mathrm{d}S_z^{n_3}}{\mathrm{d}x} \\ & 0^{n_1+n_2+n_3+4} & \ldots & 0^{n_1+n_2+n_3+n_4+4} & -\frac{\mathrm{d}N_z^2}{\mathrm{d}x} & 0 \end{bmatrix} \quad (2.81)$$

$$\mathbf{S}_{\theta_z} = \begin{bmatrix} 0 & \ldots & 0^{n_1+1} & \frac{\mathrm{d}N_y^1}{\mathrm{d}x} & \frac{\mathrm{d}S_y^1}{\mathrm{d}x} & \ldots & \frac{\mathrm{d}S_y^{n_2}}{\mathrm{d}x} & 0^{n_1+n_2+3} & \ldots & 0^{n_1+n_2+n_3+n_4+5} & \frac{\mathrm{d}N_y^2}{\mathrm{d}x} \end{bmatrix}$$
$$(2.82)$$

Where n_1, n_2, n_3 and n_4 are the number of dynamic shape functions corresponding to the degrees of freedom u_x, u_y, u_z and u_{θ_x}. The size of all S function vectors is $[1 \times (n_1 + n_2 + n_3 + n_4 + 6)]$ where the addition of 6 is due to the static shape functions. It follows that the generalized deformation coordinates $\mathbf{q}_f$ are structured as follows

$$\mathbf{q}_f = \begin{bmatrix} \mathbf{q}_x \\ \mathbf{q}_y \\ \mathbf{q}_z \\ \mathbf{q}_{\theta_x} \\ q_{\theta_y} \\ q_{\theta_z} \end{bmatrix} \quad (2.83)$$

$$\mathbf{q}_x = \begin{bmatrix} q_x^s \\ q_x^1 \\ \vdots \\ q_x^{n_1} \end{bmatrix} \qquad \mathbf{q}_y = \begin{bmatrix} q_y^s \\ q_y^1 \\ \vdots \\ q_y^{n_2} \end{bmatrix} \qquad \mathbf{q}_z = \begin{bmatrix} q_z^s \\ q_z^1 \\ \vdots \\ q_z^{n_3} \end{bmatrix} \quad (2.84)$$

$$\mathbf{q}_{\theta_x} = \begin{bmatrix} q_{\theta_x}^s \\ q_{\theta_x}^1 \\ \vdots \\ q_{\theta_x}^{n_4} \end{bmatrix} \qquad q_{\theta_y} = q_{\theta_y}^s \qquad q_{\theta_z} = q_{\theta_z}^s \quad (2.85)$$

where the index s denotes that the generalized deformation coordinate corresponds to a static shape function. The size of $\mathbf{q}_x, \mathbf{q}_y, \mathbf{q}_z, \mathbf{q}_{\theta_x}$ will depend on number of dynamic shape functions chosen. $\mathbf{q}_f$ will be of size $[6 \times 1]$ if no dynamic shape functions are used.

Chapter 3

Equations of Motion

In this Chapter a derivation of the equations of motion is presented. The mass matrix, damping matrix, stiffness matrix and forces vectors are derived according to the Floating Frame of Reference and the Euler Bernoulli beam theory.

3.1 Mass Matrix

The kinetic energy for an arbitrary body B is by definition [5, p. 200]

$$T = \frac{1}{2} \int_V \rho \dot{\mathbf{r}}_p^T \dot{\mathbf{r}}_p dV \tag{3.1}$$

where ρ is the density of the body and the velocity vector $\dot{\mathbf{r}}_p$ is defined in equation (2.25), insertion yields

$$T = \frac{1}{2} \dot{\mathbf{q}}^T \int_V \rho \mathbf{L}^T \mathbf{L} dV \dot{\mathbf{q}} \tag{3.2}$$

since the vector of generalized coordinates $\mathbf{q}$ only depends on time. The mass matrix can then be identified as

$$\mathbf{M} = \int_V \rho \mathbf{L}^T \mathbf{L} dV = \int_V \rho \begin{bmatrix} \mathbf{I} \\ -(\mathbf{A}\tilde{\mathbf{u}}\bar{\mathbf{G}})^T \\ (\mathbf{AS})^T \end{bmatrix} \begin{bmatrix} \mathbf{I} & -\mathbf{A}\tilde{\mathbf{u}}\bar{\mathbf{G}} & \mathbf{AS} \end{bmatrix} dV \tag{3.3}$$

where it clearly shows that the mass matrix is symmetric. An explicit expression for the mass matrix can be obtained by carrying out the matrix multiplication, which yields

$$\mathbf{M} = \int_V \rho \begin{bmatrix} \mathbf{I} & -\mathbf{A}\tilde{\bar{\mathbf{u}}}\bar{\mathbf{G}} & \mathbf{A}\mathbf{S} \\ & \bar{\mathbf{G}}^T\tilde{\bar{\mathbf{u}}}^T\tilde{\bar{\mathbf{u}}}\bar{\mathbf{G}} & \bar{\mathbf{G}}^T\tilde{\bar{\mathbf{u}}}\mathbf{S} \\ sym & & \mathbf{S}^T\mathbf{S} \end{bmatrix} dV = \begin{bmatrix} \mathbf{m}_{RR} & \mathbf{m}_{R\theta} & \mathbf{m}_{Rf} \\ & \mathbf{m}_{\theta\theta} & \mathbf{m}_{\theta f} \\ sym & & \mathbf{m}_{ff} \end{bmatrix} \qquad (3.4)$$

where the indices R, θ and f denotes translation, rotation and deformation respectively. The $\mathbf{m}_{RR}$, $\mathbf{m}_{\theta\theta}$ and $\mathbf{m}_{ff}$ represents the mass matrices related to rigid body translation and rotation as well as deformation, the other submatrices couples translation, rotation and deformation. While $\mathbf{m}_{RR}$ and $\mathbf{m}_{ff}$ are constant, the other submatrices depend on the rotational coordinates $\boldsymbol{\theta}$ as well as the elastic coordinates $\mathbf{q}_f$ and are therefore dependent on time.

The dependency on the generalized coordinates increases the complexity of the formulation and requires that the submatrices are derived in efficient manner. The rest of this section is devoted to explaining the derivation of the submatrices.

The most simple matrix is $\mathbf{m}_{RR}$, it can be determined as

$$\mathbf{m}_{RR} = \int_V \rho \mathbf{I} dV = \begin{bmatrix} m & 0 & 0 \\ 0 & m & 0 \\ 0 & 0 & m \end{bmatrix} \qquad (3.5)$$

where it clearly shows that this matrix is constant due to conservation of mass and it's associated with the rigid body motion.

The submatrix $\mathbf{m}_{R\theta}$ can be written as

$$\mathbf{m}_{R\theta} = -\int_V \rho \mathbf{A}\tilde{\bar{\mathbf{u}}}\bar{\mathbf{G}} dV = -\mathbf{A}\tilde{\bar{\mathbf{S}}}_t\bar{\mathbf{G}} \qquad (3.6)$$

in which the skew symmetric matrix $\tilde{\bar{\mathbf{S}}}_t$ is defined as

$$\tilde{\bar{\mathbf{S}}}_t = \int_V \rho \tilde{\bar{\mathbf{u}}} dV = \begin{bmatrix} 0 & -\bar{S}_{t_3} & \bar{S}_{t_2} \\ \bar{S}_{t_3} & 0 & -\bar{S}_{t_1} \\ -\bar{S}_{t_2} & \bar{S}_{t_1} & 0 \end{bmatrix} \qquad (3.7)$$

and its components can be calculated from the integrals in vector form

$$\bar{\mathbf{S}}_t = \int_V \rho \bar{\mathbf{u}} dV = \int_V \rho(\bar{\mathbf{u}}_0 + \bar{\mathbf{u}}_f) dV = \int_V \rho(\bar{\mathbf{u}}_0 + \mathbf{S}\mathbf{q}_f) dV \qquad (3.8)$$

It is favourable to calculate $\bar{\mathbf{S}}_t$ with $\mathbf{q}_f$ outside of the integral and define the two terms as

$$\bar{\mathbf{S}}_t = \bar{\mathbf{I}}_0 + \bar{\mathbf{S}}\mathbf{q}_f \tag{3.9}$$

where

$$\bar{\mathbf{I}}_0 = \int_V \rho \bar{\mathbf{u}}_0 dV \tag{3.10}$$

$$\bar{\mathbf{S}} = \int_V \rho \mathbf{S} dV \tag{3.11}$$

The matrix in equation (3.11) is also needed for the calculation of submatrix $\mathbf{m}_{Rf}$ since

$$\mathbf{m}_{Rf} = \mathbf{A} \int_V \rho \mathbf{S} dV = \mathbf{A}\bar{\mathbf{S}} \tag{3.12}$$

The next submatrix is $\mathbf{m}_{\theta\theta}$, which is somewhat more complex in its derivation and requires the calculation of several volume integrals. The matrix is declared in equation (3.4) as

$$\mathbf{m}_{\theta\theta} = \int_V \rho \bar{\mathbf{G}}^T \tilde{\mathbf{u}}^T \tilde{\mathbf{u}} \bar{\mathbf{G}} dV = \bar{\mathbf{G}}^T \bar{\mathbf{I}}_{\theta\theta} \bar{\mathbf{G}} \tag{3.13}$$

where $\bar{\mathbf{I}}_{\theta\theta}$ is the inertia tensor defined as

$$\bar{\mathbf{I}}_{\theta\theta} = \int_V \rho \tilde{\mathbf{u}}^T \tilde{\mathbf{u}} dV = \int_V \rho \begin{bmatrix} (\bar{u}_2)^2 + (\bar{u}_3)^2 & -\bar{u}_2\bar{u}_1 & -\bar{u}_3\bar{u}_1 \\ & (\bar{u}_1)^2 + (\bar{u}_3)^2 & -\bar{u}_3\bar{u}_2 \\ sym & & (\bar{u}_1)^2 + (\bar{u}_2)^2 \end{bmatrix} dV \tag{3.14}$$

The components in the inertia tensor can be derived as

$$\int_V \rho((\bar{u}_k)^2 + (\bar{u}_l)^2) dV = I_{kk} + 2\mathbf{I}_{kk}^{\star}\mathbf{q}_f + \mathbf{q}_f^T\bar{\mathbf{S}}_{kk}\mathbf{q}_f + I_{ll} + 2\mathbf{I}_{ll}^{\star}\mathbf{q}_f + \mathbf{q}_f^T\bar{\mathbf{S}}_{ll}\mathbf{q}_f$$

$$\int_V \rho\bar{u}_k\bar{u}_l dV = I_{kl} + \mathbf{I}_{kl}^{\star}\mathbf{q}_f + \mathbf{I}_{lk}^{\star}\mathbf{q}_f + \mathbf{q}_f^T\bar{\mathbf{S}}_{kl}\mathbf{q}_f, \qquad k, l = 1, 2, 3 \tag{3.15}$$

where the inertia shape integrals I_{kl}, $\mathbf{I}_{kl}^{\star}$ and $\bar{\mathbf{S}}_{kl}$ are defined as

$$I_{kl} = \int_V \rho x_k x_l dV \tag{3.16}$$

$$\mathbf{I}_{kl}^{\star} = \int_V \rho x_k \mathbf{S}_l dV \tag{3.17}$$

$$\bar{\mathbf{S}}_{kl} = \int_V \rho \mathbf{S}_k^T \mathbf{S}_l dV \tag{3.18}$$

$$k, l = 1, 2, 3$$

Here $\mathbf{S}_k$ is the kth row of the shape function matrix and x_1, x_2 and x_3 are the components of the initial position vector $\mathbf{u}_0$,

$$\mathbf{u}_0 = \begin{bmatrix} x \\ y \\ z \end{bmatrix} = \begin{bmatrix} x_1 \\ x_2 \\ x_3 \end{bmatrix} \tag{3.19}$$

Note that the integrals in equation (3.16), (3.17) and (3.18) are of different sizes. Calculating the integrals for all combinations of k and l yields a [3 x 3] matrix from equation (3.16), nine vectors of length $[1 \times n]$ from (3.17) and nine matrices with the size $[n \times n]$ from equation (3.18), where n is the total number of shape function used.

Some of these integrals are also needed to calculate the submatrix $\mathbf{m}_{\theta f}$, the matrix is defined in equation (3.4) as

$$\mathbf{m}_{\theta f} = \bar{\mathbf{G}}^T \int_V \rho \tilde{\mathbf{u}} \mathbf{S} dV = \bar{\mathbf{G}}^T \bar{\mathbf{I}}_{\theta f} \tag{3.20}$$

where $\bar{\mathbf{I}}_{\theta f}$ can be calculated as

$$\bar{\mathbf{I}}_{\theta f} = \int_V \rho \tilde{\mathbf{u}} \mathbf{S} dV = \int_V \rho \begin{bmatrix} \bar{u}_2 \mathbf{S}_3 - \bar{u}_3 \mathbf{S}_2 \\ \bar{u}_3 \mathbf{S}_1 - \bar{u}_1 \mathbf{S}_3 \\ \bar{u}_1 \mathbf{S}_2 - \bar{u}_2 \mathbf{S}_1 \end{bmatrix} dV \tag{3.21}$$

Using equation (2.2) makes it possible to divide the above equation into two terms

$$\bar{\mathbf{I}}_{\theta f} = \int_V \rho \begin{bmatrix} \mathbf{q}_f^T(\mathbf{S}_2^T \mathbf{S}_3 - \mathbf{S}_3^T \mathbf{S}_2) \\ \mathbf{q}_f^T(\mathbf{S}_3^T \mathbf{S}_1 - \mathbf{S}_1^T \mathbf{S}_3) \\ \mathbf{q}_f^T(\mathbf{S}_1^T \mathbf{S}_2 - \mathbf{S}_2^T \mathbf{S}_1) \end{bmatrix} dV + \int_V \rho \begin{bmatrix} x_2 \mathbf{S}_3 - x_3 \mathbf{S}_2 \\ x_3 \mathbf{S}_1 - x_1 \mathbf{S}_3 \\ x_1 \mathbf{S}_2 - x_2 \mathbf{S}_1 \end{bmatrix} dV \tag{3.22}$$

carrying on using equation (3.17) and (3.18) yields

$$\bar{\mathbf{I}}_{\theta f} = \begin{bmatrix} \mathbf{q}_f^T(\bar{\mathbf{S}}_{23} - \bar{\mathbf{S}}_{32}) \\ \mathbf{q}_f^T(\bar{\mathbf{S}}_{31} - \bar{\mathbf{S}}_{13}) \\ \mathbf{q}_f^T(\bar{\mathbf{S}}_{12} - \bar{\mathbf{S}}_{21}) \end{bmatrix} + \begin{bmatrix} \mathbf{I}_{23}^\star - \mathbf{I}_{32}^\star \\ \mathbf{I}_{31}^\star - \mathbf{I}_{13}^\star \\ \mathbf{I}_{12}^\star - \mathbf{I}_{21}^\star \end{bmatrix} \tag{3.23}$$

which is the final expression for $\bar{\mathbf{I}}_{\theta f}$. Finally the last submatrix $\mathbf{m}_{ff}$ can be written, using equation (3.18), as

$$\mathbf{m}_{ff} = \int_V \rho \mathbf{S}^T \mathbf{S} dV = \bar{\mathbf{S}}_{11} + \bar{\mathbf{S}}_{22} + \bar{\mathbf{S}}_{33} \tag{3.24}$$

and the derivation of the mass matrix is complete.

3.2 Stiffness Matrix

The stiffness matrix can be derived from the definition of strain energy, the strain energy per unit volume in index notation is defined as [9, p. 68]

$$U_0 = \int\limits_0^{\epsilon_{ij}} \boldsymbol{\sigma}_{ij} d\epsilon_{ij}^\star \tag{3.25}$$

Where $\boldsymbol{\epsilon}_{ij}$ and $\boldsymbol{\sigma}_{ij}$ denotes the current strains and stresses in the body. The other variables $\boldsymbol{\epsilon}_{ij}^\star$, denotes the integration variables, the indices i and j denotes the direction of the stresses and strains. Due to the assumptions made, associated with the Euler-Bernoulli beam theory in Section 1.5.3, most of the terms in equation (3.25) becomes zero and the equation undertakes a more explicit form

$$U_0 = \int\limits_0^{\epsilon_{xx}} \sigma_{xx} d\epsilon_{xx}^\star + 2 \int\limits_0^{\epsilon_{x\theta}} \sigma_{x\theta} d\epsilon_{x\theta}^\star \tag{3.26}$$

Where the first term is related with deformation due to axial and bending loads, the second term is due to torsional deformation. Using the constitutive relation for a linear elastic material and carrying out the calculation of the integrals yields [10, p. 93]

$$U_0 = \int\limits_0^{\epsilon_{xx}} E\epsilon_{xx} d\epsilon_{xx}^\star + 4 \int\limits_0^{\epsilon_{x\theta}} G\epsilon_{x\theta} d\epsilon_{x\theta}^\star = \frac{E}{2}\epsilon_{xx}^2 + 2G\epsilon_{x\theta}^2 \tag{3.27}$$

The two expressions for the displacements can be written as

$$u_{f1} = u_x - y\frac{du_y}{dx} - z\frac{du_z}{dx} \tag{3.28}$$

$$u_{\theta_x} = r\theta_x (= \sqrt{y^2 + z^2}\theta_x) \tag{3.29}$$

which implies that the strains are

$$\epsilon_{xx} = \frac{\partial u_{f1}}{\partial x} = \frac{du_x}{dx} - y\frac{d^2 u_y}{dx^2} - z\frac{d^2 u_z}{dx^2} \tag{3.30}$$

$$\epsilon_{x\theta} = \frac{1}{2}\frac{\partial u_{\theta_x}}{\partial x} = \frac{1}{2}r\frac{d\theta_x}{dx} \tag{3.31}$$

Insertion of equation (3.30) and (3.31) into (3.27) yields

$$U_0 = \frac{1}{2}E\left(\frac{du_x}{dx} - y\frac{d^2 u_y}{dx^2} - z\frac{d^2 u_z}{dx^2}\right)^2 + \frac{1}{2}G\left(r\frac{d\theta_x}{dx}\right)^2 \tag{3.32}$$

and the strain energy becomes

$$U = \int_V U_0 dV = \frac{1}{2} \int_V E(\frac{du_x}{dx} - y\frac{d^2u_y}{dx^2} - z\frac{d^2u_z}{dx^2})^2 dV + \frac{1}{2} \int_0^L G(r\frac{d\theta_x}{dx})^2 dV \quad (3.33)$$

Here the volume integrals can be reduced to integrals over the length L of the beam, it can be shown that all the terms except for the quadratic ones becomes zero in the first integral due to symmetry around the beam centreline. The second integral which is associated with torsion can in the easiest way be calculated for a circular cross-section, the strain energy then becomes

$$U = \frac{1}{2} \int_0^L EA(\frac{du_x}{dx})^2 + EI_z(\frac{d^2u_y}{dx^2})^2 + EI_y(\frac{d^2u_z}{dx^2})^2 + GK(\frac{d\theta_x}{dx})^2 dx \quad (3.34)$$

Where it has been used that

$$I_y = \int_A z^2 dA, \qquad I_z = \int_A y^2 dA, \qquad K = \int_A r^2 dA \quad (3.35)$$

Note that even though the assumption concerning a circular cross-section, it can be shown through St. Venants torsion theory and the relation between moment and angular displacement, that the strain energy becomes the same for any cross-section. The only difference will then be the geometry dependent torsion stiffness factor K [11, Chapter 5].

Recall the individual shape function vectors defined in equation (2.77), (2.78), (2.79) and (2.80). Inserting them into (3.34) yields

$$U = \frac{1}{2}\mathbf{q}_f^T \int_0^L EA\frac{d\mathbf{S}_x^T}{dx}\frac{d\mathbf{S}_x}{dx} + EI_z\frac{d^2\mathbf{S}_y^T}{dx^2}\frac{d^2\mathbf{S}_y}{dx^2} + EI_y\frac{d^2\mathbf{S}_z^T}{dx^2}\frac{d^2\mathbf{S}_z}{dx^2} + GK\frac{d\mathbf{S}_{\theta_x}^T}{dx}\frac{d\mathbf{S}_{\theta_x}}{dx}dx\mathbf{q}_f \quad (3.36)$$

Then the stiffness matrix associated with the generalized deformation coordinates in equation (3.36) can be identified as

$$\mathbf{K}_{ff} = \int_0^L EA\frac{d\mathbf{S}_x^T}{dx}\frac{d\mathbf{S}_x}{dx} + EI_y\frac{d^2\mathbf{S}_y^T}{dx^2}\frac{d^2\mathbf{S}_y}{dx^2} + EI_z\frac{d^2\mathbf{S}_z^T}{dx^2}\frac{d^2\mathbf{S}_z}{dx^2} + GK\frac{d\mathbf{S}_{\theta_x}^T}{dx}\frac{d\mathbf{S}_{\theta_x}}{dx}dx \quad (3.37)$$

Hence the stiffness matrix for the whole body becomes

$$\mathbf{K} = \begin{bmatrix} 0 & \cdots & 0 \\ \vdots & \ddots & \vdots \\ 0 & \cdots & \mathbf{K}_{ff} \end{bmatrix} \quad (3.38)$$

which has the size $[(7 + n) \times (7 + n)]$ where n is the total number of shape functions used.

3.3 Equations of Motion

The mass matrix and stiffness matrix have been derived and these will be used in the equations of motion. The equations of motion can be derived from Lagrange's equations [5, p. 223-224] but in this section it will be derived from the expression of virtual work since it was found to be more convenient. The virtual work of all forces δW_F acting on an arbitrary body B can be written as

$$\delta W_F = \delta W_s + \delta W_e + \delta W_g \tag{3.39}$$

Where δW_s is the virtual work of the elastic forces resulting from the deformation of the body, δW_e is the virtually work of externally applied forces, δW_g is the virtually work due to gravitation and $\delta \mathbf{q}$ is the virtual change in generalized coordinates. These can be written as [5, p. 214,216]

$$\delta W_s = -\delta \mathbf{q}^T \mathbf{K}^T \mathbf{q} \tag{3.40}$$

$$\delta W_e = \delta \mathbf{q}^T \mathbf{Q}_e \tag{3.41}$$

$$\delta W_g = \delta \mathbf{q}^T \mathbf{Q}_g \tag{3.42}$$

Where $\mathbf{K}$ is the stiffness matrix expressed in equation (3.38), $\mathbf{Q}_e$ are the generalized external forces and $\mathbf{Q}_g$ are the generalized forces caused by gravitation.

The virtual work of inertia forces are defined in [5, p. 226] as

$$\delta W_I = \int_V \rho \delta \mathbf{r}_p^T \ddot{\mathbf{r}}_p dV \tag{3.43}$$

Where $\delta \mathbf{r}_p$ is the virtual change in position of point p governing from both rigid body motion and deformation, defined as

$$\delta \mathbf{r}_p = \delta \mathbf{R} - \mathbf{A}\tilde{\bar{\mathbf{u}}}\bar{\mathbf{G}}\delta \boldsymbol{\theta} + \mathbf{A}\mathbf{S}\delta \mathbf{q}_f \tag{3.44}$$

Inserting equation (3.44) and (2.36) into (3.43) and simplifying the expression yields

$$\delta W_I = \delta \mathbf{q}^T \left(\int_V \rho \mathbf{L}^T \mathbf{L} dV \, \ddot{\mathbf{q}} + \int_V \rho \mathbf{L}^T \mathbf{a}_v dV \right) \tag{3.45}$$

where $\mathbf{a}_v$ is defined in equation (2.35). This equation can be written in a more convenient form by using equation (3.3) and introducing the quadratic velocity vector $\mathbf{Q}_v$

$$\delta W_I = \delta \mathbf{q}^T (\mathbf{M}\ddot{\mathbf{q}} - \mathbf{Q}_v) \tag{3.46}$$

$$\mathbf{Q}_v = -\int_V \rho \mathbf{L}^T \mathbf{a}_v dV \tag{3.47}$$

The virtual work of all forces acting on the body must be equal to the virtual work of inertia forces, putting $\delta W_F = \delta W_I$ yields

$$\delta \mathbf{q}^T (-\mathbf{K}^T \mathbf{q} + \mathbf{Q}_e + \mathbf{Q}_g) = \delta \mathbf{q}^T (\mathbf{M}\ddot{\mathbf{q}} - \mathbf{Q}_v) \tag{3.48}$$

Which can be rewritten in to the equations of motion

$$\mathbf{M}\ddot{\mathbf{q}} + \mathbf{C}\dot{\mathbf{q}} + \mathbf{K}\mathbf{q} = \mathbf{Q}_e + \mathbf{Q}_g + \mathbf{Q}_v \tag{3.49}$$

where damping has been added to the system through the damping matrix $\mathbf{C}$. This matrix can be defined in different ways, in this beam model Rayleigh damping is used, which defines the damping matrix as [12, p. 145]

$$\mathbf{C} = \begin{bmatrix} 0 & \cdots & 0 \\ \vdots & \ddots & \vdots \\ 0 & \cdots & \mathbf{C}_{ff} \end{bmatrix} \tag{3.50}$$

where

$$\mathbf{C}_{ff} = \eta \mathbf{m}_{ff} + \delta \mathbf{K}_{ff} \tag{3.51}$$

η and δ are parameters depending on the eigenfrequencies of the system and the critical damping at these eigenfrequencies. $\mathbf{K}_{ff}$ is defined in equation (3.37) and $\mathbf{m}_{ff}$ is defined in equation (3.24).

Note that in [5, p. 224] the equations of motion also contains a vector for kinematic constraints imposed on the body. In this project that method is not used since Dymola imposes the kinematic constraint functions through connectors, which is further explained in Chapter 5.

3.4   Generalized External Forces

The external forces acting on a body can be derived from the external virtual work written as

$$\delta W_e = \mathbf{Q}_e^T \delta \mathbf{q} = \begin{bmatrix} (\mathbf{Q}_e)_R^T & (\mathbf{Q}_e)_\theta^T & (\mathbf{Q}_e)_f^T \end{bmatrix} \begin{bmatrix} \delta \mathbf{R} \\ \delta \boldsymbol{\theta} \\ \delta \mathbf{q}_f \end{bmatrix} \tag{3.52}$$

Where $(\mathbf{Q}_e)_R$, $(\mathbf{Q}_e)_\theta$ and $(\mathbf{Q}_e)_f$ are the generalized external forces associated with the translational, rotational and generalized deformation coordinates of the body. These forces depends on the applied external loads on the body and the position they are applied at.

Consider the body being under the influence of a force and moment applied at point p, the external virtual work due to these load would be

$$\delta W_e = \mathbf{F}^T \delta \mathbf{r}_p + \mathbf{M}^T \delta \boldsymbol{\theta}_p \tag{3.53}$$

Where $\delta \boldsymbol{\theta}_p$ is the virtual change in rotations, defined as

$$\delta \boldsymbol{\theta}_p = \mathbf{A} \bar{\mathbf{G}} \delta \boldsymbol{\theta} + \mathbf{A} \mathbf{S}_\theta \mathbf{q}_f \tag{3.54}$$

where $\delta \boldsymbol{\theta}$ is the virtual change of the rotational coordinates defined in equation (2.22). Inserting equation (3.44) and (3.54) into (3.53) and simplifying the expression yields

$$\delta W_e = \mathbf{F}^T \delta \mathbf{R} + (\mathbf{M}^T \mathbf{A} \bar{\mathbf{G}} - \mathbf{F}^T \mathbf{A} \tilde{\bar{\mathbf{u}}} \bar{\mathbf{G}}) \delta \boldsymbol{\theta} + (\mathbf{F}^T \mathbf{A} \mathbf{S} + \mathbf{M}^T \mathbf{A} \mathbf{S}_\theta) \delta \mathbf{q}_f \tag{3.55}$$

or in vector formulation

$$\delta W_e = \begin{bmatrix} \mathbf{F}^T & (\mathbf{M}^T \mathbf{A} \bar{\mathbf{G}} - \mathbf{F}^T \mathbf{A} \tilde{\bar{\mathbf{u}}} \bar{\mathbf{G}}) & (\mathbf{F}^T \mathbf{A} \mathbf{S} + \mathbf{M}^T \mathbf{A} \mathbf{S}_\theta) \end{bmatrix} \begin{bmatrix} \delta \mathbf{R} \\ \delta \boldsymbol{\theta} \\ \delta \mathbf{q}_f \end{bmatrix} \tag{3.56}$$

where the generalized external forces in (3.52) can be identified as

$$(\mathbf{Q}_e)_R \Big|_p = \mathbf{F} \tag{3.57}$$

$$(\mathbf{Q}_e)_\theta \Big|_p = \bar{\mathbf{G}}^T \mathbf{A}^T \mathbf{M} + \bar{\mathbf{G}}^T \tilde{\bar{\mathbf{u}}} \mathbf{A}^T \mathbf{F} \tag{3.58}$$

$$(\mathbf{Q}_e)_f \Big|_p = \mathbf{S}^T \mathbf{A}^T \mathbf{F} + \mathbf{S}_\theta^T \mathbf{A}^T \mathbf{M} \tag{3.59}$$

Note that these components should be evaluated at the location of point p in order to obtain a correct expression for the external work.

3.5 Generalized Gravitational Forces

The derivation of the generalized gravitational forces is almost identical to the derivation of the generalized external forces, with the exception of gravitation acting as a body force at each point in the body. The virtual work caused by gravitation can be calculated through

$$\delta W_g = \mathbf{Q}_g^T \delta \mathbf{q} = \begin{bmatrix} (\mathbf{Q}_g)_R^T & (\mathbf{Q}_g)_\theta^T & (\mathbf{Q}_g)_f^T \end{bmatrix} \begin{bmatrix} \delta \mathbf{R} \\ \delta \boldsymbol{\theta} \\ \delta \mathbf{q}_f \end{bmatrix} = \int_V \rho \mathbf{g}^T \delta \mathbf{r}_p dV \tag{3.60}$$

where

$$\mathbf{g} = \begin{bmatrix} 0 \\ 0 \\ -g \end{bmatrix} \tag{3.61}$$

is expressed in the global coordinate system, $\delta \mathbf{r}_p$ is defined in equation (3.44) and g is the gravitational constant. Insertion of equation (3.44) into (3.60) yields

$$\delta W_g = \int_V \rho \mathbf{g}^T (\delta \mathbf{R} - \mathbf{A} \tilde{\mathbf{u}} \bar{\mathbf{G}} \delta \boldsymbol{\theta} + \mathbf{A} \mathbf{S} \delta \mathbf{q}_f) dV \tag{3.62}$$

which can be written in vector form as

$$\delta W_g = \begin{bmatrix} \int_V \rho \mathbf{g}^T dV & \int_V \rho \mathbf{g}^T \mathbf{A} \tilde{\mathbf{u}}^T \bar{\mathbf{G}} dV & \int_V \rho \mathbf{g}^T \mathbf{A} \mathbf{S} dV \end{bmatrix} \begin{bmatrix} \delta \mathbf{R} \\ \delta \boldsymbol{\theta} \\ \delta \mathbf{q}_f \end{bmatrix} \tag{3.63}$$

which in comparison with equation (3.52) can be used to identify the components of the generalized gravitational force vector $\mathbf{Q}_g$ as

$$(\mathbf{Q}_g)_R = m\mathbf{g} \tag{3.64}$$

$$(\mathbf{Q}_g)_\theta = -\bar{\mathbf{G}}^T \int_V \rho \tilde{\mathbf{u}} dV \mathbf{A}^T \mathbf{g} = \bar{\mathbf{G}}^T \tilde{\bar{\mathbf{S}}}_t \mathbf{A}^T \mathbf{g} \tag{3.65}$$

$$(\mathbf{Q}_g)_f = \int_V \rho \mathbf{S}^T dV \mathbf{A}^T \mathbf{g} = \bar{\mathbf{S}}^T \mathbf{A}^T \mathbf{g} \tag{3.66}$$

where equations (3.7) and (3.8) have been used.

3.6 Quadratic Velocity Vector

As with the generalized external forces, the quadratic velocity vector can be divided by their corresponding generalized coordinates, namely

$$\mathbf{Q}_v = \begin{bmatrix} (\mathbf{Q}_v)_R \\ (\mathbf{Q}_v)_\theta \\ (\mathbf{Q}_v)_f \end{bmatrix} \tag{3.67}$$

The quadratic velocity vector arises due to the coupling between rigid body motion (rotation, translation) and deformation, it includes the effect of Coriolis and centrifugal forces and is a nonlinear function of the generalized coordinates and velocities. It's components can be derived from equation (3.47) which states that

$$\mathbf{Q}_v = -\int_V \rho \mathbf{L}^T \mathbf{a}_v dV = -\int_V \rho \begin{bmatrix} \mathbf{I} \\ -\bar{\mathbf{G}}^T \tilde{\bar{\mathbf{u}}}^T \mathbf{A}^T \\ \mathbf{S}^T \mathbf{A}^T \end{bmatrix} (\mathbf{A}(\tilde{\bar{\boldsymbol{\omega}}})^2 \bar{\mathbf{u}} - \mathbf{A}\tilde{\bar{\mathbf{u}}}\bar{\mathbf{G}}\dot{\boldsymbol{\theta}} + 2\mathbf{A}\tilde{\bar{\boldsymbol{\omega}}}\mathbf{S}\dot{\mathbf{q}}_f)dV \tag{3.68}$$

The component $(\mathbf{Q}_v)_R$ can be identified as the first matrix multiplication in equation (3.68).

$$(\mathbf{Q}_v)_R = -\mathbf{A}[(\tilde{\bar{\boldsymbol{\omega}}})^2 \int_V \rho \bar{\mathbf{u}} dV - \int_V \rho \tilde{\bar{\mathbf{u}}} dV \bar{\mathbf{G}}\dot{\boldsymbol{\theta}} + 2\tilde{\bar{\boldsymbol{\omega}}} \int_V \rho \mathbf{S} dV \dot{\mathbf{q}}_f] \tag{3.69}$$

Inserting equation (3.8), (3.7) and (3.11) into (3.69) yields

$$(\mathbf{Q}_v)_R = -\mathbf{A}[(\tilde{\bar{\boldsymbol{\omega}}})^2 \bar{\mathbf{S}}_t - \tilde{\bar{\mathbf{S}}}_t \bar{\mathbf{G}}\dot{\boldsymbol{\theta}} + 2\tilde{\bar{\boldsymbol{\omega}}}\bar{\mathbf{S}}\dot{\mathbf{q}}_f] \tag{3.70}$$

Carrying on with the second matrix multiplication in equation (3.68) to get $(\mathbf{Q}_v)_\theta$

$$(\mathbf{Q}_v)_\theta = \bar{\mathbf{G}}^T \int_V \rho \tilde{\bar{\mathbf{u}}}^T (\tilde{\bar{\boldsymbol{\omega}}})^2 \bar{\mathbf{u}} dV - \bar{\mathbf{G}}^T \int_V \rho \tilde{\bar{\mathbf{u}}}^T \tilde{\bar{\mathbf{u}}} dV \bar{\mathbf{G}}\dot{\boldsymbol{\theta}} + 2\bar{\mathbf{G}}^T \int_V \rho \tilde{\bar{\mathbf{u}}}^T \tilde{\bar{\boldsymbol{\omega}}}\dot{\mathbf{u}} dV \tag{3.71}$$

where the orthogonality of the transformation matrix has been used ($\mathbf{A}\mathbf{A}^T = \mathbf{I}$) and that $\dot{\bar{\mathbf{u}}} = \mathbf{S}\dot{\mathbf{q}}_f$. Equation (3.71) can be rewritten into

$$(\mathbf{Q}_v)_\theta = -\bar{\mathbf{G}}^T \tilde{\bar{\boldsymbol{\omega}}} \int_V \rho \tilde{\bar{\mathbf{u}}}^T \tilde{\bar{\mathbf{u}}} dV \bar{\boldsymbol{\omega}} - \bar{\mathbf{G}}^T \int_V \rho \tilde{\bar{\mathbf{u}}}^T \tilde{\bar{\mathbf{u}}} dV \bar{\mathbf{G}}\dot{\boldsymbol{\theta}} - 2\bar{\mathbf{G}}^T \int_V \rho \tilde{\bar{\mathbf{u}}}^T \dot{\tilde{\bar{\mathbf{u}}}} dV \bar{\boldsymbol{\omega}} \tag{3.72}$$

by using the following operations

$$\tilde{\mathbf{x}}^T \tilde{\mathbf{y}}\tilde{\mathbf{x}}\mathbf{y} = \tilde{\mathbf{y}}\tilde{\mathbf{x}}^T \tilde{\mathbf{x}}\mathbf{y} \tag{3.73}$$

$$\tilde{\mathbf{x}}\mathbf{y} = -\tilde{\mathbf{y}}\mathbf{x} \tag{3.74}$$

which holds for any vectors $\mathbf{x}$ and $\mathbf{y}$ [13]. Insertion of equation (3.14) and making use of the chain rule

$$\dot{\bar{\mathbf{I}}}_{\theta\theta} = \frac{d\bar{\mathbf{I}}_{\theta\theta}}{d\tilde{\mathbf{u}}} \frac{\dot{\tilde{\mathbf{u}}}}{dt} = 2 \int_V \rho \tilde{\mathbf{u}}^T \dot{\tilde{\mathbf{u}}} dV \tag{3.75}$$

then equation (3.72) becomes

$$(\mathbf{Q}_v)_\theta = -\bar{\mathbf{G}}^T \tilde{\bar{\boldsymbol{\omega}}} \bar{\mathbf{I}}_{\theta\theta} \bar{\boldsymbol{\omega}} - \bar{\mathbf{G}}^T \bar{\mathbf{I}}_{\theta\theta} \dot{\bar{\mathbf{G}}} \dot{\boldsymbol{\theta}} - \bar{\mathbf{G}}^T \dot{\bar{\mathbf{I}}}_{\theta\theta} \bar{\boldsymbol{\omega}} \tag{3.76}$$

The last component of the quadratic velocity vector is obtain from the last matrix multiplication in equation (3.68), which can be simplified into

$$(\mathbf{Q}_v)_f = \int_V \rho \mathbf{S}^T \tilde{\bar{\boldsymbol{\omega}}} \tilde{\mathbf{u}} dV \bar{\boldsymbol{\omega}} + \int_V \rho \mathbf{S}^T \tilde{\mathbf{u}} dV \dot{\mathbf{G}} \dot{\boldsymbol{\omega}} + 2 \int_V \rho \mathbf{S}^T \dot{\tilde{\mathbf{u}}} dV \bar{\boldsymbol{\omega}} \tag{3.77}$$

or by using equation (3.20), in a more explicit form

$$(\mathbf{Q}_v)_f = \bar{\mathbf{I}}_{Qv} \bar{\boldsymbol{\omega}} - \bar{\mathbf{I}}_{\theta f}^T \dot{\mathbf{G}} \dot{\boldsymbol{\theta}} - 2\dot{\bar{\mathbf{I}}}_{\theta f}^T \bar{\boldsymbol{\omega}} \tag{3.78}$$

where

$$\bar{\mathbf{I}}_{Qv} = \int_V \rho \mathbf{S}^T \tilde{\bar{\boldsymbol{\omega}}} \tilde{\mathbf{u}} dV =$$

$$\begin{bmatrix} \bar{\omega}_1(\mathbf{I}_{22}^* + \mathbf{I}_{33}^*) - \bar{\omega}_2 \mathbf{I}_{21}^* - \bar{\omega}_3 \mathbf{I}_{31}^* \\ -\bar{\omega}_1 \mathbf{I}_{12}^* + \bar{\omega}_2(\mathbf{I}_{11}^* + \mathbf{I}_{33}^*) - \bar{\omega}_3 \mathbf{I}_{32}^* \\ -\bar{\omega}_1 \mathbf{I}_{13}^* - \bar{\omega}_2 \mathbf{I}_{23}^* + \bar{\omega}_3(\mathbf{I}_{11}^* + \mathbf{I}_{22}^*) \end{bmatrix}^T + \begin{bmatrix} \mathbf{q}_f^T(\bar{\omega}_1(\bar{\mathbf{S}}_{22} + \bar{\mathbf{S}}_{33}) - \bar{\omega}_2 \bar{\mathbf{S}}_{12}^T - \bar{\omega}_3 \bar{\mathbf{S}}_{13}^T) \\ \mathbf{q}_f^T(-\bar{\omega}_1 \bar{\mathbf{S}}_{12} + \bar{\omega}_2(\bar{\mathbf{S}}_{11} + \bar{\mathbf{S}}_{33}) - \bar{\omega}_3 \bar{\mathbf{S}}_{23}^T) \\ \mathbf{q}_f^T(-\bar{\omega}_1 \bar{\mathbf{S}}_{13} - \bar{\omega}_2 \bar{\mathbf{S}}_{23} + \bar{\omega}_3(\bar{\mathbf{S}}_{11} + \bar{\mathbf{S}}_{22})) \end{bmatrix}^T \tag{3.79}$$

$$\bar{\boldsymbol{\omega}} = \begin{bmatrix} \bar{\omega}_1 \\ \bar{\omega}_2 \\ \bar{\omega}_3 \end{bmatrix} \tag{3.80}$$

and the body integrals $\mathbf{I}_{kl}^*$, $\bar{\mathbf{S}}_{kl}$ are obtained from equation (3.17) and (3.18). $\dot{\bar{\mathbf{I}}}_{\theta f}$ is obtained by the time derivative of equation (3.23)

$$\dot{\bar{\mathbf{I}}}_{\theta f} = \int_V \rho \dot{\tilde{\mathbf{u}}} dV = \begin{bmatrix} \dot{\mathbf{q}}_f^T(\bar{\mathbf{S}}_{23} - \bar{\mathbf{S}}_{32}) \\ \dot{\mathbf{q}}_f^T(\bar{\mathbf{S}}_{31} - \bar{\mathbf{S}}_{13}) \\ \dot{\mathbf{q}}_f^T(\bar{\mathbf{S}}_{12} - \bar{\mathbf{S}}_{21}) \end{bmatrix} \tag{3.81}$$

This summarizes the derivation of the components of the quadratic velocity vector into

$$(\mathbf{Q}_v)_R = -\mathbf{A}[(\tilde{\bar{\boldsymbol{\omega}}})^2 \bar{\mathbf{S}}_t - \dot{\tilde{\bar{\mathbf{S}}}}_t \dot{\mathbf{G}} \dot{\boldsymbol{\theta}} + 2\tilde{\bar{\boldsymbol{\omega}}} \bar{\mathbf{S}} \dot{\mathbf{q}}_f]$$

$$(\mathbf{Q}_v)_\theta = -\bar{\mathbf{G}}^T \tilde{\bar{\boldsymbol{\omega}}} \bar{\mathbf{I}}_{\theta\theta} \bar{\boldsymbol{\omega}} - \bar{\mathbf{G}}^T \bar{\mathbf{I}}_{\theta\theta} \dot{\bar{\mathbf{G}}} \dot{\boldsymbol{\theta}} - \bar{\mathbf{G}}^T \dot{\bar{\mathbf{I}}}_{\theta\theta} \bar{\boldsymbol{\omega}}$$

$$(\mathbf{Q}_v)_f = \bar{\mathbf{I}}_{Qv} \bar{\boldsymbol{\omega}} - \bar{\mathbf{I}}_{\theta f}^T \dot{\mathbf{G}} \dot{\boldsymbol{\theta}} - 2\dot{\bar{\mathbf{I}}}_{\theta f}^T \bar{\boldsymbol{\omega}} \tag{3.82}$$

Note that $\dot{\bar{\mathbf{G}}}\dot{\boldsymbol{\theta}}$ is a null vector when quaternions are used [5, p. 52,58] and the quadratic velocity vector can be simplified.

Chapter 4

One Degree of Freedom

In this Chapter a derivation of a translational and a rotational beam model is presented. They are derived individually in two different sections by using the same principles presented in Chapter 3.

4.1 Translational Formulation

4.1.1 Position and Velocity Vector

Applying the equations from the previous Chapter to a one-dimensional problem reduces the number of equations drastically. The global and local coordinate systems are only related by a distance along one axis and there is no rotation between them. The position of an arbitrary point p on a body B then instead becomes, consult Figure 4.1

$$r_p = R + u = R + u_0 + u_f \tag{4.1}$$

Where R denotes the distance between the global and local coordinate systems, u_0 is the rigid body motion and

$$u_f = \mathbf{S}\mathbf{q}_f = \begin{bmatrix} N_x & S_x^1 & \dots & S_x^n \end{bmatrix} \begin{bmatrix} q_x^s \\ q_x^1 \\ \vdots \\ q_x^n \end{bmatrix} \tag{4.2}$$

is the deformation. Here $\mathbf{S}$ becomes a row vector instead of a matrix due to the reduction in dimensions, the length of the vector depends on the number n dynamic

shape-functions, same goes for the generalized elastic coordinates $\mathbf{q}_f$. The components of the $\mathbf{S}$ shape function vector are the same as in equation (2.77).
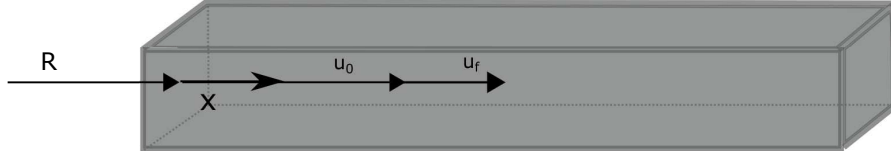

FIGURE 4.1: Position of the point p under the influence of longitudinal deformation.

The velocity and acceleration can then be expressed as

$$\dot{r}_p = \dot{R} + \dot{u}_f = \dot{R} + \mathbf{S}\dot{\mathbf{q}}_f = \mathbf{L}\dot{\mathbf{q}} \tag{4.3}$$

$$\ddot{r}_p = \ddot{R} + \mathbf{S}\ddot{\mathbf{q}}_f = \mathbf{L}\ddot{\mathbf{q}} \tag{4.4}$$

and the row vector $\mathbf{L}$ can then be identified as

$$\mathbf{L} = \begin{bmatrix} 1 & \mathbf{S} \end{bmatrix} \tag{4.5}$$

as well as the generalized coordinate vector

$$\mathbf{q} = \begin{bmatrix} R \\ \mathbf{q}_f \end{bmatrix} \tag{4.6}$$

4.1.2 Mass Matrix and Stiffness Matrix

As seen in equation (4.5) there are no matrices associated with rotation which leads to the mass matrix taking the following form

$$\mathbf{M} = \int_V \rho \mathbf{L}^{\mathbf{T}} \mathbf{L} dV = \int_V \rho \begin{bmatrix} 1 & \mathbf{S} \\ \mathbf{S}^T & \mathbf{S}^T\mathbf{S} \end{bmatrix} dV = \begin{bmatrix} m_{RR} & \mathbf{m}_{Rf} \\ sym & \mathbf{m}_{ff} \end{bmatrix} \tag{4.7}$$

The components of the mass matrix can be identified as

$$\begin{cases} m_{RR} = \int_V \rho dV = m \\ \mathbf{m}_{Rf} = \int_V \rho \mathbf{S} dV \\ \mathbf{m}_{ff} = \int_V \rho \mathbf{S}^T \mathbf{S} dV \end{cases} \tag{4.8}$$

The stiffness matrix associated with the generalized deformation coordinates becomes the same as the first term in equation (3.37) with the exception of $\mathbf{S}_x$ being replaced

with **S**. This leads to

$$\mathbf{K}_{ff} = \int\limits_0^L EA \frac{d\mathbf{S}^T}{dx}\frac{d\mathbf{S}}{dx}dx \tag{4.9}$$

and the full stiffness matrix can be written as

$$\mathbf{K} = \begin{bmatrix} 0 & \cdots \\ \vdots & \mathbf{K}_{ff} \end{bmatrix} \tag{4.10}$$

4.1.3 Generalized External Forces

Using equation (3.52) and neglecting rotation the virtual external work of a translational body may be written as

$$\delta W_e = \mathbf{Q}_e^T \delta\mathbf{q} = \begin{bmatrix} Q_R & \mathbf{Q}_f^T \end{bmatrix} \delta\mathbf{q} \tag{4.11}$$

If an external force is applied at an arbitrary point p of a body then the virtual work becomes

$$\delta W_e = F_p \delta r \tag{4.12}$$

where

$$\delta r = \delta R + \mathbf{S}\delta\mathbf{q}_f = \mathbf{L}\delta\mathbf{q} \tag{4.13}$$

Which leads to

$$\mathbf{Q}_e^T = F_p\mathbf{L} = F_p \begin{bmatrix} 1 & \mathbf{S} \end{bmatrix} \tag{4.14}$$

An the two components of the generalized external forces vector can be identified as

$$\begin{cases} Q_R = F_p \\ \mathbf{Q}_f = F_p\mathbf{S}^T \end{cases} \tag{4.15}$$

where the components should be evaluated at point p.

4.1.4 Equations of Motion

In the same manner as for the multidimensional case the equations of motion become

$$\mathbf{M}\ddot{\mathbf{q}} + \mathbf{C}\dot{\mathbf{q}} + \mathbf{K}\mathbf{q} = \mathbf{Q}_e \tag{4.16}$$

where $\mathbf{C}$ is defined in the same manner as in equation (3.50).Equation (4.16) can be written in a more explicit form

$$\begin{bmatrix} m_{RR} & \mathbf{m}_{Rf} \\ \mathbf{m}_{Rf}^T & \mathbf{m}_{ff} \end{bmatrix} \begin{bmatrix} \ddot{R} \\ \ddot{\mathbf{q}}_f \end{bmatrix} + \mathbf{C} \begin{bmatrix} \dot{R} \\ \dot{\mathbf{q}}_f \end{bmatrix} + \begin{bmatrix} 0 & \cdots \\ \vdots & \mathbf{K}_{ff} \end{bmatrix} \begin{bmatrix} R \\ \mathbf{q}_f \end{bmatrix} = \begin{bmatrix} Q_R \\ \mathbf{Q}_f \end{bmatrix} \tag{4.17}$$

Note that the quadratic velocity vector is not present in this set of equations, this is due to the absence of rotation in the system. Gravitational forces are also neglected due to the reduction in degrees of freedom.

4.2 Rotational formulation

4.2.1 Position and Velocity Vector

The rotational formulation only considers motion in one rotational degree of freedom, namely rotation around the beam centreline. The derivation is very similar to the translational formulation, the angular position of a point p can be described as, consult figure 4.2

$$\theta_p = \theta_R + \theta_0 + \theta_f \tag{4.18}$$

Where θ_p is the total angle of interest, θ_R defines the rotation of the local coordinate system relative the global, θ_0 is the initial angle of point p and θ_f is the angular deformation

$$\theta_f = \mathbf{S}\mathbf{q}_f = \begin{bmatrix} N_{\theta_x} & S_{\theta_x}^1 & \cdots & S_{\theta_x}^n \end{bmatrix} \begin{bmatrix} q_{\theta_x}^s \\ q_{\theta_x}^1 \\ \vdots \\ q_{\theta_x}^n \end{bmatrix} \tag{4.19}$$
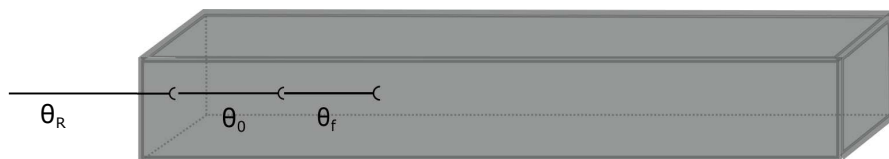

FIGURE 4.2: Angular position of the point p under the influence of torsional deformation

Differentiate equation (4.18) with respect to time yields the angular velocity

$$\dot{\theta}_p = \dot{\theta}_R + \mathbf{S}\dot{\mathbf{q}}_f = \begin{bmatrix} 1 & \mathbf{S} \end{bmatrix} \begin{bmatrix} \dot{\theta}_R \\ \dot{\mathbf{q}}_f \end{bmatrix} = \mathbf{L}\dot{\mathbf{q}} \tag{4.20}$$

The velocity for any point p on a cross-section can be described as

$$v_p = r\dot{\theta}_p = r\mathbf{L}\dot{\mathbf{q}} \tag{4.21}$$

where

$$r = \sqrt{y^2 + z^2} \tag{4.22}$$

is the distance between the beam centreline and point p in the $y - z$ plane.

4.2.2 Mass and Stiffness Matrix

Using equation (4.21) the kinetic energy becomes

$$T = \frac{1}{2}\dot{\mathbf{q}}^T \int_V \rho r^2 \mathbf{L}^T \mathbf{L} \, \mathrm{d}V \, \dot{\mathbf{q}} \tag{4.23}$$

where the mass matrix can be identified as

$$\mathbf{M} = \int_V \rho r^2 \mathbf{L}^T \mathbf{L} \, \mathrm{d}V = \int_v r^2 \begin{bmatrix} 1 & \mathbf{S} \\ \mathbf{S}^T & \mathbf{S}^T\mathbf{S} \end{bmatrix} \mathrm{d}V = \begin{bmatrix} m_{\theta\theta} & \mathbf{m}_{\theta f} \\ \mathbf{m}_{f\theta} & \mathbf{m}_{ff} \end{bmatrix} \tag{4.24}$$

and the submatrices are

$$m_{\theta\theta} = \int_V \rho r^2 \mathrm{d}V \quad \mathbf{m}_{\theta f} = \int_V \rho r^2 \mathbf{S} \, \mathrm{d}V \quad \mathbf{m}_{f\theta} = \int_V \rho r^2 \mathbf{S}^T \, \mathrm{d}V \quad \mathbf{m}_{ff} = \int_V \rho r^2 \mathbf{S}^T \mathbf{S} \, \mathrm{d}V \tag{4.25}$$

The stiffness matrix associated with torsion is derived in Section 3.2 and can be identified as the last term in equation (3.37) as

$$\mathbf{K}_{ff} = \int_0^L GK \frac{\mathrm{d}\mathbf{S}^T}{\mathrm{d}x} \frac{\mathrm{d}\mathbf{S}}{\mathrm{d}x} \, \mathrm{d}x \tag{4.26}$$

where G is the shear modulus depending on material and K is the geometry dependent torsion stiffness factor. The fully assembled stiffness matrix then becomes

$$\mathbf{K} = \begin{bmatrix} 0 & \cdots \\ \vdots & \mathbf{K}_{ff} \end{bmatrix} \tag{4.27}$$

4.2.3 Generalized External Forces

The virtual work of external forces in torsion can be written as

$$\delta W_e = \mathbf{Q}_e^T \delta \mathbf{q} = \begin{bmatrix} \mathbf{Q}_\theta^T & \mathbf{Q}_f^T \end{bmatrix} \begin{bmatrix} \delta \theta \\ \delta \mathbf{q}_f \end{bmatrix} \tag{4.28}$$

Where $\mathbf{Q}_\theta^T$ and $\mathbf{Q}_{q_f}^T$ are generalized forces associated with the generalized coordinate $\delta \theta$ and $\delta \mathbf{q}_f$ respectively. If an external moment is applied at an arbitrary point p of a body the external virtual work becomes

$$\delta W_e = M \delta \theta_p \tag{4.29}$$

where

$$\theta_p = \delta \theta_R + \mathbf{S} \delta \theta_f = \mathbf{L} \delta \mathbf{q} \tag{4.30}$$

This leads to

$$\mathbf{Q}_e^T = M \mathbf{L} \tag{4.31}$$

and the generalized external forces becomes

$$Q_\theta = M \qquad \mathbf{Q}_f = M \mathbf{S}^T \tag{4.32}$$

4.2.4 Equation of motion

The equations of motion takes the form

$$\mathbf{M} \ddot{\mathbf{q}} + \mathbf{C} \dot{\mathbf{q}} + \mathbf{K} \mathbf{q} = \mathbf{Q}_e \tag{4.33}$$

and in a more explicit form

$$\begin{bmatrix} m_{\theta\theta} & \mathbf{m}_{\theta f} \\ \mathbf{m}_{f\theta} & \mathbf{m}_{ff} \end{bmatrix} \begin{bmatrix} \ddot{\theta} \\ \ddot{\mathbf{q}}_f \end{bmatrix} + \mathbf{C} \begin{bmatrix} \dot{\theta} \\ \dot{\mathbf{q}}_f \end{bmatrix} + \begin{bmatrix} 0 & 0 \\ 0 & \mathbf{K}_{ff} \end{bmatrix} \begin{bmatrix} \theta \\ \mathbf{q}_f \end{bmatrix} = \begin{bmatrix} Q_\theta^T \\ \mathbf{Q}_{q_f} \end{bmatrix} \tag{4.34}$$

The quadratic velocity vector and the gravitational force vector are not present in this equation. This due to the reduction of degrees of freedom in the system.

Chapter 5

Implementation in Dymola

This Chapter gives a introduction to Dymola, a computer modeling software used in this Thesis. The implementation of the theoretical beam model and the structure of the model is presented and different aspects of the implementation are discussed.

5.1   Introduction to Dymola

Dymola is an object orientated computer software with the possibility to model large physical systems. The program spans over different fields of engineering such as electrical, mechanical, hydraulic, thermodynamic. One of the advantages with Dymola is the possibility to integrate different fields of engineering in the same system model. Each specific field has its own library with all the necessary tools required to build a model such as components, connectors, sources. These can be used to build models with a drag and drop technique. The language used in Dymola is named Modelica and is an equation based language. Every component is described by physical equations and the connections between components contains flow and potential couple equations, i.e. for a component in the Mechanical library the flow equation is the force and the position is the potential equation. Dymola is designed to solve ordinary differential equations efficiently and the Modelica language has an in-built time derivative operator which makes it easy to break down differential equations of higher order in to sets of first order. When the equations of the model are defined, Dymola solves it using numerical time integration schemes integrated within the software.

5.2 Frames

In the Modelica Multibody Dynamics library frames are used to describe an objects spatial position and orientation. Each frame can be seen as a local coordinate system attached at some point in the body. A frame contains a position vector, $\mathbf{r_0}$, rotation object $\mathbf{R}$, force vector $\mathbf{f}$ and torque vector $\mathbf{t}$. The position vector $\mathbf{r_0}$ describes the position of the frame relative an inertial frame. This vector is defined in the inertial frame. The rotation object $\mathbf{R}$ contains a transformation matrix $\mathbf{T}$ and the angular velocity vector $\boldsymbol{\omega}$. The transformation matrix $\mathbf{T}$ transforms the inertial frame into the local frame. $\boldsymbol{\omega}$ is the angular velocity of the local frame with respect to the inertial frame, defined in the local frame. The force vector $\mathbf{f}$ and the torque vector $\mathbf{t}$ are both defined in the local frame. An illustration of frame variables is presented in Figure 5.1.
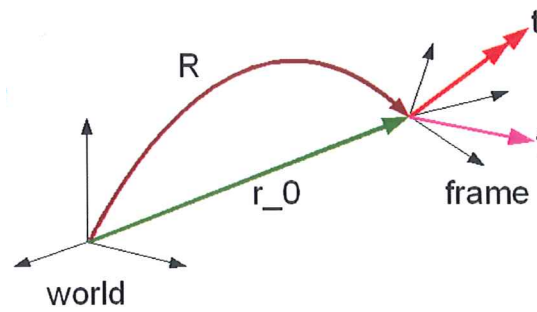

FIGURE 5.1: Illustration of the connection between two frames in Dymola. World is the inertial frame.

There are two different approaches available in order to define the rotation object $\mathbf{R}$ in the Multibody library, quaternions(i.e. Euler parameters) or angles. Quaternions defines a three angle rotation through four parameters and therefore an additional equation is required in the implementation, see equation (2.24). Angles uses three different angles and requires the user to specify in what sequence the rotation should be preformed e.g. Euler angles or Bryant angles. In Dymola there are implemented functions that can be used to create a rotation object from chosen angular description or vice versa.

Mentioned above is the use of an inertial frame. In Dymola this is represented by a model called *Worldframe*. This model creates a frame fixed to ground that all other components will refer to. *Worldframe* is also used to activate gravity or enable animation in a system model. There are three options for the gravity parameter namely uniform gravity field, point gravity or no gravity. The animation parameter can be set to true if animation should be enabled or false if no animation is required.

5.3 States

Dymola uses a set of states to describe the dynamics of a multibody model. The states can be position, angular representation or their time derivatives. The states corresponds to each degree of freedom in the model. Since there might be several potential states for each degree of freedom, the user can manually specify the set of states directly. If not, Dymola will select a suitable set.

The states describe the motion of the body. If the body is deformable then additional states are necessary to describe the deformation of the body. Hence all generalized deformation coordinates $\mathbf{q}_f$ and their time derivatives are used as state when the beam model is simulated. Therefore the number of states in the beam model is depending on the number of shape functions used.

When a multibody model is simulated in Dymola there are a lot of possible states. Before the simulation starts Dymola uses the kinematic constraint equations to reduce the number of states to a minimum.

5.4 Roots and branches

Each of the components have a set of states and some kinematic constraints. For example a revolute joint constraints the angular motion around two directions and all translational motion. This component has two internal states, namely a angle and it's time derivative. The revolute joint will give a kinematic connection between two bodies.

When solving the model Dymola needs to know where to start. This is handled with a flag that tells Dymola if the component is a root or not. If the component is a root then Dymola start with this component and works through the model. The beam model in this thesis is a potential root which mean that the beam is used as a root if necessary, e.g. a beam in free fall. If for instance the beam is connected to a fixed frame, then the fixed frame will be the root and the beam will use the known states of the fixed frame to calculate the states within the beam i.e. the beam is no root in this case.

When building a multibody model in Dymola its possible to construct kinematic loops. A kinematic loop is when several components are connected with kinematic constraints and more than one component is selected as root. The tool needs to take extra care to handle this automatically. Dymola builds an abstract connection graph of the model and sees if there is any loops present. If so it contains an algebraic loop and need to cut it. The Modelica modelling language features language elements for building such a graph, and letting the component developer tell the tool how the component interacts in

the connection graph. Components with no internal kinematic constraints e.g. spherical joints can be used as a cut to divide a kinematic loop in to different branches. Then Dymola solves each branch individually to later "bind" them together again by iterating a nonlinear system of equations. An example of such a problem is illustrated in Figure 5.2.
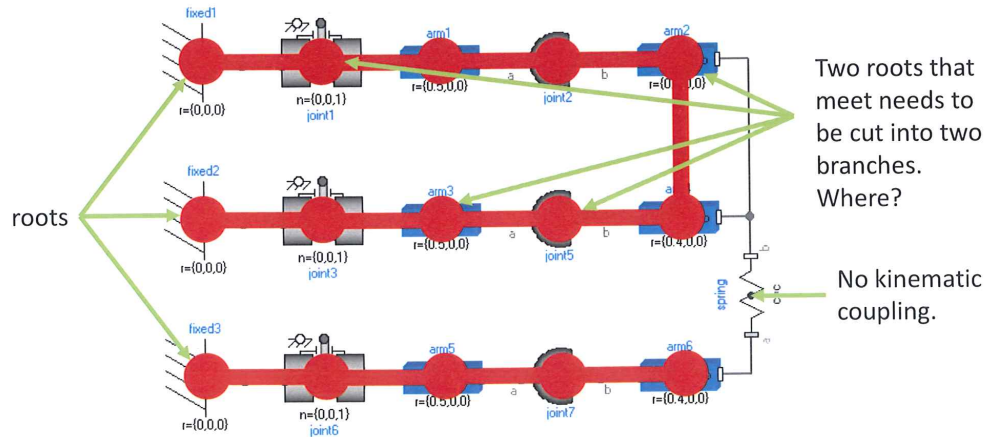

FIGURE 5.2: Dymola schematic illustration of the concepts roots, branches and cuts.

5.5 Beam Model

5.5.1 Model Structure

The theory described in Chapter 2, 3 and 4 was implemented as components in Dymola. Each component were created in individual libraries named after the their degree of freedoms, a total of three libraries were created, namely *Translational*, *Rotational* and *Multibody*. Each library has a main component, a *Functions* package and a *TestModels* package. The main component includes the equation of motion and all other necessary equations to describe the beam. *Functions* include functions used to calculate the necessary information needed to describe the dynamics of the beam. *TestModels* include different test models. The geometry dependent parameters are calculated in the package *Geometry*. A scheme of the libraries can be seen in Figure 5.3
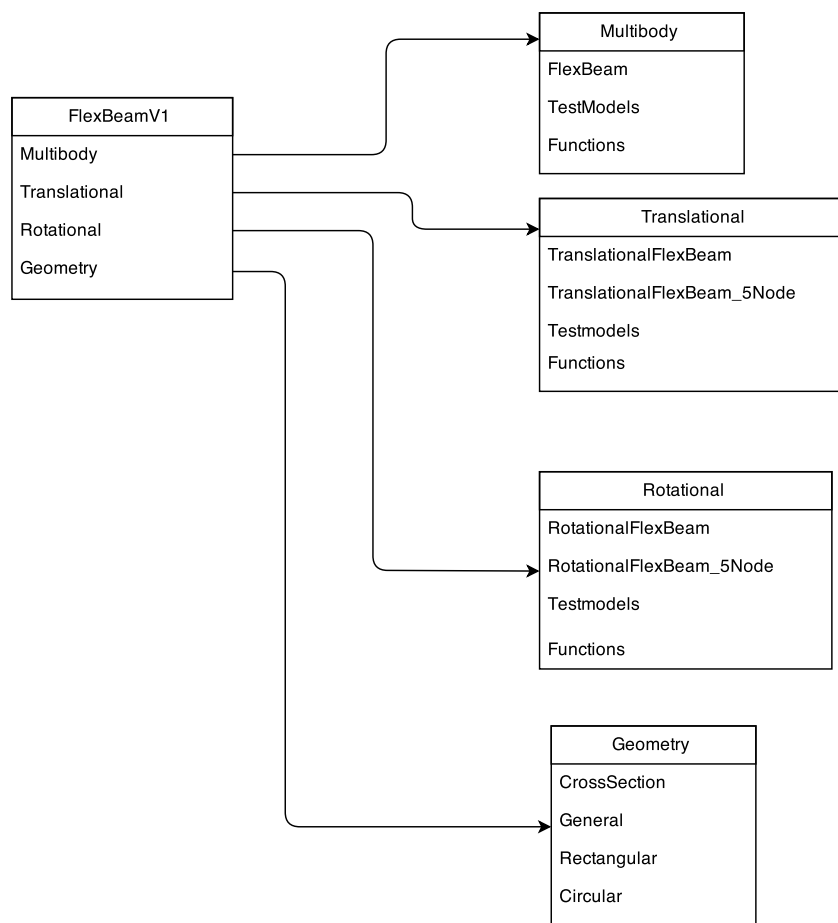
FIGURE 5.3: Libraries scheme.

The *Functions* package in the *Multibody* library were divided into different packages dependent on which equations it is associated with, these groups were: *MassMatrix*, *S_functions*, *Frequencies*, *ForceVectors* and *Graphics*. Consult figure 5.4.
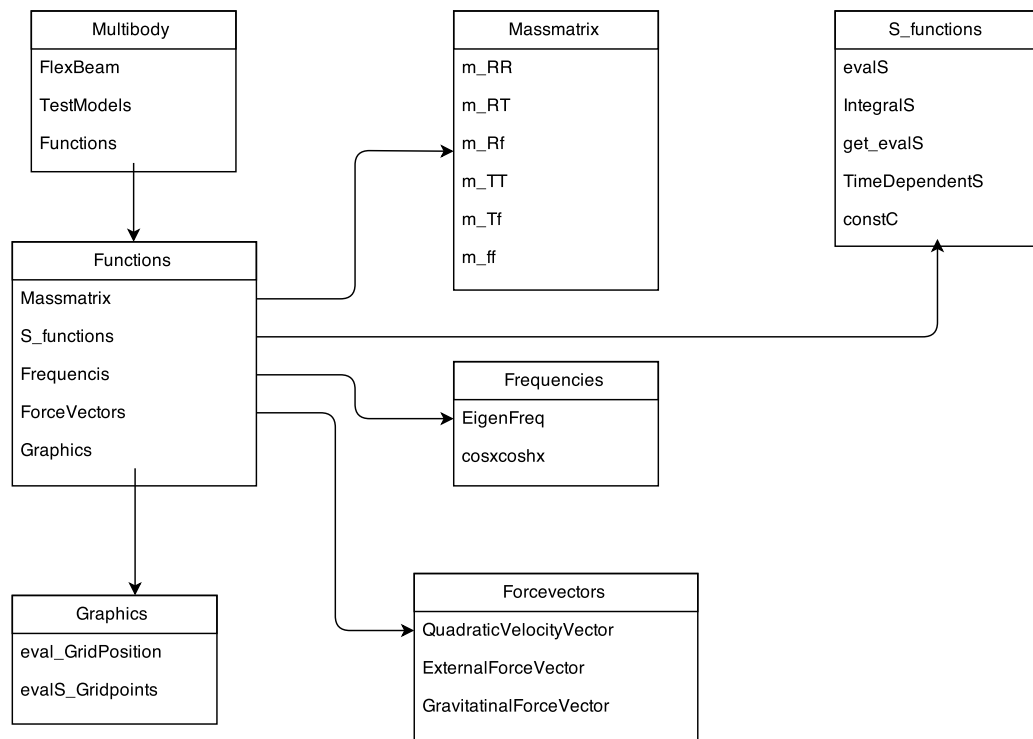
FIGURE 5.4: Multibody functions scheme

Most importantly the *S_functions* package contains all functions associated with the shape functions and their integrals. The functions in the package were designed so that all time independent integrals could be calculated in a pre-processor to save computation time, therefore they were divided into time independent and time dependent functions. The time independent functions comprises calculation of (3.10), (3.11), (3.16), (3.17) and (3.18) as well as the integrals shown in (3.37). While the time dependent functions comprises calculation of (3.9), (3.14) and (3.21).

The packages *MassMatrix* contains functions calculating individual submatrices defined in (3.4) as well as a function that assembles it to full size. The stiffness matrix only contains one submatrix and therefore the assembly is done in the same function that calculate equation (3.37). Furthermore the package *Frequencies* includes functions to calculate the eigenfrequencies of the beam and *Graphics* calculate necessary properties for the visualization. Finally the last mentioned package, *ForceVectors*, contains functions used to evaluate the external force vector, the gravitational force vector and the quadratic velocity vector.

In Figure 5.5 a work flow scheme can be seen. This scheme gives an idea of how the beam model works.
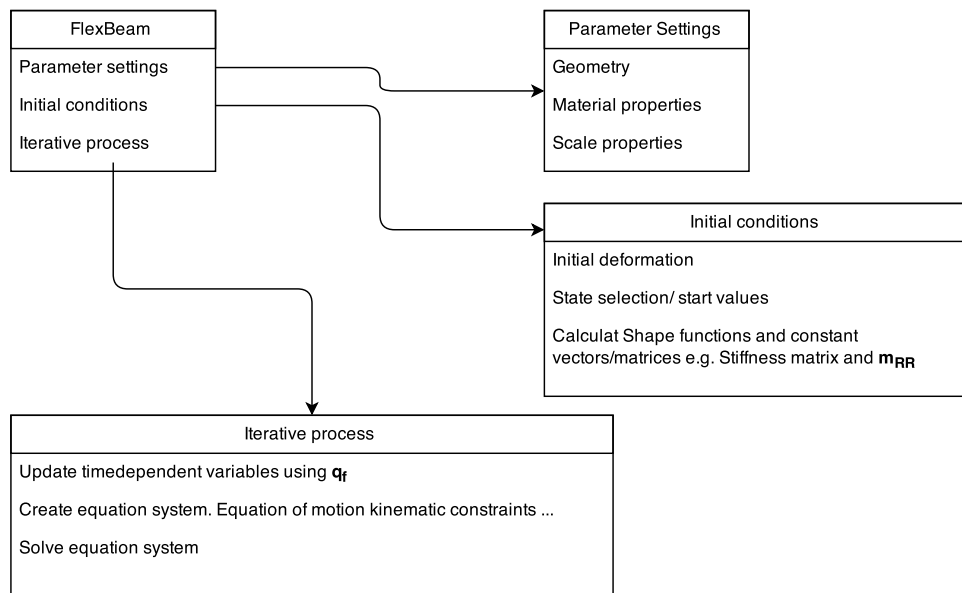
FIGURE 5.5: Work flow scheme of the main component FlexBeam.

5.5.2 Main Component

The equations of motion described in Section 3.3 were implemented in the model main component named *FlexBeam*. The main component connects the *Functions* package with information regarding given geometry and material properties as well as the equations of motion. The size of the equations of motion depends on the number of shape functions used, which also depends on the number of normal modes used for each DoF.

Each mechanical component in Dymola needs connectors to be able to connect to other components. These connectors uses frames that are placed at points where the boundary conditions are described. It could be another component but also external loads or prescribed motions. In the main component *FlexBeam* two frames are used, that is one at each end.

The two frames are named *frame_a* and *frame_b*, the beam component uses *frame_a* as a reference for its local coordinate system and uses the equations of motion to calculate the position, orientation and angular velocity of *frame_b*. If another component is connected to *frame_a* then the beam component receives position, orientation and angular velocity from that component. If nothing is connected then the beam component uses its internal initial states to solve the equations of motion. This is handled through roots and branches as mentioned in Section 5.4.

5.5.3 Graphical Representation

To visualize the beam a Dymola model called SurfaceFrame is used. This model makes a parametrized surface out of given input coordinates. Two parameters are used to define the number of grid point used to parametrize the beam surface, namely nu and nv. Where nu is the number of grid points along the beam axis and nv is the number of grid points needed to describe the boundary of the cross-section. The beam model only supports rectangular visualisation and therefore nv is set to five. This due to the fact that all four corners of the cross-section are needed to describe the surface. The fifth point is the same as the starting corner coordinates and enables the cross-section to be closed. nu can be set to a suitable integer value chosen by the user. Necessary coordinates are calculated with the help of two functions *evalS_gridpoints* and *eval_gridPosition*. Where *evalS_gridpoints* evaluates the shape function matrix in every grid point, which is done before the iteration process starts. *eval_gridPosition* calculate the position of each grid point in every iteration using the shape functions for each grid point and the generalized coordinate vector $\mathbf{q}_f$.

Since the deformations of the beam are assumed to be small, a scaling option has been implemented. This was done to enable visualization of the deformation. It is possible to scale the deformation in the x-, y- and z-direction. A blue beam is used to visualize the scaled deformation and a red beam is used to visualize the unscaled deformation as seen in Figure 5.6.
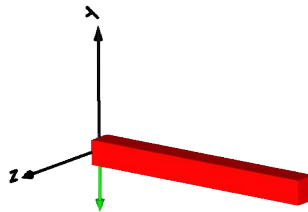

FIGURE 5.6: An animation of a beam with rectangular cross section before deformation. The x-axis coincide with the beam centreline. Direction of gravity is shown by the green arrow.

5.5.4 Geometry

There are a lot of parameters depending on the cross-section geometry in the beam model, for instant torsion stiffness, inertia and planar second moment of area. These parameter are calculated in a function called *Rectangle*. This function extend the partial

function *CrossSection*. The idea of this structure is to enabled the user to chose a cross-section, define the geometry and then all necessary parameters can be calculated. The three-dimensional beam model however only supports a rectangular cross-section.

5.5.5 Equations of Motion using ω

Mentioned above is the use of states when solving models in Dymola. If quaternions are used four parameters and one constraint function describes the rotation. This means that Dymola can make the choice to use these parameters as states. The formulation using quaternions as possible states works fine if the body is a root. In this case the angular velocity and transformation matrix are calculated using the quaternions. If the body is not a root information regarding angular velocity and the transformation matrix will be know at one of the frames. In this case the quaternions are calculated from the angular velocity and transformation matrix. Due to the complexity of the relation between the angular velocity, the transformation matrix and the quaternions it is more convenient to rewrite the equation of motion with angular velocity instead of quaternions. This can be done using equation (2.21) and its time derivative

$$\bar{\boldsymbol{\alpha}} = \dot{\bar{\boldsymbol{\omega}}} = \dot{\bar{\mathbf{G}}}\dot{\boldsymbol{\theta}} + \bar{\mathbf{G}}\ddot{\boldsymbol{\theta}} \tag{5.1}$$

The first therm in equation 5.1 will be a null vector when quaternions are used according to [5, p. 227]. If equation 5.1 is used in 3.4 then the mass matrix can be written as

$$\mathbf{M} = \int\limits_{V} \rho \begin{bmatrix} \mathbf{I} & -\mathbf{A}\tilde{\mathbf{u}} & \mathbf{A}\mathbf{S} \\ & \bar{\mathbf{G}}^T\tilde{\mathbf{u}}^T\tilde{\mathbf{u}} & \bar{\mathbf{G}}^T\tilde{\mathbf{u}}\mathbf{S} \\ sym & & \mathbf{S}^T\mathbf{S} \end{bmatrix} dV \tag{5.2}$$

By multiply the second row of the equation of motion by $\bar{\mathbf{G}}$ and make use of the quaternions identities from [5, p. 58] and the definition of $\bar{\mathbf{G}}$ [5, p. 52].

$$\bar{\mathbf{G}} = 2\bar{\mathbf{E}} \tag{5.3}$$

$$\bar{\mathbf{G}}\bar{\mathbf{G}}^T = 4\bar{\mathbf{E}}\bar{\mathbf{E}}^T = 4\mathbf{I} \tag{5.4}$$

The equation of motion can be rewritten.

$$
\begin{bmatrix}
\mathbf{m}_{RR} & \mathbf{A}\tilde{\bar{\mathbf{S}}}_t^T & \mathbf{A}\bar{\mathbf{S}} \\
 & \bar{\mathbf{I}}_{\theta\theta} & \bar{\mathbf{I}}_{\theta f} \\
symmetric & & \mathbf{m}_{ff}
\end{bmatrix}
\begin{bmatrix}
\ddot{\mathbf{R}} \\
\bar{\boldsymbol{\alpha}} \\
\ddot{\mathbf{q}}_f
\end{bmatrix}
=
\begin{bmatrix}
(\mathbf{Q}_e)_R \\
(\mathbf{Q}_e)_\alpha \\
(\mathbf{Q}_e)_f - \mathbf{K}_{ff}\mathbf{q}_f - \mathbf{C}_{ff}\dot{\mathbf{q}}_f
\end{bmatrix}
+
\begin{bmatrix}
(\mathbf{Q}_v)_R \\
(\mathbf{Q}_v)_\alpha \\
(\mathbf{Q}_v)_f
\end{bmatrix}
+
\begin{bmatrix}
(\mathbf{Q}_g)_R \\
(\mathbf{Q}_g)_\alpha \\
(\mathbf{Q}_g)_f
\end{bmatrix}
$$

$$(5.5)$$

where the components in the mass matrix are defined in Chapter 3. The components in the force vectors associated with rotation will be

$$(\mathbf{Q}_e)_\alpha = \mathbf{A}^T\mathbf{M} + \tilde{\mathbf{u}}\mathbf{A}^T\mathbf{F} \tag{5.6}$$

$$(\mathbf{Q}_g)_\alpha = \tilde{\bar{\mathbf{S}}}_t\mathbf{A}^T\mathbf{g} \tag{5.7}$$

$$(\mathbf{Q}_v)_\alpha = -\tilde{\bar{\boldsymbol{\omega}}}\bar{\mathbf{I}}_{\theta\theta}\bar{\boldsymbol{\omega}} - \dot{\bar{\mathbf{I}}}_{\theta\theta}\bar{\boldsymbol{\omega}} \tag{5.8}$$

5.5.6 Calculations of the Inertia Shape Integrals

In Section 3.1 the mass matrix was derived. The mass matrix contains different integrals of the shape functions that needs to be evaluated. This was done using the software Maple and the free computational knowledge engine Wolframalpha. When evaluating equation (3.10), (3.11), (3.16) and (3.17) only one shape function vector is present and no special treatment is necessary. However when equation (3.18) is calculated there are vector multiplications of the shape function vectors. To simplify the calculations the orthogonal properties of the dynamic shape functions were used. This states that the integral over the length of two shape functions with two different frequencies will be zero. This can be shown by using integration by part combined with the boundary conditions.

Making use of equation (2.49) with the two different eigenfrequencies p_n and p_m

$$\frac{d^2S_x^n(x)}{dx^2} = -p_n^2 S_x^n(x) \qquad\qquad \frac{d^2S_x^m(x)}{dx^2} = -p_m^2 S_x^m(x)$$

By multiplication of the first equation with S_x^m and the second with S_x^n and subtracting the first with the second one gets

$$\frac{p_m^2 - p_n^2}{a^2} S_x^n S_x^m = S_x^m \frac{d^2S_x^n}{dx^2} - S_x^n \frac{d^2S_x^m}{dx^2}$$

Integrating both sides over the length and using integration by parts yields

$$\frac{p_m^2 - p_n^2}{a^2} \int_0^L S_x^n S_x^m = \left[S_x^m \frac{dS_x^n}{dx} - S_x^n \frac{dS_x^m}{dx} \right]_0^L - \int_0^L \frac{dS_x^m}{dx}\frac{dS_x^n}{dx} - \frac{dS_x^m}{dx}\frac{dS_x^n}{dx}dx = 0$$

Where the boundary conditions in equation 2.53 has been used.

This proves the orthogonality for longitudinal dynamic mode shapes. In the same way the orthogonality for the torsional dynamic mode shapes can be proved. The proof for orthogonality of lateral vibrations can be done in a similar way [3, p. 334].

The dynamic mode shapes of the slope S_{θ_y} and S_{θ_z} are related to the lateral shape functions by equation (2.73) and (2.74). In this master thesis these shape functions are assumed to have the orthogonality properties, but this has not been proven.

Chapter 6

Validation

In this Chapter, test cases for validation are presented for both the one-dimensional and three-dimensional models. The results are compared with analytical solutions from the Euler Bernoulli beam theory, described in Section 1.5.

6.1 Three-Dimensional Model

In order to verify the three-dimensional model it was required to test each degree of freedom and their response in different loading situations. The test was divided into three main categories: static loading, free vibration and forced vibration. The tests were carried out on a beam fixed in frame a and free in frame b, i.e. the load was applied at frame b. The displacements were calculated at frame b.

During static loading the beam was subjected to a linearly increasing load. The displacements were measured and the results were compared with the analytical solution for a Euler Bernoulli beam. In the free vibration test case the displacement of the beam was set to an initial value which caused the beam to vibrate freely. The natural frequency of the beam was observed and measured and then compared with the analytical solution. The forced vibration test case investigated if the beam model could enter mechanical resonance when subjected to a harmonic force.

In addition to verification of the shape functions some additional tests regarding gravitational and centrifugal forces were made in order to verify the beam response to these phenomenons.

6.1.1 Static Loading

The following material and geometric parameters were used for the static force load cases: $E = 210GPa$, $\rho = 2700Kgm^{-3}$, $L = 1m$, $h = 0.1m$, $b = 0.07m$ and $v = 0.3$. Where E is the Young's modulus, ρ material density, L length of the beam, h and b are the hight and width respectively. Possion's ratio is denoted by v. The force at frame b was set to increase linearly from $F = 0N$ to $F = 1000N$ during one second while the other directions were set to zero. After one second the force remain constant. The damping of the stiffness matrix was set to $\delta = 10^{-4}$ to avoid vibrations in the beam. This damping was introduce to reduce simulation time and numerical noise. The mass matrix damping coefficient η was set to zero during all simulations. The models were simulated during 1.5 seconds with 5000 steps.

The same material and geometric parameters were used in the static torque load cases, with exception of the width b being changed to $b = 0.08m$ to simplify the analytical solution. The torque or bending moment was set to increase linearly from $M = 0Nm$ to $M = 3000Nm$ during one second and then kept constant. The torque/bending moment around the other axes were set to zero. Simulations were carried out with the same number of steps and simulation time as the static force models.

6.1.1.1 Force x-direction
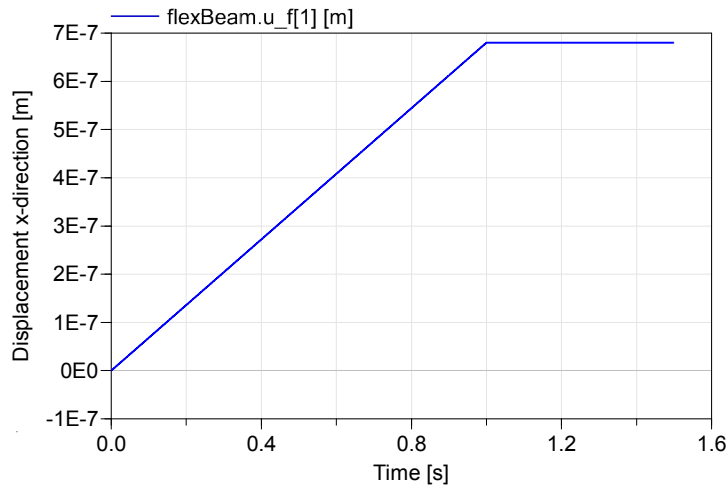
FIGURE 6.1: Displacement $u_{x,dym}$ at frame b, force applied in x-direction

Dymola solution

$$u_{x,dym} = 6.80272 \cdot 10^{-7}m$$

Analytical solution [4, p. 21]

$$u_{x,analytic} = \frac{FL}{AE} = 6.802721088 \cdot 10^{-7} m$$

Error difference

$$error_{u_x} = \frac{|u_{x,dym} - u_{x,analytic}|}{|u_{x,analytic}|} = 1.599936 \cdot 10^{-5}\%$$
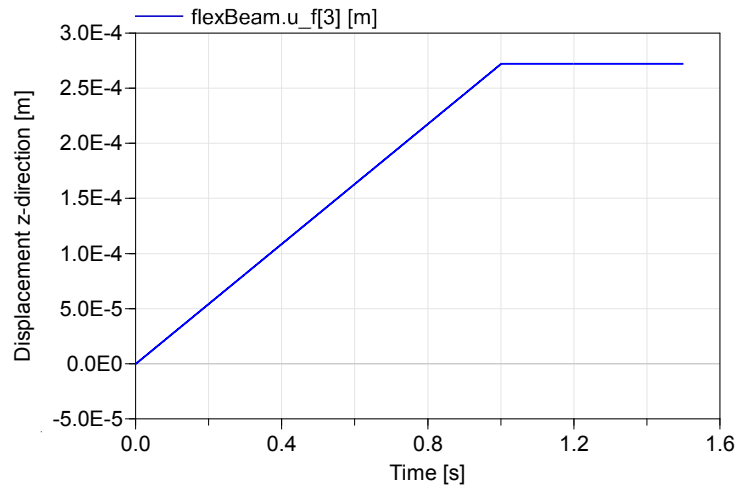
6.1.1.2 Force y-direction
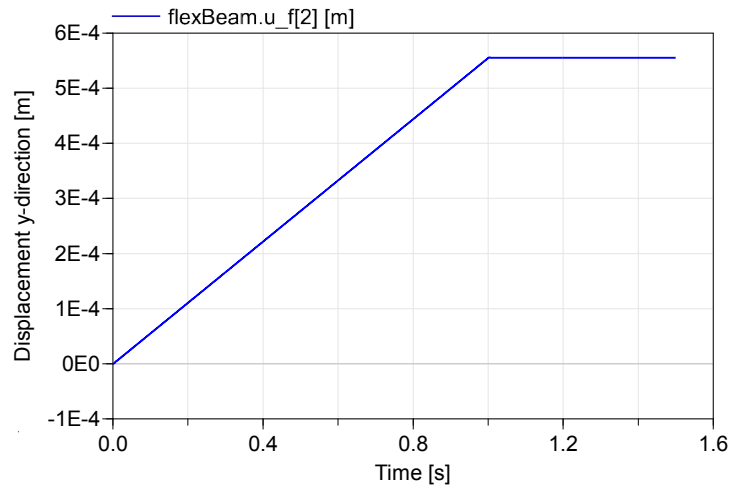
FIGURE 6.2: Displacement $u_{y,dym}$ at frame b, force applied in y-direction
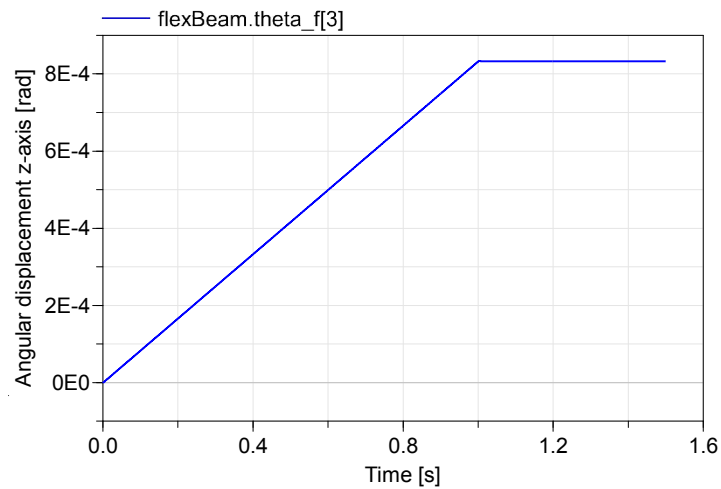
FIGURE 6.3: Angular deformation $\theta_{z,dym}$ around the z-axis at frame b, force applied in y-direction

Dymola solution

$$u_{y,dym} = 5.55325 \cdot 10^{-4} m$$

$$\theta_{z,dym} = 8.32987 \cdot 10^{-4} rad$$

Analytical solution [8, p. 344]

$$u_{y,analytic} = \frac{FL^3}{3EI_z} = 5.553241705 \cdot 10^{-4} m$$

$$\theta_{z,analytic} = \frac{FL^2}{2EI_z} = 8.329862557 \cdot 10^{-4} rad$$

Error difference

$$error_{u_y} = \frac{|u_{y,dym} - u_{y,analytic}|}{|u_{y,analytic}|} = 1.493722125 \cdot 10^{-4} \%$$

$$error_{\theta_z} = \frac{|\theta_{z,dym} - \theta_{z,analytic}|}{|\theta_{z,analytic}|} = 8.9353215 \cdot 10^{-5} \%$$

6.1.1.3 Force z-direction
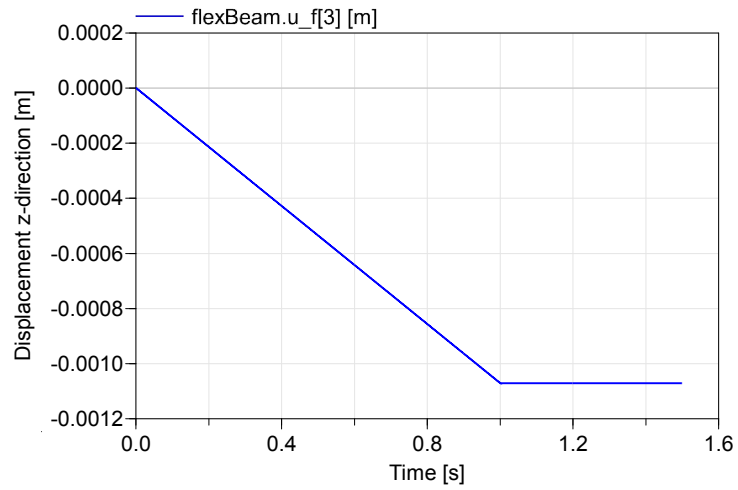

FIGURE 6.4: Displacement $u_{z,dym}$ at frame b, force applied in z-direction
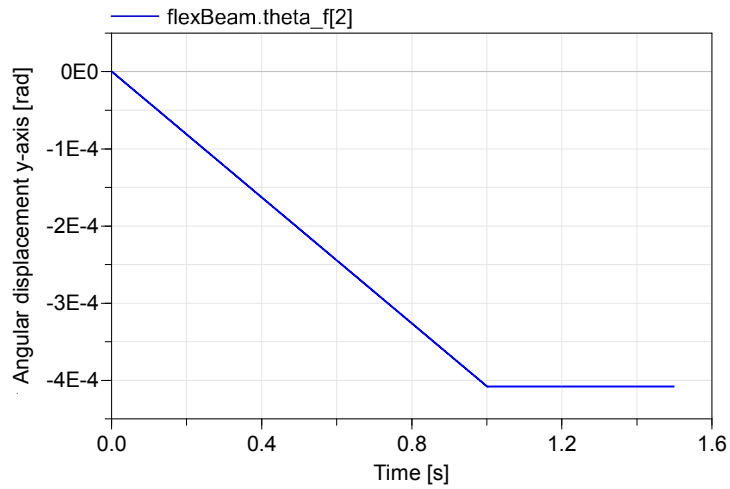
FIGURE 6.5: Angular deformation $\theta_{y,dym}$ around the y-axis at frame b, force applied in z-direction

Dymola solution

$$u_{z,dym} = 2.72109 \cdot 10^{-4} m$$

$$\theta_{y,dym} = -4.08163 \cdot 10^{-4} rad$$

Analytical solution

$$u_{z,analytic} = \frac{FL^3}{3EI_y} = 2.721088435 \cdot 10^{-4} m$$

$$\theta_{y,analytic} = -\frac{FL^2}{2EI_y} = -4.081632653 \cdot 10^{-4} rad$$

Error difference

$$error_{u_z} = \frac{|u_{z,dym} - u_{z,analytic}|}{|u_{z,analytic}|} = 5.751375001 \cdot 10^{-5} \%$$

$$error_{\theta_y} = \frac{|\theta_{y,dym} - \theta_{y,analytic}|}{|\theta_{y,analytic}|} = 6.49985 \cdot 10^{-5} \%$$
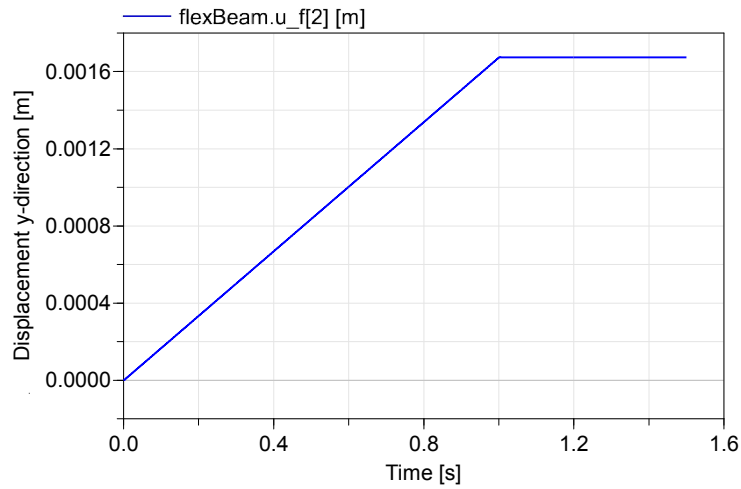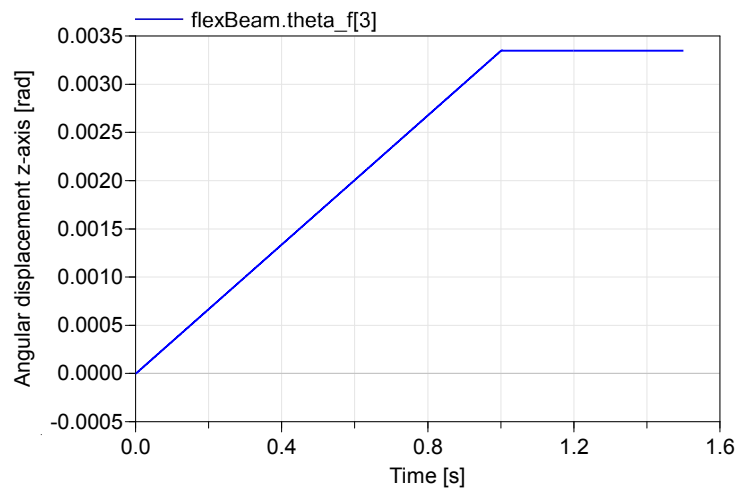
6.1.1.4 Torque x-axis
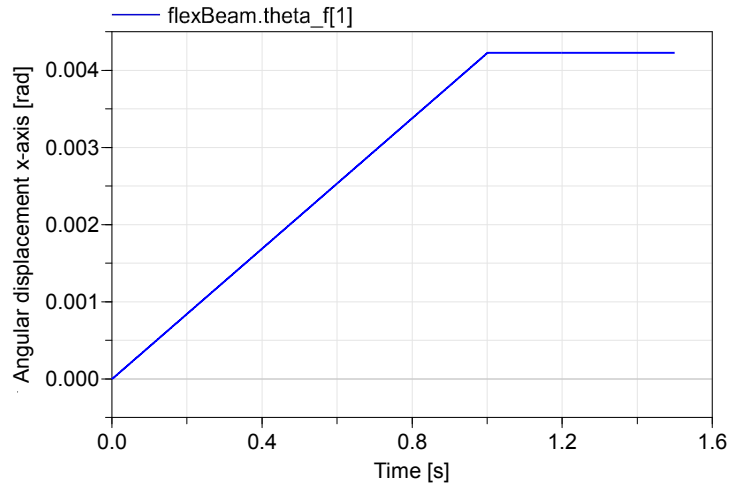
FIGURE 6.6: Angular deformation $\theta_{x,dym}$ at frame b, torque applied around the x-axis

Dymola solution

$$\theta_{x,dym} = 4.2259 \cdot 10^{-3} rad$$

Analytical solution [4, p. 65]

$$\theta_{x,analytic} = \frac{ML}{GK} = 4.2259015 \cdot 10^{-3} rad$$

Error difference

$$error_{\theta_x} = \frac{|\theta_{x,dym} - \theta_{x,analytic}|}{|\theta_{x,analytic}|} = 3.549538483 \cdot 10^{-5}\%$$

6.1.1.5 Torque y-axis

FIGURE 6.7: Displacement $u_{z,dym}$ at frame b, torque applied applied around the y-axis
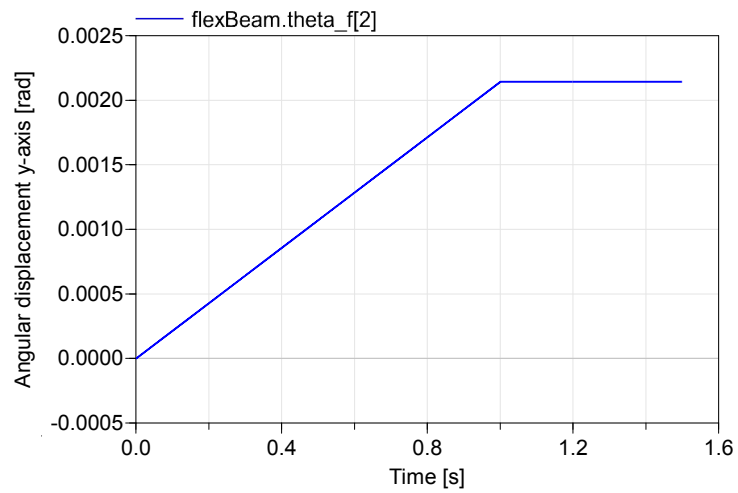
FIGURE 6.8: Angular deformation $\theta_{y,dym}$ at frame b, torque applied around the y-axis

Dymola solution

$$u_{z,dym} = -1.07143 \cdot 10^{-3} m$$

$$\theta_{y,dym} = 2.14286 \cdot 10^{-3} rad$$

Analytical solution [8, p. 344]

$$u_{z,analytic} = -\frac{ML^2}{2EI_y} = 1.0714286 \cdot 10^{-3} m$$

$$\theta_{y,analytic} = \frac{ML}{EI_y} = 2.142857 \cdot 10^{-3} rad$$

Error difference

$$error_{u_z} = \frac{|u_{z,dym} - u_{z,analytic}|}{|u_{z,analytic}|} = 1.306666632 \cdot 10^{-4}\%$$

$$error_{\theta_y} = \frac{|\theta_{y,dym} - \theta_{y,analytic}|}{|\theta_{y,analytic}|} = 1.35333336 \cdot 10^{-4}\%$$

6.1.1.6   Torque z-axis

FIGURE 6.9: Displacement $u_{y,dym}$ at frame b, torque applied around the z-axis

FIGURE 6.10: Angular deformation $\theta_{z,dym}$ at frame b, torque applied around the z-axis

Dymola solution

$$u_{y,dym} = 1.67411 \cdot 10^{-3} m$$
$$\theta_{z,dym} = 3.34821 \cdot 10^{-3} rad$$

Analytical solution

$$u_{y,analytic} = \frac{ML^2}{2EI_z} = 1.6741071 \cdot 10^{-3} m$$
$$\theta_{z,analytic} = \frac{ML}{EI_z} = 3.3482143 \cdot 10^{-3} rad$$

Error difference

$$error_{u_y} = \frac{|u_{y,dym} - u_{y,analytic}|}{|u_{y,analytic}|} = 1.732266711 \cdot 10^{-4} \%$$
$$error_{\theta_z} = \frac{|\theta_{z,dym} - \theta_{z,analytic}|}{|\theta_{z,analytic}|} = 1.28426666 \cdot 10^{-4} \%$$

6.1.2 Free Vibration

The geometric and material parameters used for the free vibration test case were: $E = 210GPa$, $\rho = 2700Kgm^{-3}$, $L = 1m$, $h = 0.1m$, $b = 0.08m$ and $v = 0.3$. The free vibration test was modelled by setting the deformation at frame b to an initial value which caused the beam to exhibit a harmonic motion.

The test was conducted using three different settings for each degree of freedom. One undamped model with one dynamic shape function, one undamped model with ten dynamic shape functions and one damped model with three dynamic shape functions. The damped model had $\delta \neq 0$, i.e. the stiffness matrix coefficient of the damping matrix was not equal to zero. This coefficient vary between $10^{-3} - 10^{-6}$ depending on load case used. The damping was used to reduce numerical noise and to reduce simulation time. The mass matrix coefficient of the damping matrix η was set to zero during all simulations.

The period of the vibration in each case was measured in Dymola and a natural frequency calculated from the period. The natural frequency was then compared to the analytical solution provided in 2.6.

6.1.2.1 Initial Deformation x-direction

The initial displacement at frame b was set to $u_{x,0} = 2.5 \cdot 10^{-4} m$ while the displacements in the other directions were set to zero.
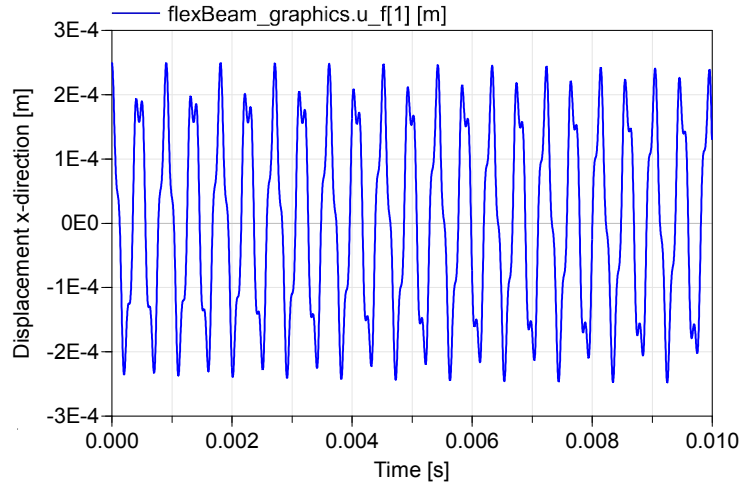

FIGURE 6.11: Displacement $u_{x,dym}$ at frame b, one dynamic shape function, no damping
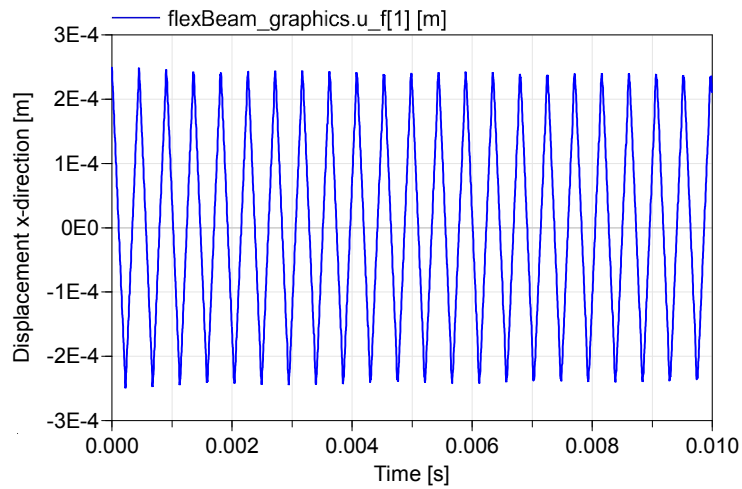

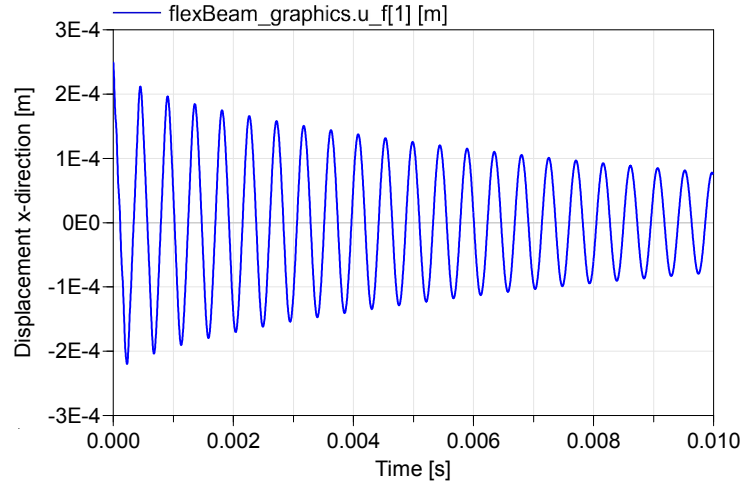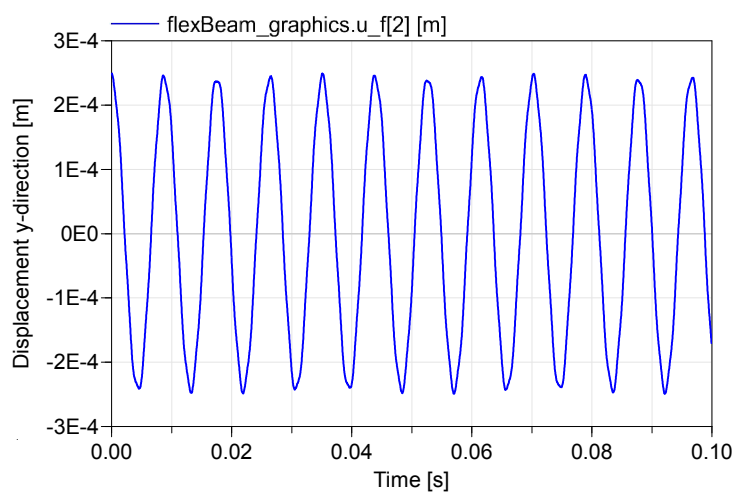FIGURE 6.12: Displacement $u_{x,dym}$ at frame b, ten dynamic shape functions, no damping

FIGURE 6.13: Displacement $u_{x,dym}$ at frame b, three dynamic shape functions, damping set to $\delta = 10^{-6}$

The first natural frequency for a beam fixed in one end and free in another is [3, p. 309-310]

$$f_{x,analytic} = \frac{1}{4L}\sqrt{\frac{E}{\rho}} = 2204.792751 Hz$$

The period from the test cases in Dymola was measured as

$$T_{x,dym} = 0.00045s \tag{6.1}$$

which yields the natural frequency

$$f_{x,dym} = \frac{1}{T_{x,dym}} = 2222.222222 Hz$$

Error

$$error_{f_x} = \frac{|f_{x,dym} - f_{x,analytic}|}{|f_{x,analytic}|} = 0.7905261459\%$$

6.1.2.2 Initial Deformation y-direction

The initial displacement at frame b was set to $u_{y,0} = 2.5 \cdot 10^{-4} m$, $\theta_{z,0} = 3.75 \cdot 10^{-4}$ while the displacements in the other directions were set to zero. The initial value of $\theta_{z,0}$ was calculated according to Section 6.1.1.2, i.e. for a static load case with constant force applied at frame b.

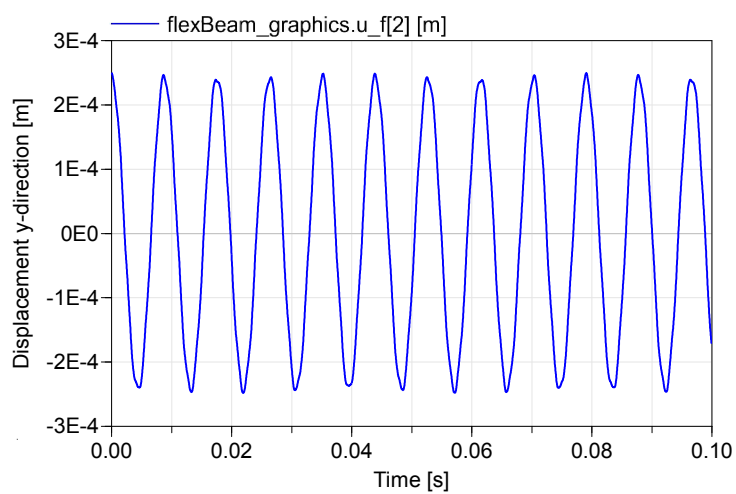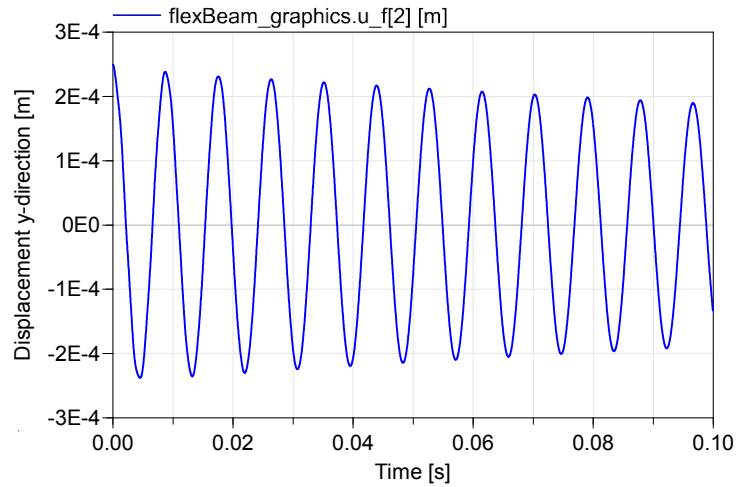FIGURE 6.14: Displacement $u_{y,dym}$ at frame b, one dynamic shape function, no damping

FIGURE 6.15: Displacement $u_{y,dym}$ at frame b, ten dynamic shape functions, no damping

FIGURE 6.16: Displacement $u_{y,dym}$ at frame b, three dynamic shape functions, damping set to $\delta = 10^{-5}$

The first natural frequency for a beam fixed in one end and free in the other is [3, p. 344]

$$f_{y,analytic} = \frac{1}{2\pi} \sqrt{\frac{EI_z}{A\rho}} k^2 = 113.9593084 Hz$$

where $A = bh$ is the cross section area and $k = 1.875$. The period from the test case in Dymola was measured as

$$T_{y,dym} = 0.0087s \tag{6.2}$$

which yields the natural frequency

$$f_{y,dym} = \frac{1}{T_{y,dym}} = 114.9425287 Hz$$

Error

$$error_{f_y} = \frac{|f_{y,dym} - f_{y,analytic}|}{|f_{y,analytic}|} = 0.8627819121\%$$

6.1.2.3 Initial Deformation z-direction

The initial displacement at frame b was set to $u_{z,0} = 2.5 \cdot 10^{-4} m$, $\theta_{y,0} = -3.75 \cdot 10^{-4}$ while the displacements in the other directions were set to zero.
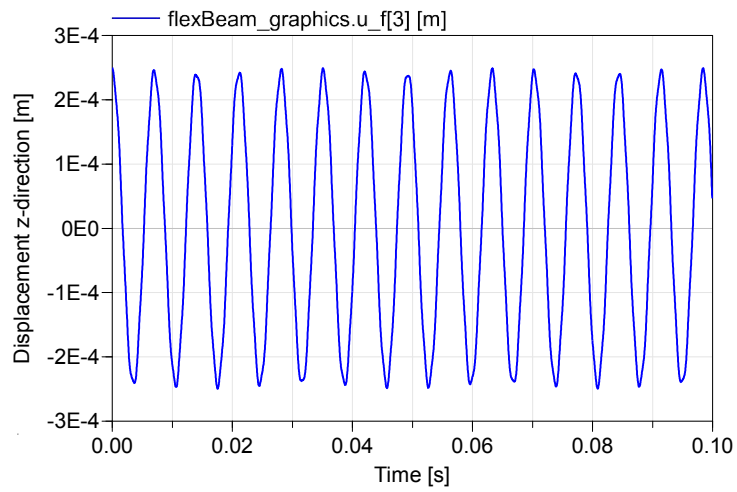
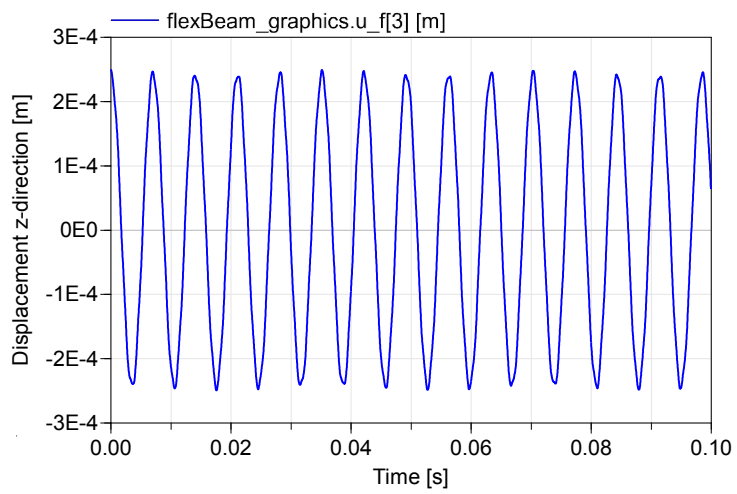FIGURE 6.17: Displacement $u_{z,dym}$ at frame b, one dynamic shape function, no damping

FIGURE 6.18: Displacement $u_{z,dym}$ at frame b, ten dynamic shape functions, no damping
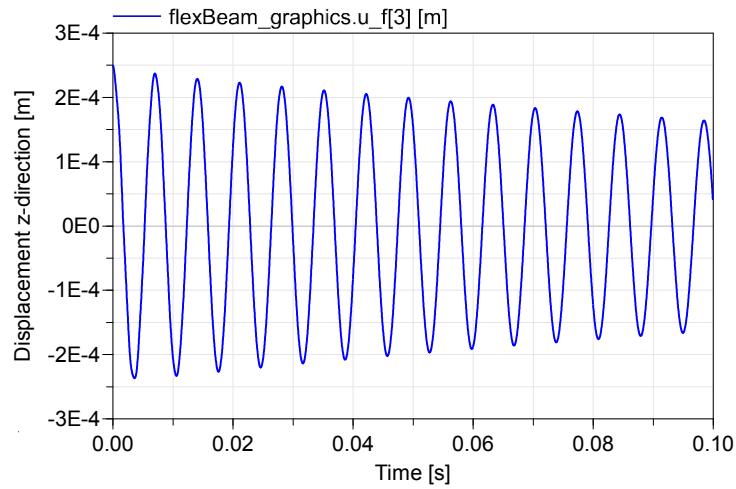
FIGURE 6.19: Displacement $u_{z,dym}$ at frame b, three dynamic shape functions, damping set to $\delta = 10^{-5}$

The first natural frequency for a beam fixed in one end and free in another is

$$f_{z,analytic} = \frac{1}{2\pi}\sqrt{\frac{EI_y}{A\rho}}k^2 = 142.4491355 Hz$$

where $A = bh$ is the cross section area and $k = 1.875$. The period from the test case in Dymola was measured as

$$T_{z,dym} = 0.00698s \tag{6.3}$$

which yields the natural frequency

$$f_{z,dym} = \frac{1}{T_{z,dym}} = 143.2664756 Hz$$

Error

$$error_{f_z} = \frac{|f_{z,dym} - f_{z,analytic}|}{|f_{z,analytic}|} = 0.5737768061\%$$

6.1.2.4 Initial Angular Deformation around the x-axis

The initial deformation at frame b was set to $\theta_{x,0} = 3.75 \cdot 10^{-4}$ while the angular deformation in the other directions were set to zero.
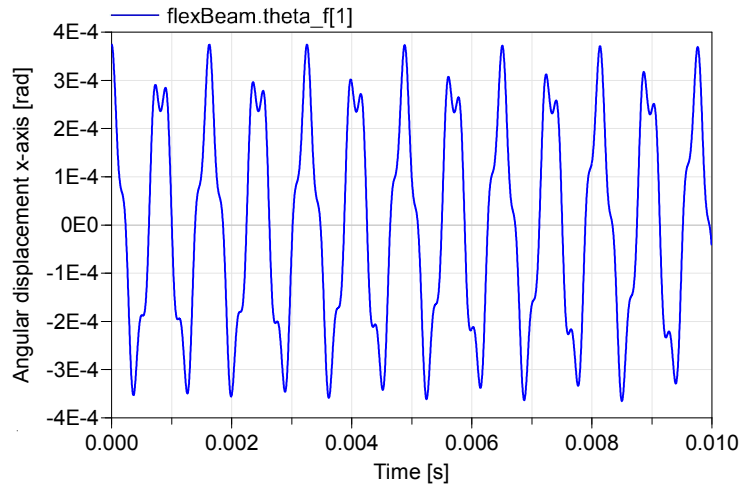
FIGURE 6.20: Angular deformation $\theta_{x,dym}$ at frame b, one dynamic shape function, no damping
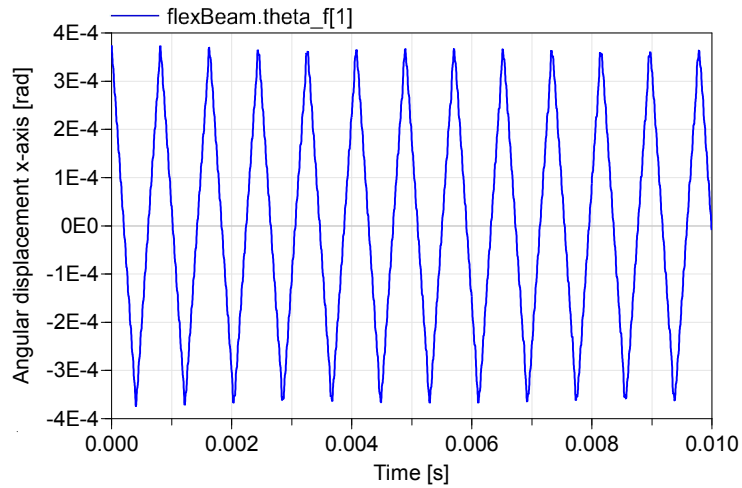

FIGURE 6.21: Angular deformation $\theta_{x,dym}$ at frame b, ten dynamic shape functions, no damping

The first natural frequency for a beam fixed in one end and free in the other is [3, p. 325-326]

$$f_{\theta_x,analytic} = \frac{1}{4L}\sqrt{\frac{GK}{J_x}} = 1225.978272Hz$$

where J_x is the moment of inertia around the x-axis per unit length calculated as $J_x = \frac{\rho A}{12}(b^2 + h^2)$. The period from the test case in Dymola was measured as
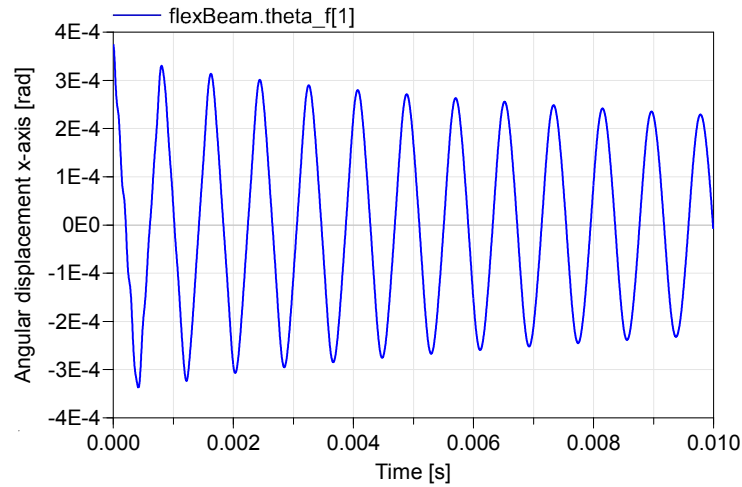
$$T_{\theta_x,dym} = 0.000804s \tag{6.4}$$

FIGURE 6.22: Angular deformation $\theta_{x,dym}$ at frame b, three dynamic shape functions, damping set to $\delta = 10^{-6}$

which yields the natural frequency

$$f_{\theta_x,dym} = \frac{1}{T_{x,dym}} = 1243.781095 Hz$$

Error

$$error_{f_{\theta_x}} = \frac{|f_{\theta_x,dym} - f_{\theta_x,analytic}|}{|f_{\theta_x,analytic}|} = 1.452132016\%$$

6.1.3 Forced Vibration

The forced vibration test cases used the same geometric and material properties as the free vibration test cases i.e. $E = 210GPa$, $\rho = 2700Kgm^{-3}$, $L = 1m$, $h = 0.1m$, $b = 0.08m$ and $v = 0.3$, no damping was applied. The tests were modelled by applying a harmonic force at frame b, the frequency of the harmonic force was set to the analytical frequency as well as the frequency of free vibration derived in Section 6.1.2. The displacement at frame b was calculated and analysed to see if the beam was under the influence of mechanical resonance.

6.1.3.1 Force x-direction

The force in the x-direction at frame b was set to $F = 1000sin(f2\pi t)$ while the other directions were set to zero. The frequency f was set as either the analytical solution

$$f_{x,analytic} = 2204.792759 Hz$$

or the solution from the free vibration test
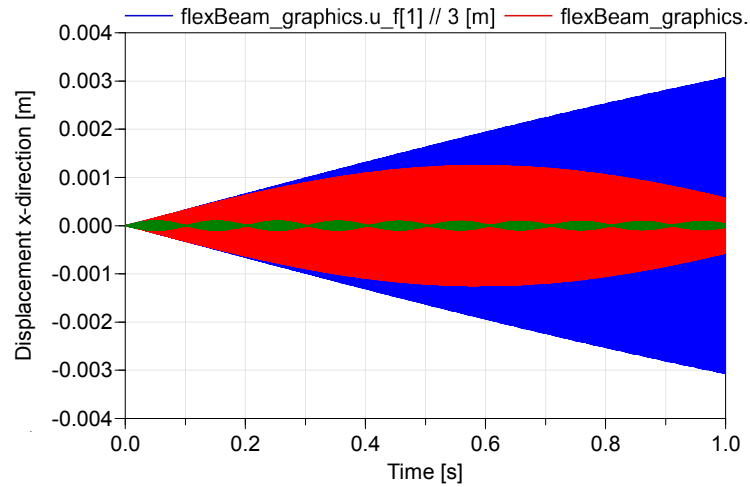
$$f_{x,dym} = 2222.222222 Hz$$

FIGURE 6.23: Displacement $u_{x,dym}$ at frame b as an response to the frequency $f_{x,analytic}$. One, three and five dynamic shape functions shown in green, red and blue colors.
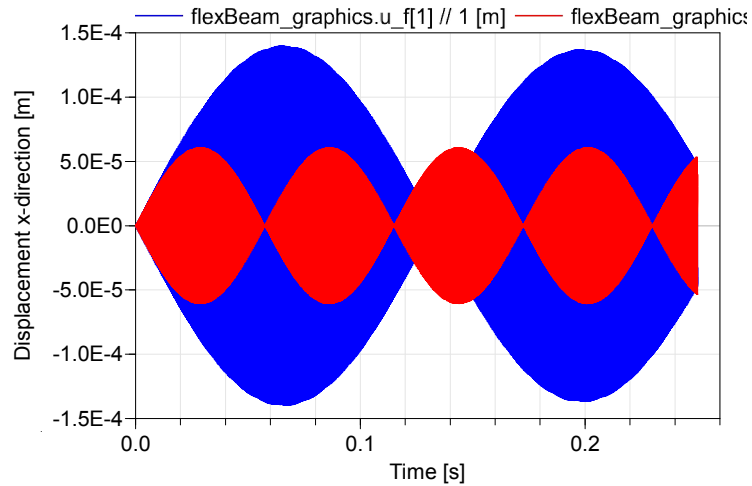

FIGURE 6.24: Displacement $u_{x,dym}$ at frame b as an response to the frequency $f_{x,dym}$. One and ten dynamic shape functions shown in blue and red colors.

Clearly the analytical frequency causes the beam to excite it's natural frequency. The beat frequency of the red graph in figure 6.24 are equal to the difference between $f_{x,analytical}$ and $f_{x,dym}$, i.e.

$$f_{beat} = f_{x,dym} - f_{x,analytical} = 17.429463 Hz$$

which is a phenomenon that occurs when the harmonic force is close to the natural frequency.

6.1.3.2 Force y-direction

The force in the y-direction at frame b was set to $F = 1000sin(f2\pi t)$ while the other directions were set to zero. The frequency f was set as either the analytical solution

$$f_{y,analytic} = 113.9593084Hz$$

or the solution from the free vibration test
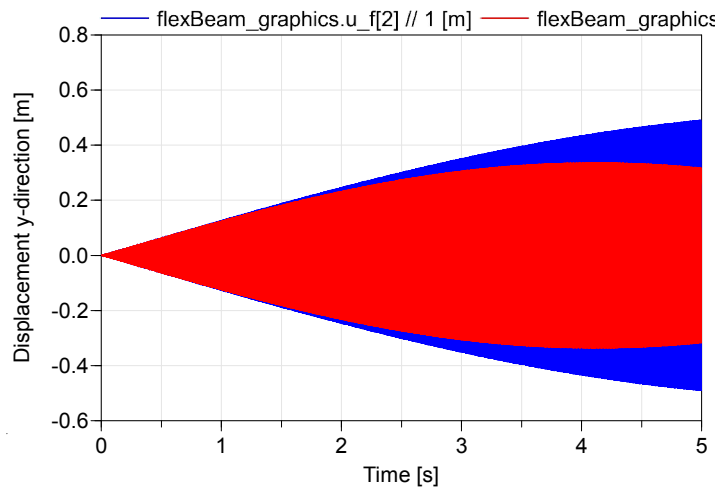
$$f_{y,dym} = 114.9425287Hz \tag{6.5}$$

FIGURE 6.25: Displacement $u_{y,dym}$ at frame b as an response to the frequency $f_{y,analytic}$. One and ten dynamic shape functions shown in blue and red colors.

As shown in Figure 6.25 the analytical frequency doesn't excite the beam in to mechanical resonance. The same result occurred with the frequency from the free vibration test. The beat frequency of the red graph in Figure 6.25 can be calculated as

$$f_{y,beat} = 0.1223391241Hz$$

Subtracting the beat frequency from the analytical frequency and the actual natural frequency of the system is obtained as

$$f_{y,actual} = f_{y,analytic} - f_{y,beat} = 113.8370449Hz$$

The displacement response from this frequency is shown in Figure 6.26 which clearly indicates mechanical resonance.
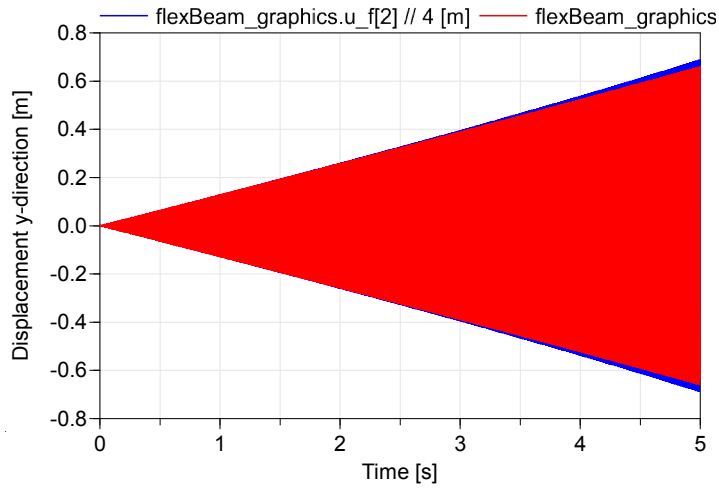

FIGURE 6.26: Displacement $u_{y,dym}$ at frame b as a response to the frequency $f_{y,actual}$. One and ten dynamic shape functions shown in blue and red colors.

The error of $f_{y,actual}$ compared to the analytical can be calculated as

$$error_{f_y} = \frac{|f_{y,beat}|}{|f_{y,analytic}|} = 0.1073533403\%$$

6.1.3.3 Force z-direction

The force in the z-direction at frame b was set to $F = 1000sin(f2\pi t)$ while the other directions were set to zero. The frequency f was set as either the analytical solution

$$f_{z,analytic} = 142.4491355 Hz$$

or the solution from the free vibration test
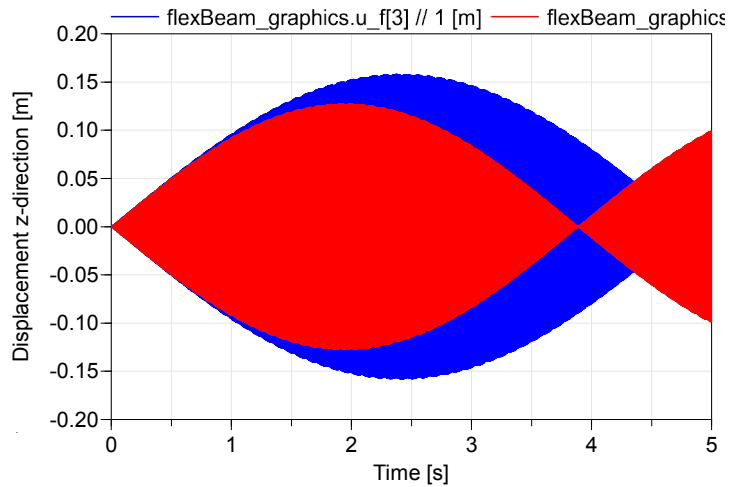
$$f_{z,dym} = 143.2664756 Hz$$

FIGURE 6.27: Displacement $u_{z,dym}$ at frame b as an response to the frequency $f_{z,analytic}$. One and ten dynamic shape functions shown in blue and red colors.

As with the forced vibration in y-direction the analytical frequency doesn't cause mechanical resonance which is presented in Figure 6.27. The same result occurred with the frequency from the free vibration test. The beat frequency of the red graph in Figure 6.27 can be calculated as

$$f_{z,beat} = 0.2571798176 Hz$$

Subtracting the beat frequency from the analytical frequency and the actual natural frequency of the system is obtained as

$$f_{z,actual} = f_{z,analytic} - f_{z,beat} = 142.1919557 Hz$$

The displacement response from this frequency is shown in Figure 6.28 which clearly indicates mechanical resonance.
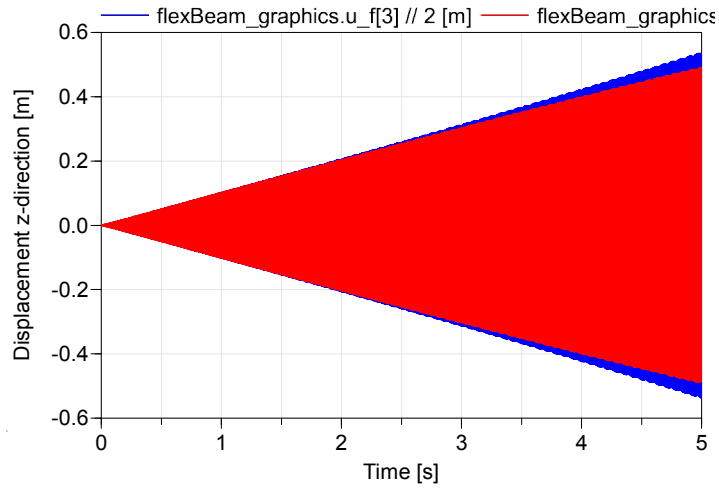
FIGURE 6.28: Displacement $u_{z,dym}$ at frame b as an response to the frequency $f_{z,actual}$. One and ten dynamic shape functions shown in red and blue colors.

The error of $f_{z,actual}$ compared to the analytical can be calculated as

$$error_{f_z} = \frac{|f_{z,beat}|}{|f_{z,analytic}|} = 0.1805415082\%$$

6.1.3.4 Torque x-axis

The torque around the x-axis at frame b was set to $M = 3000sin(f2\pi t)$ while the other directions were set to zero. The frequency f was set as either the analytical solution

$$f_{\theta_x,analytic} = 1225.978272 Hz$$

or the solution from the free vibration test

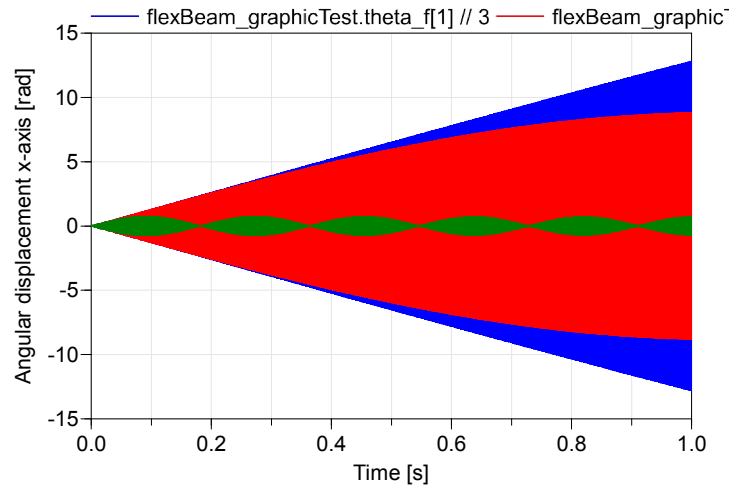$$f_{\theta_x,dym} = 1243.781095 Hz$$

FIGURE 6.29: Displacement $\theta_{x,dym}$ at frame b as a response to the frequency $f_{\theta_x,analytic}$. One, three and five dynamic shape functions shown in green, red and blue colors.

As seen in Figure 6.29, the analytical natural frequency $f_{\theta_x,analytic}$ causes the beam to excite with enough dynamic shape functions. The frequency from the free vibration test $f_{\theta_x,dym}$ had an identical behaviour as seen in Figure 6.24 for forced vibration in x-direction, although it is not presented here.

6.1.4 Gravitational Force

The implementation of the gravitational force was tested with two simple models. One model where an arbitrary beam fell freely for the duration of 1 second and it's position relative to the inertial frame was recorded, where the initial velocity and position was set to zero. One model in which the beam was fixed in frame a and free in frame b, the displacement at frame b was calculated and compared with an analytical solution for a fixed-free beam with distributed load. The geometric and material properties for the beam were: $E = 210GPa$, $\rho = 2700Kgm^{-3}$, $L = 1m$, $h = 0.1m$, $b = 0.1$ and $v = 0.3$. The models were simulated with 15000 steps and the gravitation was set to $g = 9.81ms^{-2}$ in the negative y-direction.
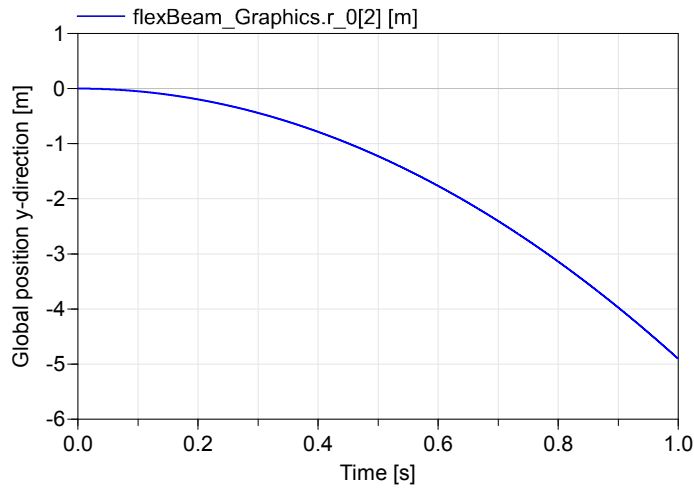
FIGURE 6.30: The y-position of the beam relative the inertial frame during free fall in the gravitational field.

As seen in Figure 6.30 the y-position of the beam is $r_{y,dym} = -4.905m$ after 1 second of free fall. The analytical solution to the problem at $t = 1s$ is

$$r_{y,analytic} = -\frac{gt^2}{2} = -4.905m$$

Which implies that the solution in Dymola and the analytical solution are identical.
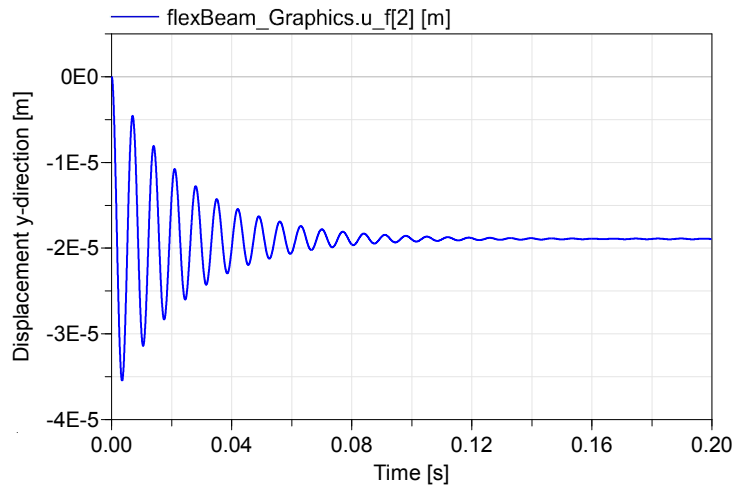

FIGURE 6.31: Displacement $u_{y,dym}$ at frame b due to gravitation, the beam is fixed in frame a. The beam is modelled with three dynamic modeshapes for the y-direction and damping set to $\delta = 10^{-3}$.

The displacement in figure 6.31 stabilizes after $t = 0.2s$ at the value

$$u_{y,dym} = -1.88872 \cdot 10^{-5}m$$

The analytical solution is obtained by approximating the gravitational force as a distributed load Q such as

$$Q = -\frac{gm}{L} = -\frac{g\rho AL}{L} = -g\rho hb = -264.87\frac{N}{m}$$

where m is the beam mass, A the cross section area. The displacement at the free end for a fixed-free beam with distributed load is [8, p. 344]

$$u_{y,analytic} = \frac{QL^3}{8EI_z} = -1.89192857 \cdot 10^{-5}m$$

The error between the analytical solution and the solution from Dymola is

$$error_{u_y} = \frac{|u_{y,dym} - u_{y,analytic}|}{|u_{y,analytic}|} = 0.169592555\%$$

6.1.5 Centrifugal Force

To test the centrifugal forces, a model was created with a beam connected to a revolute joint at frame a. The revolute joint was connected to a fixed inertial frame in the other end. Frame b was considered free and not connected to any other component. By setting the angular velocity or torque at the revolute joint to a constant value the beam would start rotating around the y-axis of the inertial frame and deform due to the arising centrifugal forces. The geometric and material properties of the beam were the same as in Section 6.1.4 and the test included three dynamic shape functions in the x- and z-direction. The test was simulated for 1 second with 15000 steps for two different setups at the revolute: the angular velocity set to $\omega = 50 rads^{-1}$ or the torque set to $M = 100Nm$. The deformation of the beam was calculated at frame b.
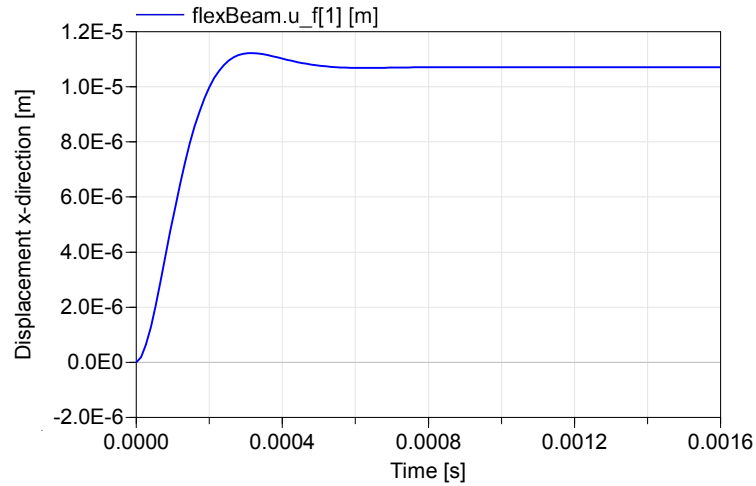
6.1.5.1 Constant Angular Velocity

FIGURE 6.32: The displacement in the x-direction $u_{x,dym}$ at frame b with constant angular velocity $\omega = 50 rads^{-1}$. Damping was set to $\delta = 10^{-4}$.

Figure 6.32 shows that the deformation $u_{x,dym}$ stabilizes after some time at

$$u_{x,dym} = 1.07144 \cdot 10^{-5} m$$

The analytical solution to the problem can be obtained by integrating the incremental elongation over the beam's length. Let the incremental elongation be defined as

$$du_{x,analytic} = \frac{x}{AE} dF = \frac{x}{E} \rho \omega^2 x dx$$

where $dF = \rho A \omega^2 x dx$ is the centrifugal force acting on an incremental mass. Integrating the incremental elongation yields

$$u_{x,analytic} = \frac{\rho \omega^2}{E} \int_0^L x^2 dx = \frac{\rho \omega^2 L^3}{3E} = 1.071428571 \cdot 10^{-5} m$$

The error between the solution in Dymola and the analytical solution can be calculated as

$$error_{u_x} = \frac{|u_{x,dym} - u_{x,analytic}|}{|u_{x,analytic}|} = 0.0010667067\%$$
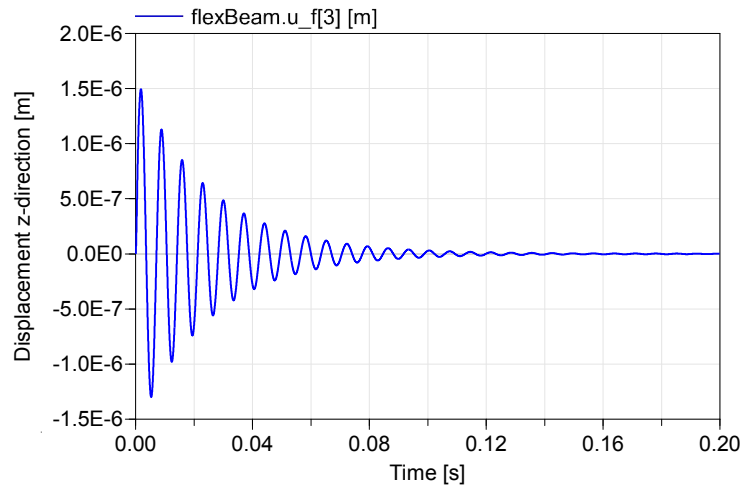
FIGURE 6.33: The displacement in the z-direction $u_{z,dym}$ at frame b with constant angular velocity $\omega = 50 rads^{-1}$. Damping was set to $\delta = 10^{-4}$.

Figure 6.33 indicates that the beam vibrates for a short duration of time in the beginning since the starting angular velocity is zero. After some time the displacement $u_{z,dym}$ stabilizes at zero due to damping.
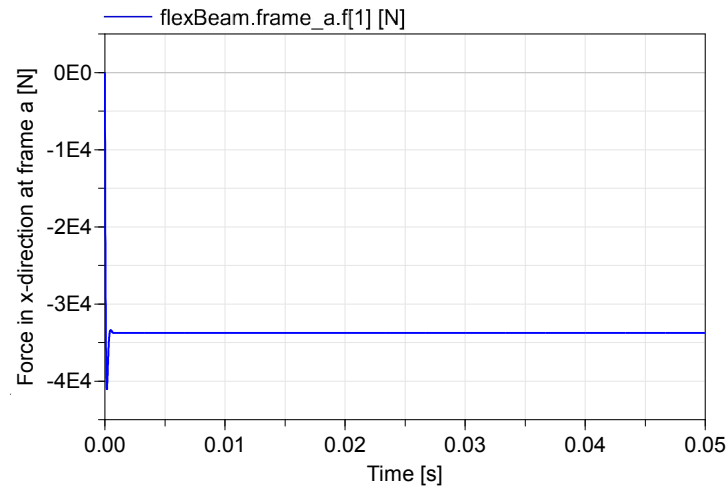

FIGURE 6.34: The force in the x-direction at frame a with constant angular velocity $\omega = 50 rads^{-1}$. Damping was set to $\delta = 10^{-4}$.

The reaction force at frame a is shown in figure 6.34, it stabilizes at the constant value

$$F_{x,dym} = -33750N$$

The analytical calculation of the force is derived by integrating the incremental centrifugal force $dF = \rho A \omega^2 x dx$ over the beam's length.

$$F_{x,analytic} = -\int_0^L \rho A \omega^2 x dx = -\frac{\rho A \omega^2 L^2}{2} = -33750N$$

Which is identical to the solution obtained in Dymola.
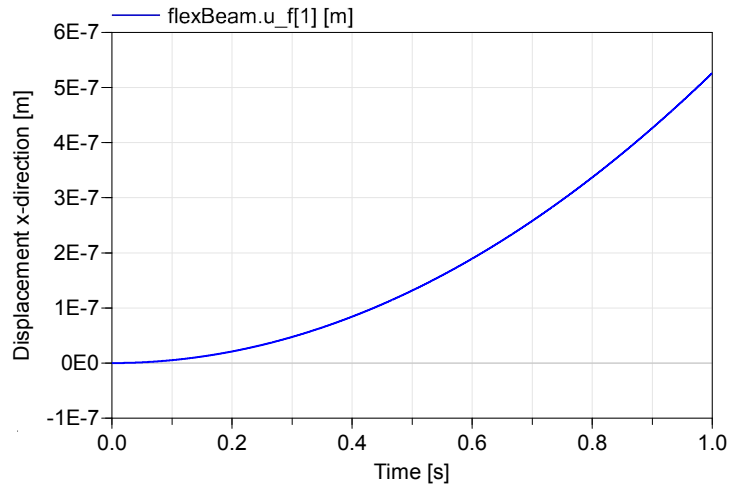
6.1.5.2 Constant Torque

FIGURE 6.35: The displacement in the x-direction $u_{x,dym}$ at frame b with constant torque $M = 100Nm$. Damping was set to $\delta = 10^{-4}$.

Figure 6.35 shows that the elongation $u_{x,dym}$ of the beam increases with time. At $t = 0.5s$ and $t = 1s$ the displacements are

$$u_{x,dym}|_{t=0.5} = 1.31563 \cdot 10^{-7}m$$
$$u_{x,dym}|_{t=1} = 5.26358 \cdot 10^{-7}m$$

The analytical solution can be obtained in a similar approach as in the case with constant angular velocity. The angular velocity at an arbitrary time t_1 is defined as

$$\omega = \int_0^{t_1} \alpha dt = \int_0^{t_1} \frac{M}{I_a} dt = \frac{M}{I_a} t_1$$

where α is the constant angular acceleration, M the applied moment at frame a, I_a the constant inertia at frame a around the y-axis. The incremental centrifugal force can then be defined as

$$dF = \rho A \omega^2 x dx = \rho A x dx (\frac{Mt_1}{I_a})^2$$

Recall that $du_{x,analytic} = \frac{x}{AE}dF$ which implies that the elongation can be calculated as

$$u_{x,analytic} = \frac{\rho}{E}\left(\frac{Mt_1}{I_a}\right)^2 \int_0^L x^2 dx = \frac{\rho M^2 L^3}{3EI_a^2}t_1^2$$

Evaluating $u_{x,analytic}$ at $t_1 = 0.5s$ and $t_1 = 1s$ yields

$$u_{x,analytic}|_{t=0.5} = 1.316162285 \cdot 10^{-7}m$$

$$u_{x,analytic}|_{t=1} = 5.264649141 \cdot 10^{-7}m$$

where it has been used that

$$I_a = \frac{m(h^2 + L^2)}{12} + m\frac{L^2}{4}$$

The error between the solution in Dymola and the analytical solution at these two points becomes

$$error_{u_x,t=0.5} = 0.0404422248\%$$
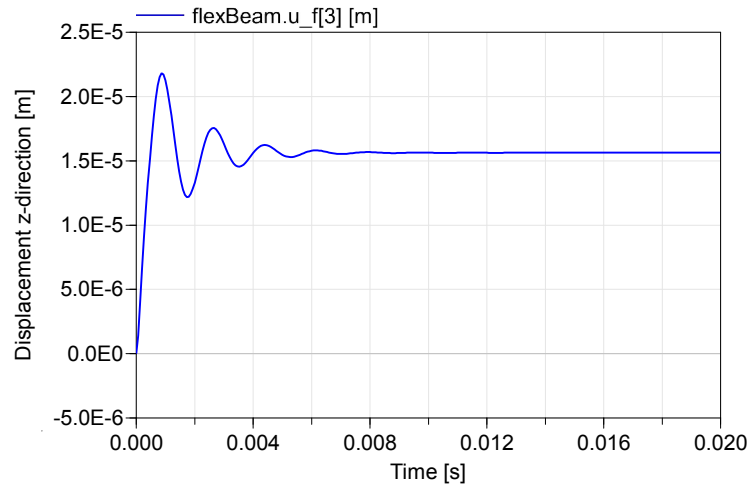
$$error_{u_x,t=1} = 0.0203079256\%$$

FIGURE 6.36: The displacement in the z-direction $u_{z,dym}$ at frame b with constant torque $M = 100Nm$. Damping was set to $\delta = 10^{-4}$.

The bending deformation in the z-direction at frame b, $u_{z,dym}$, is shown in Figure 6.36. The deformation at $t = 0.02s$ is

$$u_{z,dym} = 1.563 \cdot 10^{-5}m$$

The analytical solution can be derived considering that the tangential acceleration a_t acting on a infinitesimal thin section can be written as

$$a_t = \frac{dv_t}{dt} = \frac{d(\omega x)}{dt} = \alpha x = \frac{M}{I_a} x$$

Where v_t is the tangential velocity of the section. The incremental force acting on this section becomes

$$dF = a_t dm = \frac{M}{I_a} x \rho A dx$$

Which indicates that the force acts as a linear increasing distributed load with respect to the x coordinate. The distributed load Q can be calculated as

$$Q = \frac{F}{L} = \frac{M\rho A}{L I_a} \int_0^L x dx = 149.6259352 \frac{N}{m}$$

The displacement can be derived considering that the load causes the beam to deflect relative it's local coordinate system in frame a. In the local coordinate system the beam is considered fixed in frame a and free in frame b, which implies that the displacement is given by [8, p. 344]

$$u_{z,analytic} = \frac{11QL^3}{60EI_y} = 1.567509797 \cdot 10^{-5} m$$

The error between the solution in Dymola and the analytical solution is

$$error_{u_z} = \frac{|u_{z,dym} - u_{z,analytic}|}{|u_{z,analytic}|} = 0.2877045708\%$$

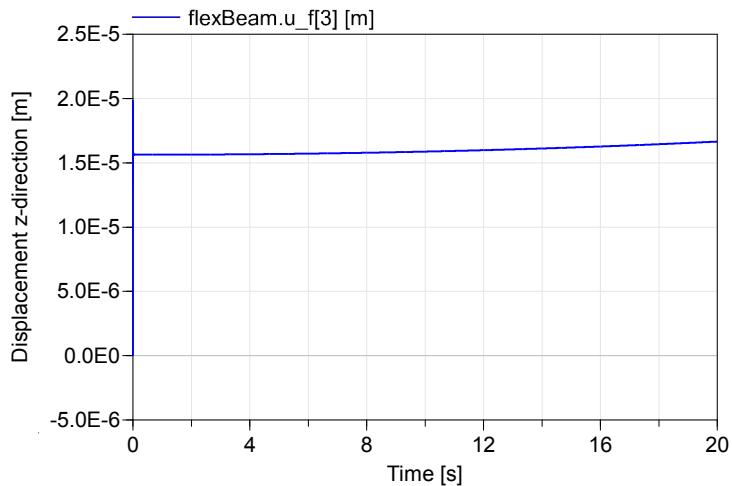### 6.1.5.3 Constant Torque - Increased Simulation Time

FIGURE 6.37: The deformation in the z-direction $u_{z,dym}$ at frame b with constant torque $M = 100Nm$. Damping was set to $\delta = 10^{-4}$. Simulation time is 20 seconds.

The analytical solution $u_{z,analytic}$ proposed in Section 6.1.5.2 implies that the deformation is constant for a constant torque applied at frame a. The results from the simulation in Dymola and the analytic solution coincide if the simulation time is short. If the simulation time is increased, i.e. the force is applied for a longer duration, then $u_{z,dym}$ increases with time. The phenomenon is presented in Figure 6.37 where the same model has been simulated for 20 seconds with 30000 steps.

Consequently the reaction force in the z-direction at frame a increases as shown in Figure 6.38.
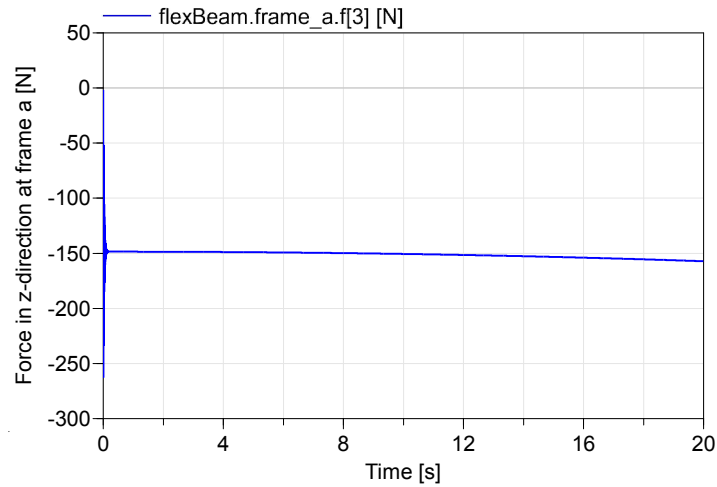

FIGURE 6.38: The force in the z-direction at frame a with constant torque $M = 100Nm$. Damping was set to $\delta = 10^{-4}$. Simulation time is 20 seconds.

The angular acceleration of the revolute joint slightly decreases at the same time presented in Figure 6.39.
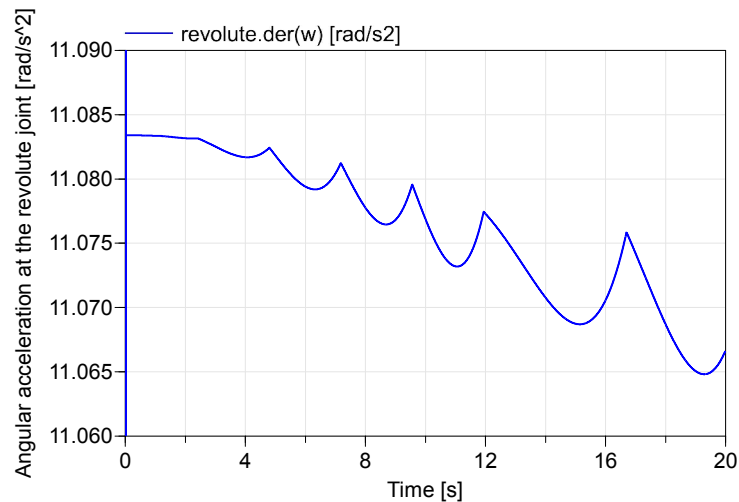

FIGURE 6.39: The angular acceleration at the revolute joint with constant torque $M = 100Nm$. Damping was set to $\delta = 10^{-4}$. Simulation time is 20 seconds.

6.2 One-Dimensional Models

To verify the one-dimensional the models same tests were preformed as those done for the three-dimensional model. Hence three tests were made: static loading, free vibration and force vibrations. A cantilever beam was used i.e. the beam is fixed in *flange_a* and free at *flange_b*. Force was applied at *flange_b* and the displacement was calculated at the same flange. A flange is a connector used for one-dimensional bodies in the same way as frames are used in three-dimensional bodies.

During the static load case the beam was subjected to a linearly increasing load for a specified time and then kept constant. The displacement at the end of the simulation was then compared to analytical solution of an Euler Bernoulli beam. In the free vibration test the initial displacement was set to a specific value and then the beam could vibrate freely. The time period of the response was measured and the natural frequency was calculated and compared to analytical solutions. To test the forced vibration a periodic force with a frequency equal to the natural frequency was applied.

6.2.1 Static Loading

In the translational test the same parameters were used as in the static loading of the three-dimensional beam model. The load case was identical to the load case in x-direction preformed in section 6.1.1.1.

In the rotational test the same parameters were used as in the static loading of the three-dimensional beam model. This test was identical to the load case, Torque x-axis in section 6.1.1.4.

6.2.1.1 Translational

Dymola solution, figure 6.40

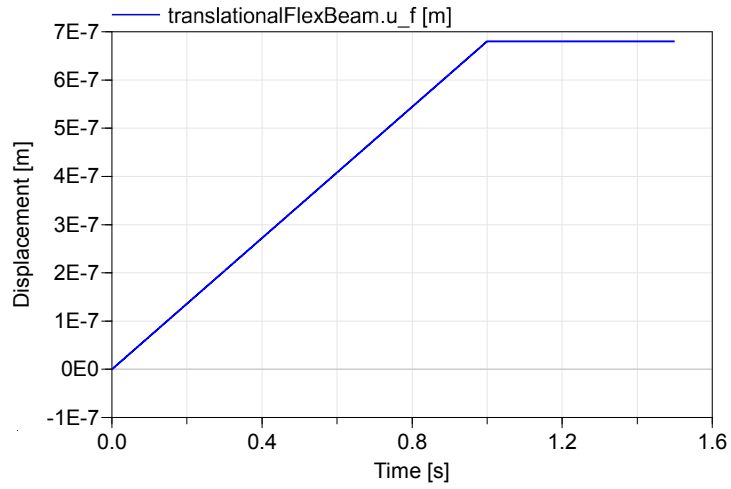$$u_{dym} = 6.80272 \cdot 10^{-7} m$$

FIGURE 6.40: Displacement u_{dym} at flange b as a response to the static load

Analytical solution [4, p. 21]

$$u_{x,analytic} = \frac{FL}{AE} = 6.802721088 \cdot 10^{-7} m$$

Error difference

$$error_{u_x} = \frac{|u_{dym} - u_{analytic}|}{|u_{analytic}|} = 1.599936 \cdot 10^{-5} \%$$

6.2.1.2 Rotational
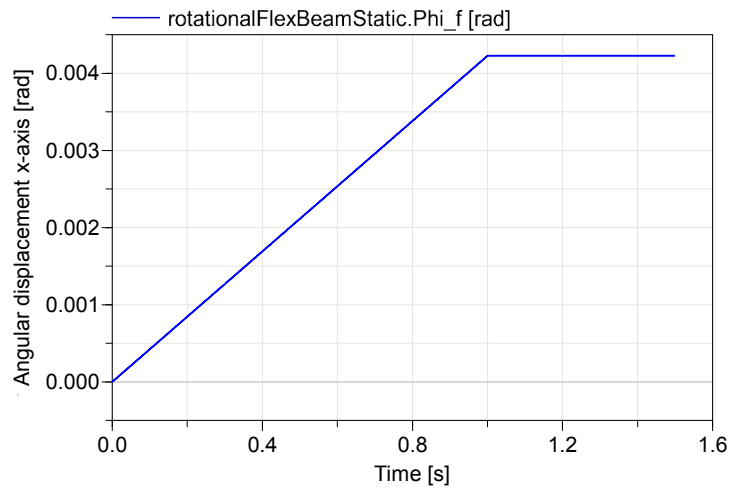
Dymola solution

$$\theta_{dym} = 4.2259 \cdot 10^{-3}$$

FIGURE 6.41: Angular deformation θ_{dym} at flange b as a response to the static torque

Analytical solution [4, p. 65]

$$\theta_{analytic} = \frac{ML}{GK} = 4.2259015 \cdot 10^{-3}$$

Error difference

$$error_\theta = \frac{|\theta_{dym} - \theta_{analytic}|}{|\theta_{analytic}|} = 3.549538483 \cdot 10^{-5}\%$$

6.2.2 Free Vibrations

In this test the same parameters as in the three-dimensional test case were used, see Section 6.1.2. Tests were done with one, three and ten dynamic shape functions respectively. The natural frequency were calculated from the time period measured in Dymola. This frequency was then compared with the analytical solution. Note that the test preformed with three dynamic mode shapes had damping in the system with $\delta = 10^{-6}$.

6.2.2.1 Translational

The initial deformation at flange b was set to $u_0 = 2.5 \cdot 10^{-4}m$. The responses for the different number of dynamic mode shapes can be seen in Figures 6.42, 6.43 and 6.44
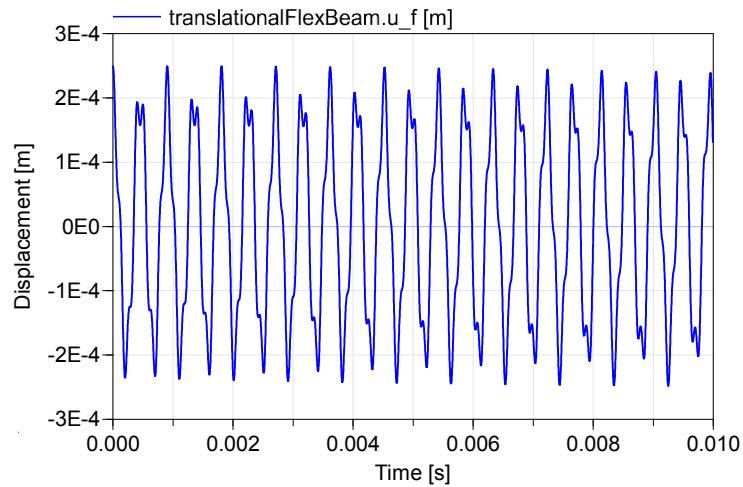

FIGURE 6.42: Free vibration of the translational model, one dynamic mode shape
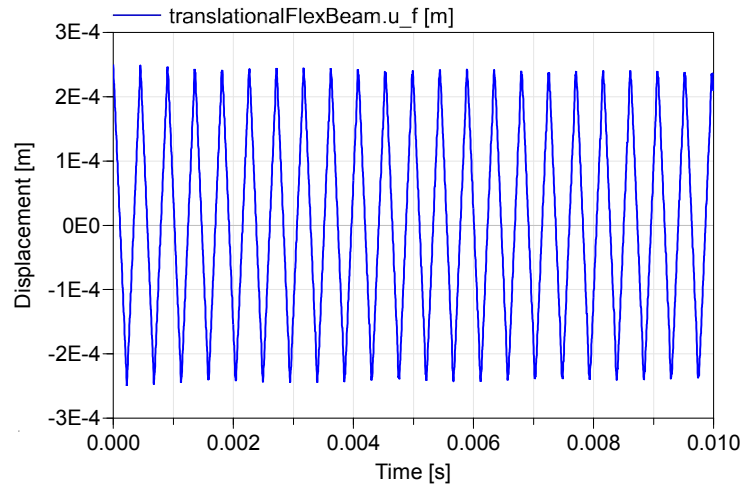
FIGURE 6.43: Free vibration of the translational model, ten dynamic modes shapes

FIGURE 6.44: Free vibration of the translational model, three dynamic modes shapes.
Damping $\delta = 10^{-6}$

The first natural frequency for a beam, fixed in one end and free in the other, is [3, p. 309-310]

$$f_{x,analytic} = \frac{1}{4L}\sqrt{\frac{E}{\rho}} = 2204.792751 Hz$$

The period from the test cases in Dymola was measured as

$$T_{x,dym} = 0.00045s \tag{6.6}$$

which yields the natural frequency

$$f_{x,dym} = \frac{1}{T_{x,dym}} = 2222.222222 Hz$$

Error

$$error_{f_x} = \frac{|f_{x,dym} - f_{x,analytic}|}{|f_{x,analytic}|} = 0.7905261459\%$$

6.2.2.2 Rotational

The initial deformation at flange b was set to $\theta_{x,0} = 3.75 \cdot 10^{-4}$. The response can be seen in Figures 6.45, 6.43 and 6.47. Note that the test preformed with three dynamic mode shapes had damping in the system $\delta = 10^{-6}$.

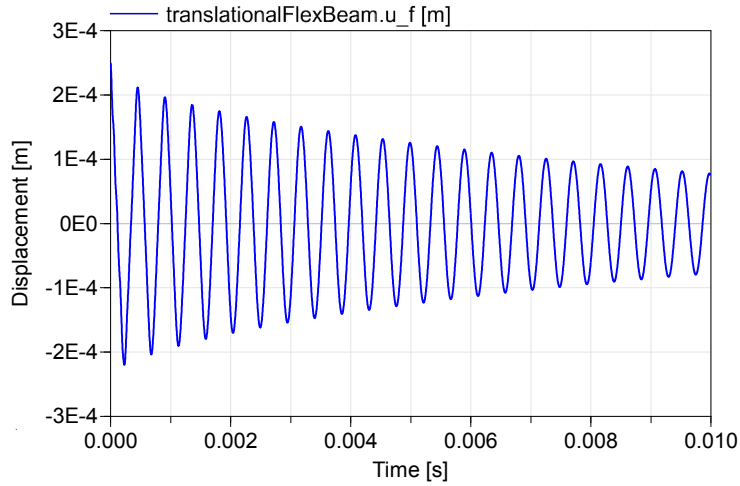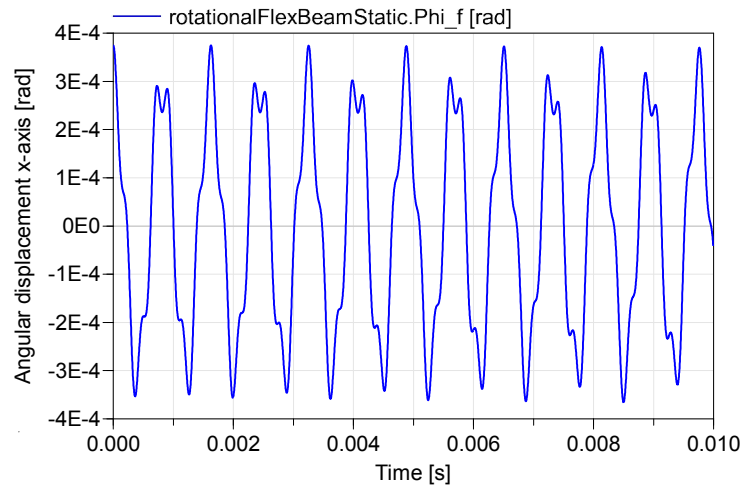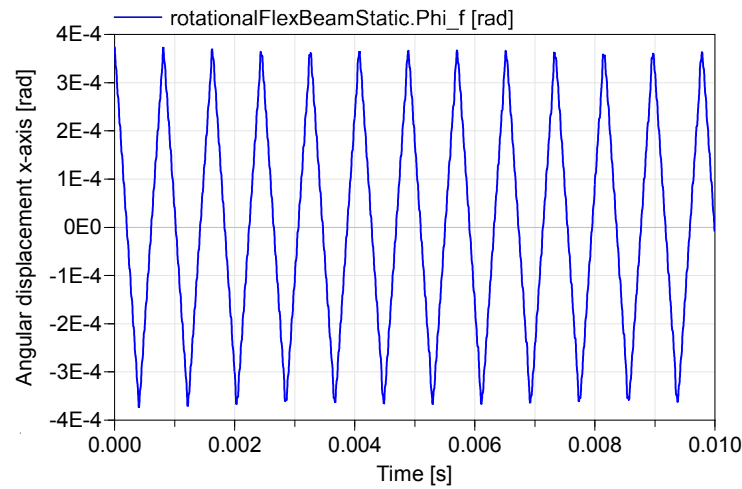FIGURE 6.45: Free vibration of the rotational model, one dynamic mode shape.

FIGURE 6.46: Free vibration of the rotational model, ten dynamic mode shapes.
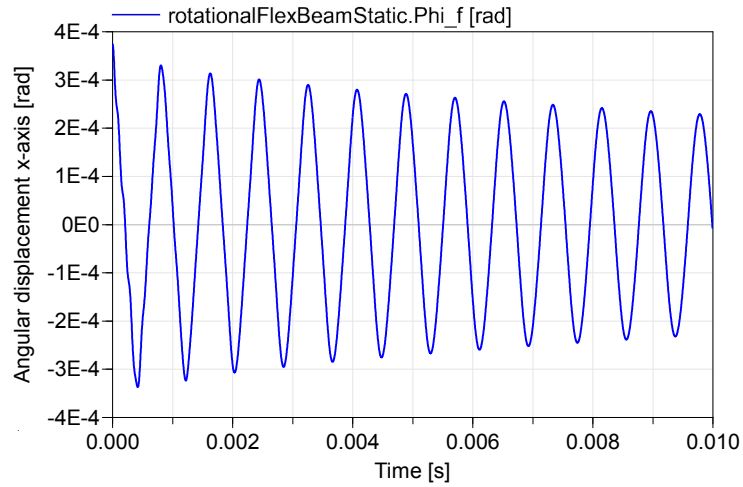
FIGURE 6.47: Free vibration of rotational model, three dynamic mode shape. Damping $\delta = 10^{-6}$

The first natural frequency for a beam fixed in one end and free in the other is [3, p. 325-326]

$$f_{\theta_x,analytic} = \frac{1}{4L}\sqrt{\frac{GK}{J_x}} = 1225.978272Hz$$

where J_x is the moment of inertia around the x-axis per unit length calculated as $J_x = \frac{\rho A}{12}(b^2 + h^2)$. The period from the test cases in Dymola was measured as

$$T_{\theta_x,dym} = 0.000804s \tag{6.7}$$

which yields the natural frequency

$$f_{\theta_x,dym} = \frac{1}{T_{x,dym}} = 1243.781095Hz$$

Error

$$error_{f_{\theta_x}} = \frac{|f_{\theta_x,dym} - f_{\theta_x,analytic}|}{|f_{\theta_x,analytic}|} = 1.452132016\%$$

6.2.3 Forced Vibrations

The force vibration test used a harmonic applied force at flange b with a frequency corresponding to the eigenfrequency of the beam.

6.2.3.1 Translational

The force in flange b was set to $F = 1000sin(f2\pi t)$. The frequency f was set to the analytical solution

$$f_{analytic} = 2204.792759 Hz$$

The responses can be seen in Figure 6.48

FIGURE 6.48: Displacement u_{dym} at flange b as a response to the frequency $f_{analytic}$. One, three and five dynamic shape functions shown in green, red and blue colors.

Figure 6.48 shows that excitation occurs for the analytical eigenfrequency. It's clear that more dynamic mode shapes gives a better excitation behaviour. The beating phenomena is also present in this model.

6.2.3.2 Rotational

The torque at flange b was set to $M = 3000sin(f2\pi t)$. The frequency f was set to the analytical solution

$$f_{\theta,analytic} = 1225.978272 Hz$$

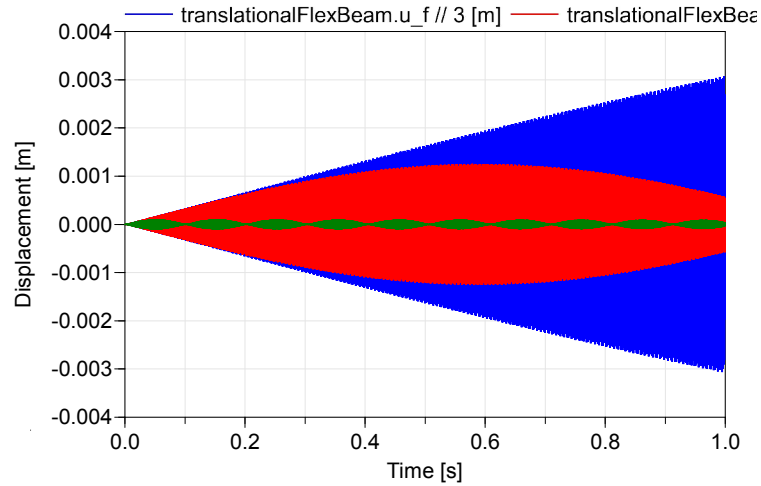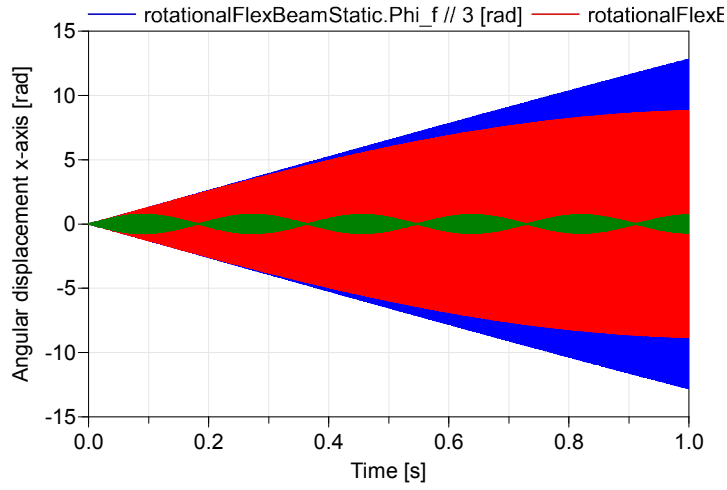The response can be seen in Figure 6.49.

FIGURE 6.49: Deformation θ_{dym} at flange b as an response to the frequency $f_{\theta,analytic}$. One, three and five dynamic shape functions shown in green, red and blue colors.

Figure 6.49 show the same kind of response as the translational model. More dynamic mode shapes give a better excitation behaviour. The beating behaviour occur in this model as well due to the differences of $f_{\theta,dym}$ and $f_{\theta,analytic}$

6.2.4 Comparison in Dynamic Response

A comparison was made between the one-dimensional models, three-dimensional model and an analytical solution of a dynamic response in a cantilever beam. The analytical solution was taken from problem 5.6 in [14, p. 3]. The problem is a cantilever beam that is subjected to a force in the direction of the beam. The solution can be written as [14, p. 24]

$$u(x,t) = \frac{P}{EA}x - \frac{8PL}{\pi^2 AE} \sum_{i=1}^{n} \frac{(-1)^{i-1}}{(2i-1)^2} sin\left(\frac{(2i-1)\pi x}{2L}\right) cos\left((2i-1)\frac{\pi c}{2L}t\right) \qquad (6.8)$$

with the parameter values $P = 10000N$, $\rho = 8000\frac{kg}{m^3}$, $L = 1m$, $A = 2 \times 10^{-4}m^2$, $c = \sqrt{\frac{EA}{m}}$, $m = \rho A$ $t = 0 \ldots 0.05$. In this simulation 5000 time steps were used and $n = 10$ is the number of mode shapes used. The displacement was investigated at $x = 0.5m$.

This solution was compared with the one-dimensional and three-dimensional model with the same values on parameters and force. Ten dynamic mode shapes were used in the simulations. The responses can be seen in Figures 6.50, 6.51 and 6.52.
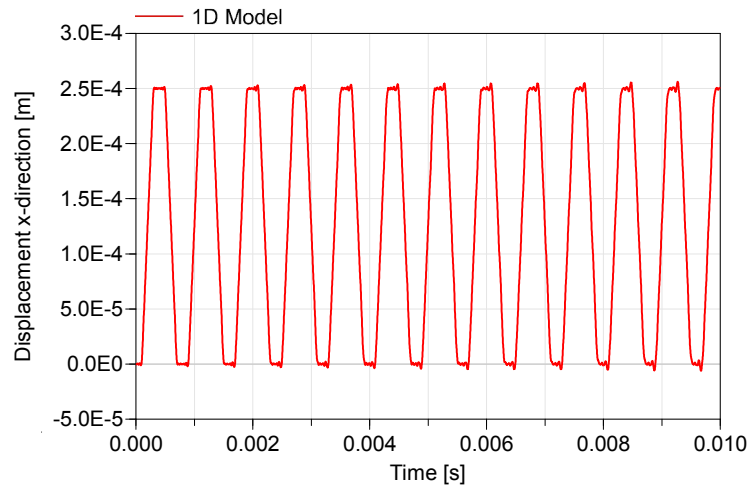
FIGURE 6.50: Dynamic response of the one-dimensional translational beam model at $x = 0.5m$
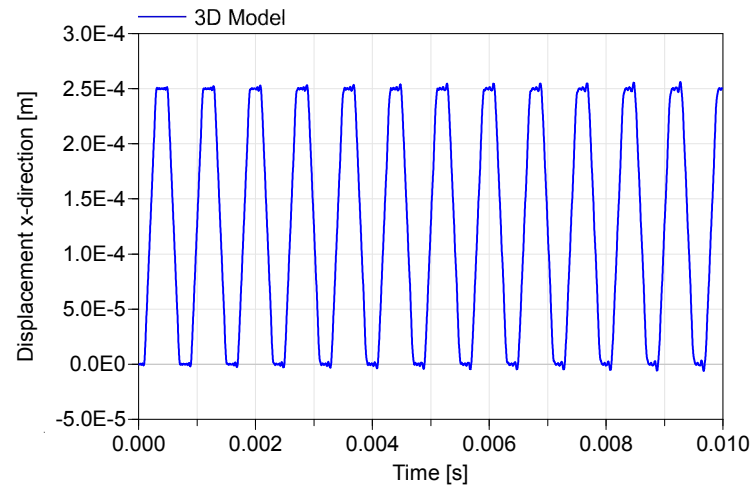

FIGURE 6.51: Dynamic response of the three-dimensional beam model in the x-direction at $x = 0.5m$
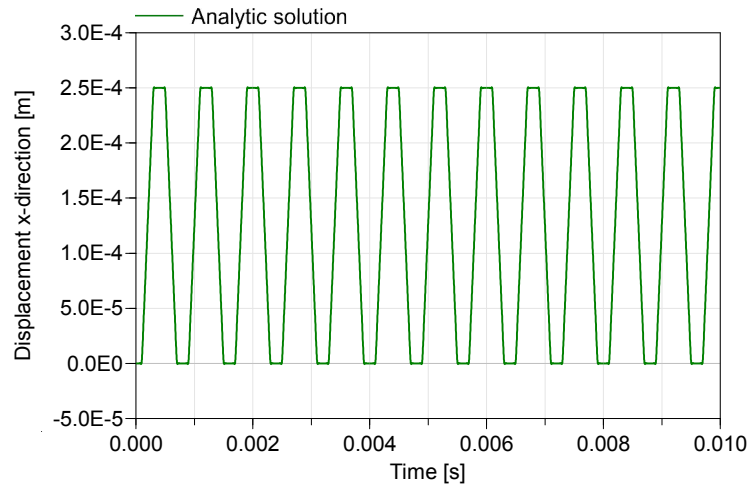
FIGURE 6.52: Dynamic response of the analytical solution at in the x-direction at
$x = 0.5m$

The solution of problem 5.6 in [14, p. 3] can be used as a solution to the rotational problem as well. This is due to the similarities in the governing equation in 1.1 and 1.2. The solution will be

$$\theta(x,t) = \frac{M}{GK}x - \frac{8ML}{\pi^2 GK} \sum_{i=1}^{n} \frac{(-1)^{i-1}}{(2i-1)^2} sin\left(\frac{(2i-1)\pi x}{2L}\right) cos\left((2i-1)\frac{\pi c}{2L}t\right) \quad (6.9)$$

with $M = 100Nm$, $\rho = 8000\frac{kg}{m^3}$, $L = 1m$, $b = 0.1m$, $h = 0.1m$, $E = 200 \times 10^9$, $v = 0.3$ $G = \frac{E}{2(v+1)}$, $c = \sqrt{\frac{GK}{\rho I_p}}$, $I_p = \frac{bh(b^2+h^2)}{12}$ $t = 0 \dots 0.05$ During the simulation 5000 time steps were used. The number of shape functions used is $n = 10$. In the one-dimensional and three-dimensional models, ten dynamic mode shapes are used. The displacement was investigated at $x = 0.5m$. Note that M is a constant torque applied in flange b. The responses can be seen in Figures 6.53, 6.54 and 6.55.

FIGURE 6.53: Dynamic response of the one-dimensional rotational beam model at $x = 0.5m$

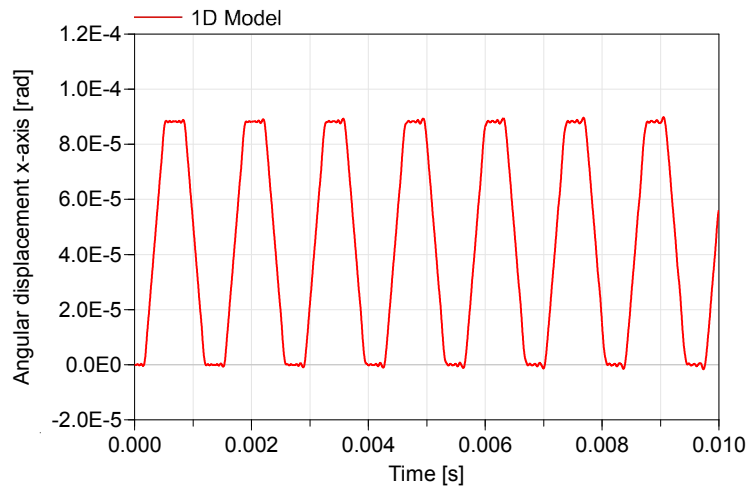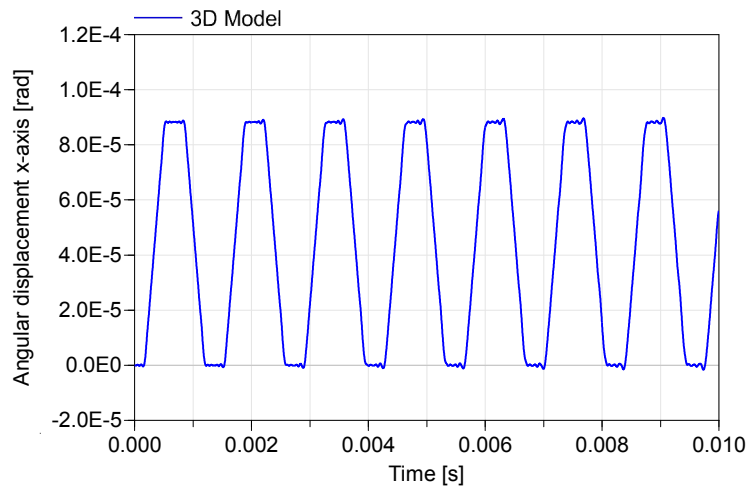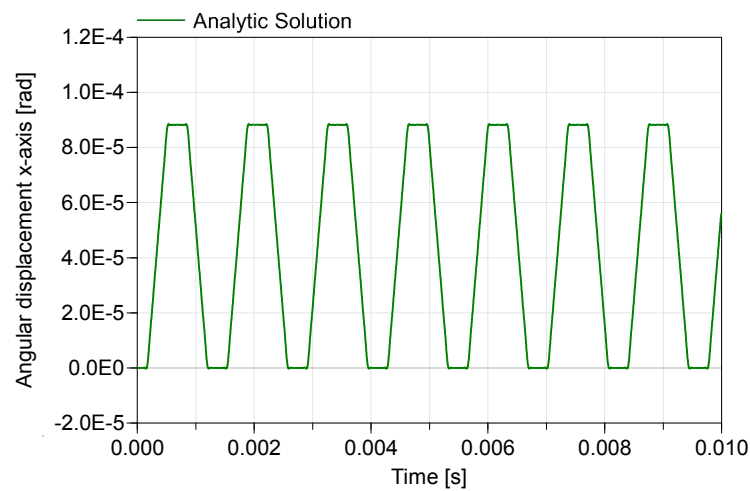FIGURE 6.54: Dynamic response of the three-dimensional beam model at $x = 0.5m$

FIGURE 6.55: Dynamic response of the analytic solution at $x = 0.5m$

6.3 Summary of Errors from the Validation

The substantial results from the validation process are gathered here in a more compact format to give the reader an overview of the accuracy of the model.

6.3.1 Three Dimensional Model

The errors from the different test cases for the three-dimensional model are presented in Tables 6.1, 6.2, 6.8, 6.4 and 6.5.

Static Load/ Error	$u_x(\%)$	$u_y(\%)$	$u_z(\%)$	$\theta_x(\%)$	$\theta_y(\%)$	$\theta_z(\%)$
Force x	$1.6 \cdot 10^{-5}$	–	–	–	–	–
Force y	–	$1.49 \cdot 10^{-4}$	–	–	–	$8.94 \cdot 10^{-5}$
Force z	–	–	$5.75 \cdot 10^{-5}$	–	$6.5 \cdot 10^{-5}$	–
Torque x	–	–	–	$3.55 \cdot 10^{-5}$	–	–
Torque y	–	–	$1.31 \cdot 10^{-4}$	–	$1.35 \cdot 10^{-4}$	–
Torque z	–	$1.73 \cdot 10^{-4}$	–	–	–	$1.28 \cdot 10^{-4}$

TABLE 6.1: The deformation error results from the static loading test cases for the three dimensional model.

Free Vibration/ Error	$f_x(\%)$	$f_y(\%)$	$f_z(\%)$	$f_{\theta_x}(\%)$
Initial Deformation x-dir.	0.79	–	–	–
Initial Deformation y-dir.	–	0.86	–	–
Initial Deformation z-dir.	–	–	0.57	–
Initial Deformation x-axis.	–	–	–	1.45

TABLE 6.2: The frequency error results from the free vibration test cases for the three-dimensional model.

Forced Vibration/ Error	$f_x(\%)$	$f_y(\%)$	$f_z(\%)$	$f_{\theta_x}(\%)$
Force x-dir.	0	–	–	–
Force y-dir.	–	0.11	–	–
Force z-dir.	–	–	0.18	–
Torque x-axis.	–	–	–	0

TABLE 6.3: The frequency error results from the forced vibration test cases for the three-dimensional model.

Gravitational Force/ Error	$r_y(\%)$	$u_y(\%)$
Free Fall	0	–
Fixed-Free Grav. Load	–	0.17

TABLE 6.4: The error results from the gravitational test cases for the three-dimensional model.

Centrifugal Force/ Error	$u_x(\%)$	$u_x|_{t=0.5}(\%)$	$u_x|_{t=0.5}(\%)$	$u_z(\%)$	$F_x(\%)$
Const. Ang. Vel.	0.001	–	–	–	0
Const. Torque	–	0.04	0.02	0.29	–

TABLE 6.5: The error results from the centrifugal test cases for the three-dimensional model.

6.3.2 One Dimensional Models

The errors from the different test cases for the one-dimensional models are presented in Tables 6.6, 6.7 and 6.8.

Static Load/ Error	$u_x(\%)$	$\theta_x(\%)$
Translational	$1.6 \cdot 10^{-5}$	–
Rotational	–	$3.55 \cdot 10^{-5}$

TABLE 6.6: The deformation error results from the static loading test cases for the one-dimensional models.

Free Vibration/ Error	$f_x(\%)$	$f_{\theta_x}(\%)$
Translational	0.79	–
Rotational	–	1.45

TABLE 6.7: The frequency error results from the free vibration test cases for the one-dimensional models.

Forced Vibration/ Error	$f_x(\%)$	$f_{\theta_x}(\%)$
Translational	0	—
Rotational	—	0

TABLE 6.8: The frequency error results from the forced vibration test cases for the one-dimensional models.

Chapter 7

Applications

In addition to the validation of displacements and dynamic behaviour the beam was tested in a common mechanical application, namely the slider crank mechanism. The idea was to verify that the beam model works properly when connected to other components in a more complex mechanical system than those presented in Chapter 6. Additionally it was also of interest to sample the computational time of such an application and compare the required computational time for models with rigid or flexible beams.

7.1   Slider Crank

The slider crank model (Figure 7.2) was constructed in three different ways, one with both crank and rod as rigid beams, one with crank as rigid and rod as flexible and one with both crank and rod as flexible beams. The rigid model worked as a reference to validate the forces in the flexible models. All three of the models were connected in identical ways and the material properties of the components in the models were equal. The crank was connected to the inertial frame through a revolute joint in order to constrain the movement in the $x-y$ plane. The crank, rod and piston were connected together with a universal and a spherical joint as seen in Figure 7.1. The movement of the piston was constrained by connecting with a prismatic joint which only allowed a translational movement along the x-axis of the inertial frame.
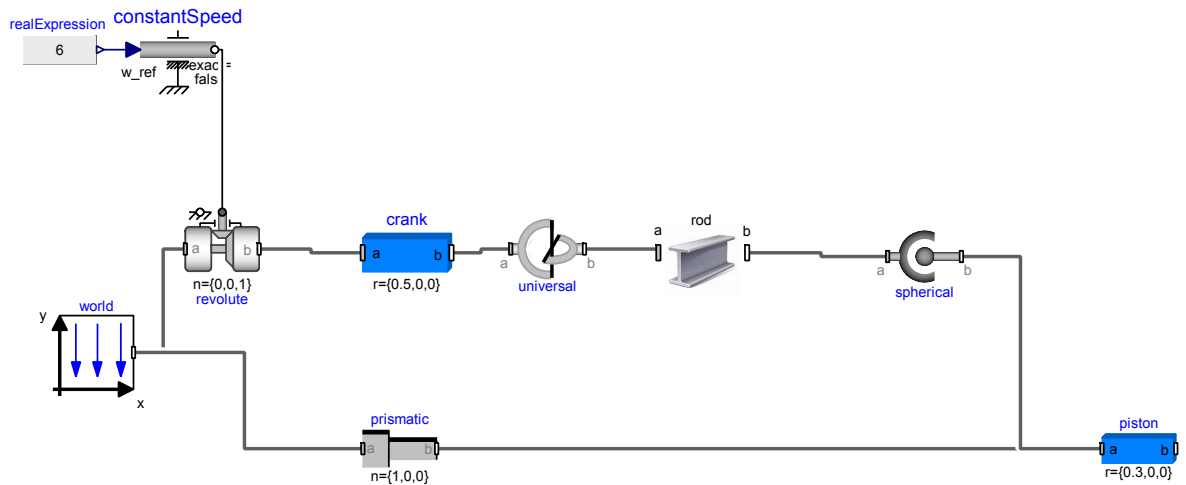
FIGURE 7.1: Overview of the slider crank model with rigid crank and flexible rod.

The angular velocity at the revolute joint was set to $\omega_z = 6 rads^{-1}$ and the initial angle to $\phi_z = 45 \deg$ relative the x-axis of the inertial frame. The initial position of the model can be seen in Figure 7.2. The geometric and material properties of the crank, rod and piston is shown in Table 7.1.
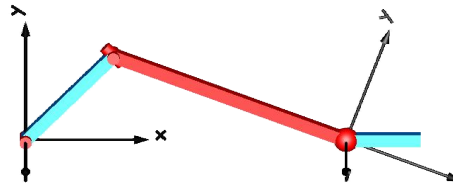

FIGURE 7.2: Animation of the initial position of the slider crank model. Frame b is visualized at the right end of the red beam. The crank, rod and piston is seen from left to right in the same order.

Property	Crank	Rod	Piston
Length L	$0.5\ m$	$1\ m$	$0.3\ m$
Height h	$0.05\ m$	$0.05\ m$	$0.05\ m$
Width b	$0.05\ m$	$0.05\ m$	$0.05\ m$
Density ρ	$2700\ \frac{kg}{m^3}$	$2700\ \frac{kg}{m^3}$	$7700\ \frac{kg}{m^3}$
Mass m	$3.375\ kg$	$6.75\ kg$	$5.775\ kg$
Young's Modulus E	$210\ GPa$	$210\ GPa$	(Rigid)
Poisson's Ratio	0.3	0.3	(Rigid)

TABLE 7.1: Geometric and material properties for the different components. The elastic properties are only applied to the flexible parts.

7.1.1   Forces and Deformation

The number of dynamic shape functions used in the flexible beams were chosen to be three in the x-direction and three in the y-direction since they were the only directions of possible deformation. The three models were simulated for 3 seconds with 5000 steps and damping set to $\delta = 10^{-4}$. The forces at frame b of the rod in the rigid model are shown in Figures 7.3 and 7.4. Note that all the forces and displacements presented here are defined in the local coordinate system of frame b, which is rotated relative the inertial frame depending on the orientation of the beam (see Figure 7.2).

FIGURE 7.3: Force in the x-direction at frame b of the rod (rigid model).

FIGURE 7.4: Force in the y-direction at frame b of the rod (rigid model).

The forces in the rigid model can be compared with the forces at the same location in the model with a flexible rod shown in Figures 7.5 and 7.6 or the model with both flexible crank and rod presented in Figures 7.7 and 7.8.
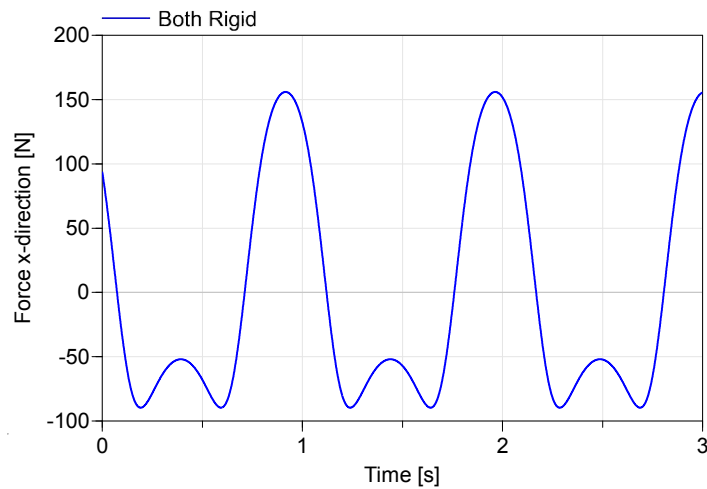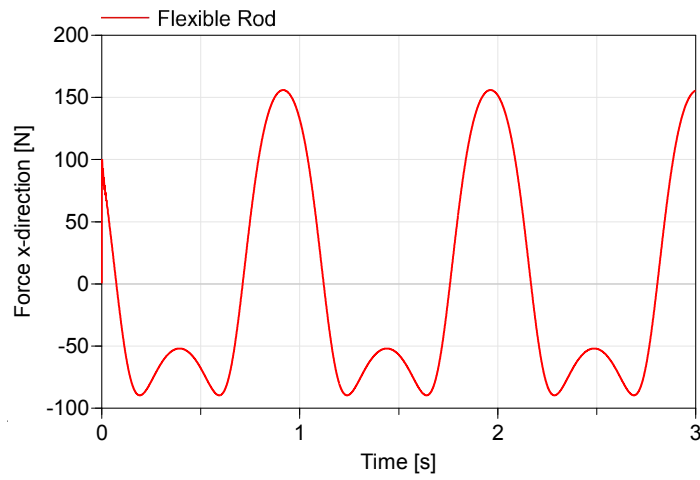
FIGURE 7.5: Force in the x-direction at frame b of the rod (rigid crank, flexible rod).
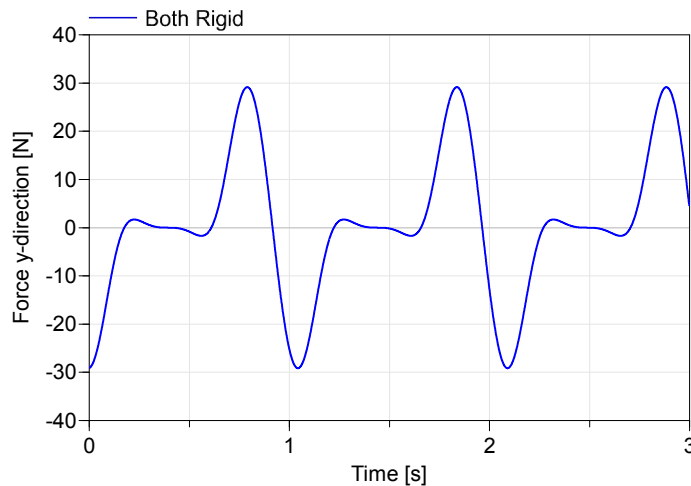

FIGURE 7.6: Force in the y-direction at frame b of the rod (rigid crank, flexible rod).
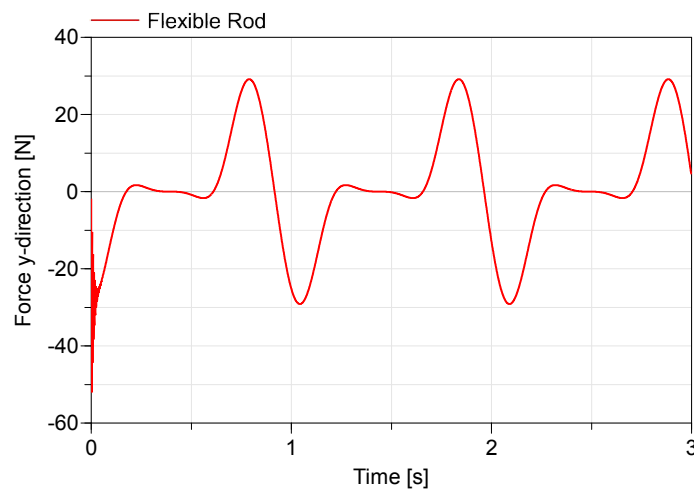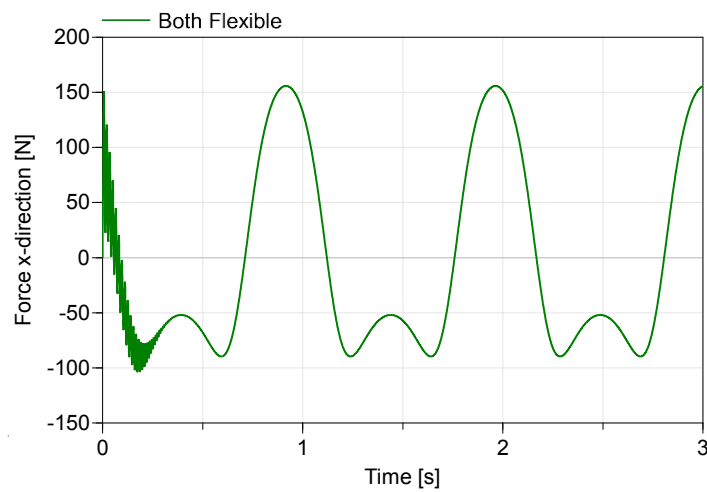

FIGURE 7.7: Force in the x-direction at frame b of the rod (flexible crank, flexible rod).

FIGURE 7.8: Force in the y-direction at frame b of the rod (flexible crank, flexible rod).

The response in deformation to these forces are presented in Figure 7.9 and 7.10 for the model with rigid crank and flexible rod as well as Figures 7.11 and 7.12 for the model with flexible crank and rod.
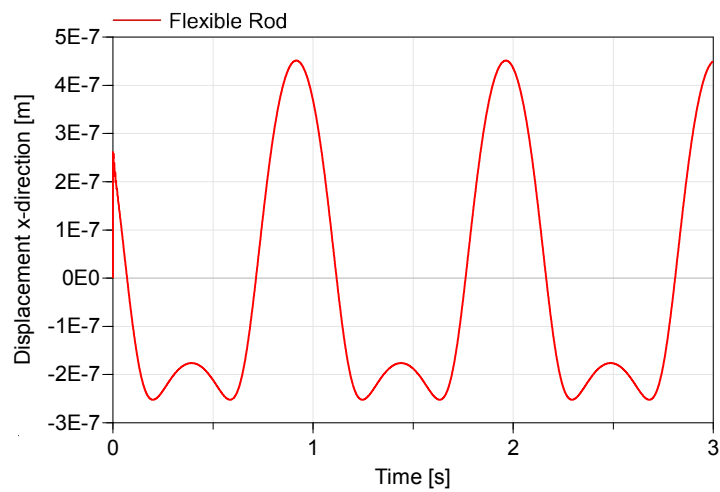
FIGURE 7.9: Displacement in the x-direction at frame b of the rod (rigid crank, flexible rod).
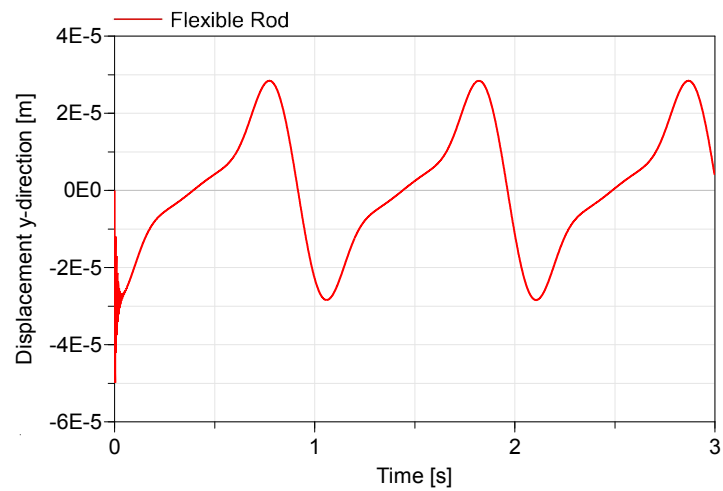
FIGURE 7.10: Displacement in the y-direction at frame b of the rod (rigid crank, flexible rod).

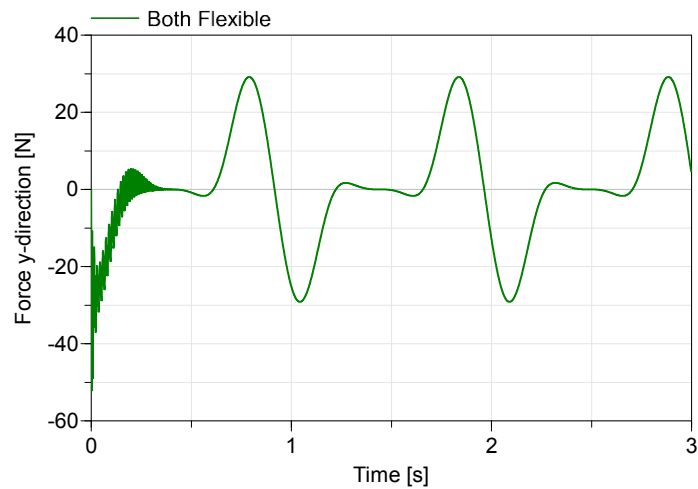FIGURE 7.11: Displacement in the x-direction at frame b of the rod (flexible crank, flexible rod).
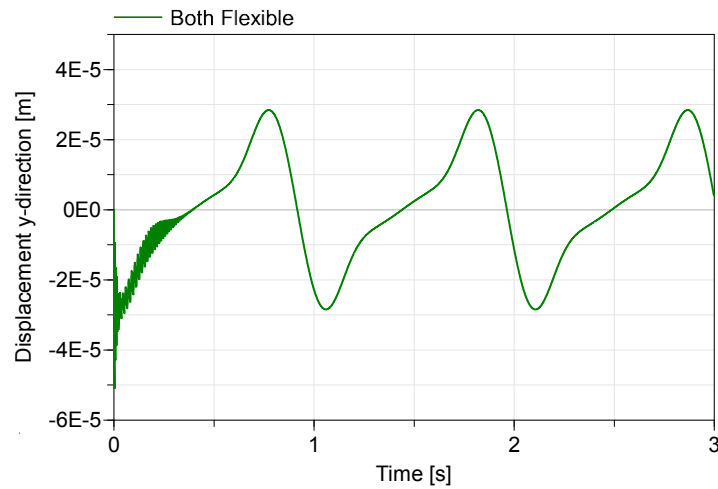
FIGURE 7.12: Displacement in the y-direction at frame b of the rod (flexible crank, flexible rod).

As seen in Figures 7.9, 7.10, 7.11 and 7.12 the rod is influenced by vibrations in the beginning of the simulation which later disappears due to damping. By comparing the figures one can see that the model with two flexible beams vibrates differently and more intense than the one with only a flexible rod. A close up on the displacements of the model with flexible crank and rod is presented in Figures 7.13 and 7.14.
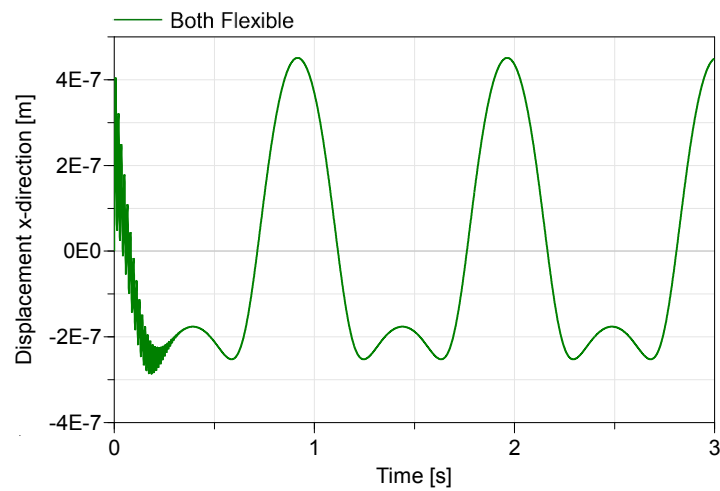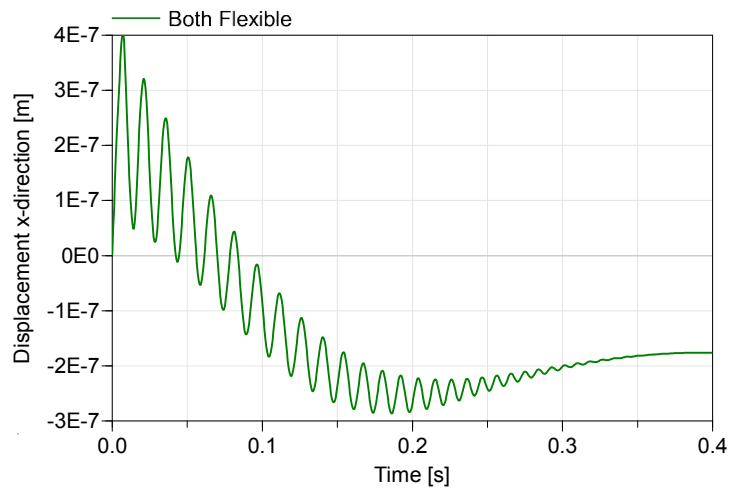

FIGURE 7.13: Close up on the displacement in the x-direction at frame b of the rod (flexible crank, flexible rod).
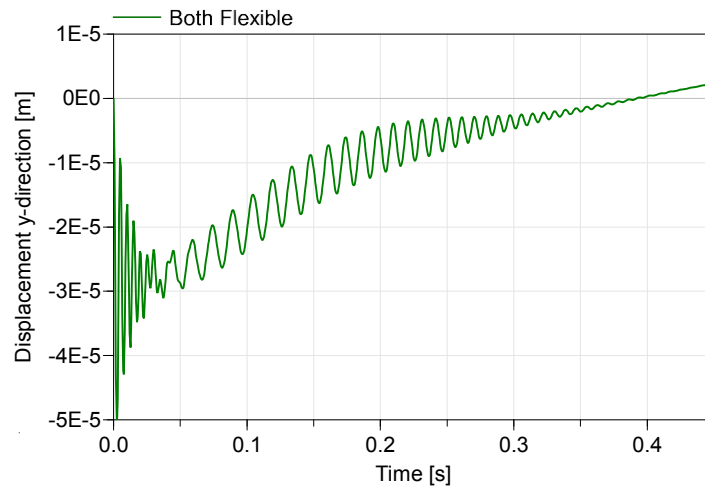
FIGURE 7.14: Close up on the displacement in the y-direction at frame b of the rod (flexible crank, flexible rod).

7.1.2 CPU Benchmark

The slider crank models with flexible beam components were also a part of a CPU benchmark. The benchmark compared the computational time required to simulate the models depending on the number of dynamic shape functions. Additionally the number of states and time-varying variables were recorded during the tests. The two flexible slider crank models were run with one, three and five dynamic shape functions in the x- and y-direction. In the model with two flexible beams, both beams were set with equal number of dynamic shape functions in each test. All the simulated tests were conducted on a laptop with 6 GB RAM and a Intel Core i5 CPU with four cores at 2.6 GHz and animation was set to on.

The benchmark for the model with a rigid crank and a flexible rod is presented in Table 7.2 while the benchmark for the model with both crank and rod as flexible is presented in Table 7.3. The required computational time versus the elapsed simulation time for the two models is shown in Figures 7.15 and 7.16. The results can be compared with the same variables for the rigid model which are CPUTime $= 0.126s$, Continuous Time States $= 1$ (one degree of freedom system) and Time Varying Variables $= 91$.

CPU Variable	One shape function	Three shape functions	Five shape functions
CPU Time	1.714 *s*	2.737 *s*	4.699 *s*
Continuous Time States	18	26	34
Time Varying Variables	681	733	785

TABLE 7.2: CPU variables for different number of dynamic shape functions (x-, y-direction) used in the model with rigid crank and flexible rod.

FIGURE 7.15: Required computational time for different number of dynamic shape functions (x-, y-direction) used in the model with rigid crank and flexible rod.

CPU Variable	One shape function	Three shape functions	Five shape functions
CPU Time	9.737 *s*	21.3 *s*	43.324 *s*
Continuous Time States	34	50	66
Time Varying Variables	1214	1314	1414

TABLE 7.3: CPU variables for different number of dynamic shape functions (x-, y-direction) used in the model with flexible crank and flexible rod.
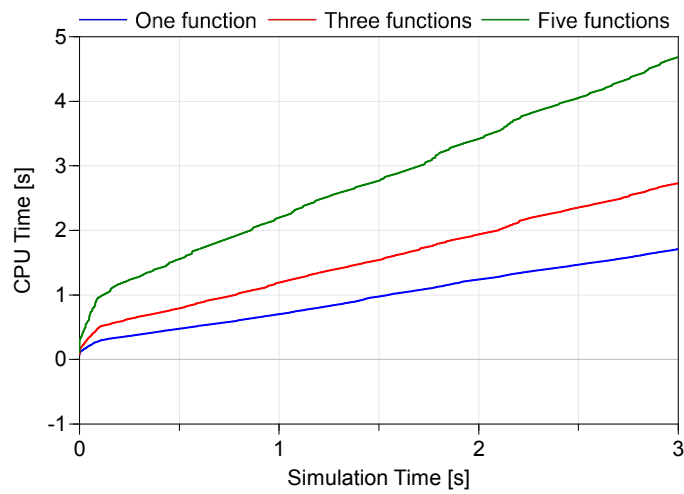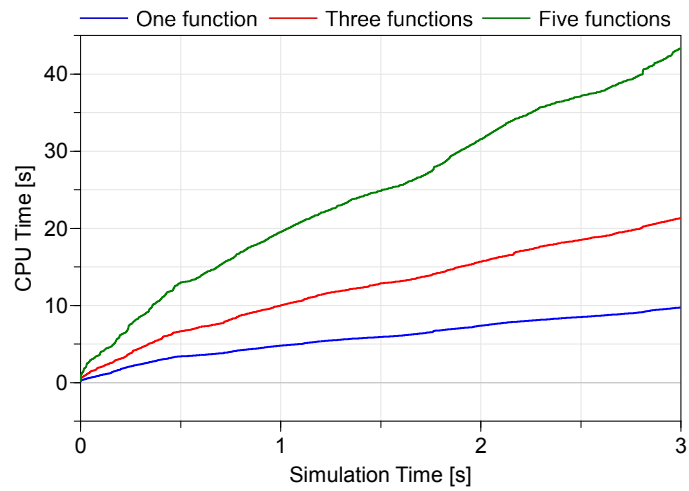
FIGURE 7.16: Required computational time for different number of dynamic shape functions (x-, y-direction) used in the model with flexible crank and flexible rod.

Chapter 8

Discussion

8.1 Response and Behaviour

The beam models respond well to the static loading cases as presented in Sections 6.1.1 and 6.2.1. The Figures in these Sections indicates that a slowly linearly increasing force implies an identical behaviour in displacement. The angular displacement respond well to lateral forces and vice versa to applied torques.

By comparing the Figures from the free vibration test cases in Sections 6.1.2 and 6.2.2, the model seem to work much better with damping applied. The damping seems to remove numerical noise and lessen the activation of dynamic shape functions that doesn't provide any substantial contribution to the solution. By increasing the number of dynamic shape functions, the free vibration response in x-direction and around the x-axis provides a more realistic behaviour. This doesn't seem to be the case for the same tests in the y- and z-directions in which Figures 6.14 and 6.15 shows almost identical behaviour. This phenomenon could be due to differences in coverage of frequencies and modeshapes between a Fixed-Free and a Fixed-Fixed beam as implied by the Craig-Bampton method.

The results from the forced vibration test cases in Sections 6.1.3 and 6.2.3 proves that the beam model can represent mechanical resonance. If the applied force is not acting precisely in the model's eigenfrequency then the model responds with vibrations in a overriding beat frequency. The beat frequency is a natural behaviour in any mechanical system and something expected when vibrations do not occur in the eigenfrequency.

The displacements seem realistic when the model is subjected to gravitational and centrifugal forces. The Figures in Section 6.1.5.1 shows that the displacement in the x-direction stabilises at a constant value while the displacement in the z-direction is zero, which should be the case when the angular velocity is constant.

However when the torque is constant and the angular velocity is linearly increasing, the displacement in the x-direction increases exponentially with time while the displacement in the z-direction seem to adjust to a constant value as seen in Figures 6.35 and 6.36. This should be the case when the torque is constant but when the simulation time is increased it seems as if additional energy is added to the model as indicated by Figures 6.37 and 6.38 even though the torque is constant. That additional energy would be added to the model doesn't align with the fact that the angular acceleration is slightly decreasing as seen in Figure 6.39. The results indicates that something could be wrong in the implementation of the quadratic velocity vector described in Section 3.6, but it could as well be a numerical error in Dymola. At the moment there is not enough information to make any conclusions regarding this issue.

The results from all the test cases done with both the three-dimensional and one-dimensional models are identical which indicates that the implementation of these degrees of freedoms have been done correctly. Especially the results from Section 6.2.4 shows that the displacement and frequency response of the beam models are very similar to the analytical solution. However, it seems as if the results from the beam models shows an overshoot in displacement that increases with time as seen in Figures 6.50, 6.51, 6.53 and 6.54. This is something that could be related to the additional energy associated with the results from the centrifugal force test cases. It could also be a consequence to the absence of damping and the models capability in modeling free vibration of undamped beams as previously discussed. Another hypothesis is that it's related with the simplifications made with the Craig-Bampton method. Setting up a identical test case where the beam is modeled with several beam components would be of interest to further investigate this behaviour.

8.2   Accuracy

As presented in Table 6.1, the errors in the displacement in the static loading cases are close to non-existent and the model's accuracy in prescribing static deformation is almost equivalent to the theory described in Section 1.5.

The errors in frequency are larger in the free vibration test cases compared to the forced vibration test cases as seen in Tables 6.2 and 6.8. Interestingly there are errors for the

free vibration test cases in the x-direction and around the x-axis which are not in the result from the forced vibration test cases where these errors are zero.

It seems as if the model has a different stiffness, mass or inertia depending on the applied forces or displacements and therefore different eigenfrequencies. The model underestimates the eigenfrequencies in the free vibration test cases in comparison to the forced vibration test cases where the frequencies are overestimated in the y- and z-directions. Furthermore this shouldn't be the case since the beams in both test cases have the same geometric and material parameters and therefore should result in equal eigenfrequencies.

The errors presented in Section 6.3, with the exception of the free vibration test cases, are much lower than one percent. This indicates that the beam model in question has the potential of representing the Euler Bernoulli beam theory, in both static and dynamic load cases.

8.3   Compatibility with the Dymola Library

The flexible slider crank models presented in Chapter 7 shows that the beam model can be connected and run with other components in the standard mechanical library in Dymola. The results in Figures 7.3, 7.4, 7.5, 7.6, 7.7 and 7.8 indicate that the forces are almost identical in the flexible and rigid models. The displacements in the flexible model follows the change in direction of the forces as presented in Figures 7.9, 7.10, 7.11 and 7.12, which indicates that a successful connection between external forces and internal displacements has been made.

The vibrational response in the system can be captured by exchanging rigid components with flexible components as seen in Figures 7.13 and 7.14. Adding additional flexible components increases the vibrational response which seems logical since the system has become more elastic.

In the slider crank models the flexible beams were attached with their respective frame a closest to the fixed inertial frame (see Figure 7.1). This was done intentionally since the local coordinate system of the beam model is attached to frame a as described in Section 7.1. Connecting the components differently causes the model to calculate the inverse of the equations of motion since Dymola evaluates the system according to the defined roots and branches. This is due to the kinematic description, where the displacement is described relative a local coordinate system that needs to be attached at one end (see equation (2.6)). However, it works to connect the beams with frame b closest to the root but it is far from ideal since it forces Dymola to select variables as states that were

not thought of as states in the implementation (e.g. the transformation matrix between frame a and b). Connecting the beams in this manner might cause Dymola to crash during the simulations.

8.4 Computational Efficiency

The benchmark presented in Table 7.2 shows that a common mechanical application with one flexible beam can without any problems run on a low performance laptop with a CPU time below the elapsed simulation time.

The simulation time increases non-linearly when adding further complexity to the model by increasing the number of dynamic shape functions as seen in Figure 7.15. If another flexible beam is added to the system the number of time varying variables and time states are almost doubled while the CPU time increases more drastically as presented in Table 7.3.

Since the models haven't been run on any other computer software it is hard to know weather the beam model is efficient or not. However, the results indicate that the model runs smoothly if few dynamic shape functions are used (one to three), which should be sufficient for most applications.

Chapter 9

Conclusion and Future Work

9.1 Conclusion

A flexible beam library has been implemented in Dymola using the Craig-Bampton method in a Floating Frame of Reference formulation. The library contains three different components, one translational, one rotation and one multibody component, each one compatible with the standard mechanical library in Dymola. The implemented models are based on the Euler Bernoulli beam theory and have shown significantly promising results throughout the validation process. Especially impressive is the models accuracy in representing static deformation which is better than the accuracy in representing dynamic deformation. The models show different response in eigenfrequencies depending on the given case of dynamic deformation. The eigenfrequency deviates further from the analytical solution in free vibration in comparison to forced vibration. Furthermore an increase in the systems energy has been observed while the beam is subjected to certain loads. It is recommended to further investigate whether the mentioned issues are due to the simplifications made with the Craig-Bampton method, if there are faults within the implementation or if it could be due to numerical errors in Dymola.

Modeling an elastic beam with coupled substructures provides the advantage of neglecting prescribed kinematic boundary conditions. In large mechanical systems this is a great advantage since the user can connect multiple elastic beam components without providing any information concerning kinematic constraints. In combination with the Floating Frame of Reference formulation, it leads to a compact format, suitable with the object-oriented equation based environment in Dymola, providing short computational times on low performance computers.

9.2   Future Work

As a concluding remark we recommend Modelon AB to put further effort in developing and investigating the following:

- Differences in eigenfrequencies in free and forced vibrational cases of deformation and if this can be related to the Craig-Bampton method.

- Run more and longer simulations in order to identify other situations in which additional energy seem to appear in the system.

- Model a single beam with several beam components to investigate if this increases the accuracy of the solution.

- Test the models in larger mechanical applications such as a vehicle suspension or drive line and compare with similar models in other modeling software products.

- Test the models with other material properties that are more common in mechanical applications than those presented in Chapters 6 and 7.

- Implement a material database with the properties of common materials so that these can easily be exchanged in the models.

- The Rayleigh damping coefficients should be evaluated according to chosen material properties and model structure.

- The beam component should identify which frame is closest to the root and automatically define the origin of the local coordinate system in that frame.

- Circular cross sections should be implemented in the three-dimensional component.

- The user should be able to turn static shape functions on and off in order to conveniently exchange flexible components with rigid ones.

- An implementation of Euler/Bryant angles as rotational coordinates to add extended compatibility with the standard libraries.

Bibliography

[1] Caroline Malmberg. Flexible beams in dymola. Master's thesis, Lund University, LTH, Department of Construction Sciences, 2010.

[2] Eric Saad. Modelling of flexible beams in dymola. Master's thesis, Lund University, LTH, Devision of Mechanics, 2011.

[3] S. Timoshenko. *Vibration Problems in Engineering*. D. Van Nostrand Company, New York, USA, 2nd edition, 5th printing edition, 1937.

[4] Christer Ljung, Niels Saabye Ottosen, and Matti Ristinmaa. *Introduktion till Hållfasthetslära, Enaxliga tillstånd*. Studentlitteratur 2007, 1:1 edition, 2007.

[5] Ahmed A. Shabana. *Dynamics of Multibody Systems*. Cambridge University Press, 3rd edition, 2005.

[6] Roy R. Craig JR and C.C. Bampton. Coupling of substructures for dynamic analysses. *AIAA Journal*, 6(7):1313–1319, July 1968.

[7] Niels Saabye Ottosen and Hans Petersson. *Introduction to the Finite Element Method*. Prentice Hall Europe, 1st edition, 1992.

[8] *Handbok och formelsamling i Hållfasthetslära*. Institutionen för hållfasthetslära KTH, 7th edition, 2010.

[9] Niels Saabye Ottosen and Matti Ristinmaa. *The Mechanics of Constitutive Modelling*, volume 1. Division of Solid Mechanics Lund University, 1999.

[10] J. N. Reddy. *Energy Principles and Variational Methods in Applied Mechanics*. John Wiley & Sons, 2nd edition, 2002.

[11] Christer Ljung, Niels Saabye Ottosen, and Matti Ristinmaa. *Hållfasthetslära, Allmänna tillstånd*. Studentlitteratur 2007, 1:1 edition, 2007.

[12] Per Lidström. *Lecture Notes on Mechanical Vibrations*. Lund University, Faculty of Engineering LTH, Division of Mechanics, 2013.

[13] Karim Sherif and Karin Nachbagauer. A detailed derivation of the velocity-dependent inertia forces in the floating frame of reference formulation. *Journal of Computational and Nonlinear Dynamics*, 9(4), July 2014.

[14] Per Lidström. *Mechanical Vibrations Exercises*. Lund University, Faculty of Engineering LTH, Division of Mechanics, 2013.